Measuring and Improving Time-of-Flight Camera Light Source Electrical-to-Optical Power Conversion Efficiency

A thesis
submitted in fulfilment
of the requirements for the degree

of

Master of Engineering

at

The University of Waikato

by

DALE OWEN CORLETT

THE UNIVERSITY OF
WAIKATO
Te Whare Wānanga o Waikato

2020

Abstract

Time of Flight (ToF) cameras capture three-dimensional depth images of a scene. They do this by transmitting a modulated light signal from a light source, which scatters off objects in the scene and returns to the camera's modulated image sensor. Distance values for each pixel of the image sensor are calculated from the measured difference in phase between the transmitted and received signal.

There are two circuit topologies typically used for ToF camera light sources, shunt switching and series switching. Chronoptics Limited (Hamilton, New Zealand) is a company that develops ToF cameras. The light source of their Kea ToF camera drives four laser diodes using the iC-HG (iC-Haus GmbH, Bodenheim, Germany) Integrated Circuit (IC). The iC-HG IC, and therefore the Kea light source, has a series switching topology. Texas Instruments (Dallas, Texas) has designed a ToF camera with a light source that has the shunt switching topology. Texas Instruments claim that the shunt switching topology has a better electrical input power to optical output power than the series switching topology.

The aim of this project is to investigate the shunt topology, in particular the Texas Instruments implementation, and to determine if the shunt topology could provide a substantial increase in efficiency for the Kea light source and future Chronoptics' light source designs.

In this thesis, we measure the electrical input to optical output power efficiency of the Texas Instruments TIDA-01173 light source and compare it to the Kea light source and find the TIDA1173 does indeed have a higher power efficiency than the Kea light source. However, it is not as efficient as we anticipated, so we also investigate options for improving the power efficiency of the TIDA-01173 light source to maximise the benefits of designing a new light source.

To achieve the aim, an apparatus is designed and constructed to measure the electrical input power and optical output power of the TIDA-01173 and Kea light sources. The input and output power measurements are used to calculate the

efficiency of the light sources over a range of modulation frequencies from 10 MHz to 100 MHz. The electrical to optical power efficiency results show that the shunt switching topology TIDA-01173 light source is more power efficient than the series switching topology Kea light source. The TIDA-01173 has a measured power efficiency of 22% at 10 MHz modulation frequency, and Kea has an efficiency of 11% at the same frequency. These hardware measurement results are corroborated by the results of SPICE simulations made for each of the ToF light sources. To make these simulations, the electrical and optical properties of the BOB850T1000 laser diode (Bob Laser Co, Guangdong, China) used in the ToF light sources are extracted to make a laser diode SPICE model.

An account of the power consumption of each component in both light sources is conducted using the light source SPICE simulations. This account shows that the linear current limiter in the TIDA-01173 consumes the most power, so it is swapped for a buck current regulator. This modification increases the power efficiency of the TIDA-01173 light source to 28% at 10 MHz modulation frequency. The power efficiency of the Kea light source is increased to 13% at 10 MHz modulation frequency by decreasing the input voltage from 5 V to 4 V. Improving the efficiency of the ToF camera light sources allows higher optical output power for a given input power. This enables ToF cameras to be powered from low power sources such as, Universal Serial Bus (USB) ports or battery packs, therefore improving the versatility of ToF cameras.

Acknowledgements

I am grateful for the funding provided for my work by the Callaghan Innovation Research and Development Fellowship, and the University of Waikato Research Masters Scholarship. I would like to thank Chronoptics team for welcoming me, giving me the opportunity to do my master's with them, organising the Callaghan Innovation Research and Development Fellowship, and providing me with their technical support and knowledge. I am very thankful for my supervisors, Dr Adrian Dorrington and Dr Lee Streeter. I greatly appreciate all the help they provided me. I am very fortunate to have met so many nice people over the course of my studies, and I owe a lot to the friends that I have made. It wouldn't have been the same without you. And finally, thanks to my parents and siblings for the immense support they have provided me.

Abbreviations

ToF	Time of Flight
IC	Integrated Circuit
AMCW	Amplitude Modulated Continuous Wave
OD	Optical Density
USB	Universal Serial Bus
PPE	Personal Protective Equipment
IS	Saturation Current
N	Ideality Factor
RS	Series Resistance
TT	Transit-Time
CJO	Zero-Bias Junction Capacitance
VJ	Junction Potential
M	Grading Coefficient
LD	Laser Diode
IPM	Input Power Measurement
GPIO	General-Purpose Input Output
I^2C	Inter-Integrated Circuit
FWHM	Full Width at Half Maximum
CMOS	Complacentry Metal-Oxide-Semiconductor
DAC	Digital to Analogue Converter
SMA	SubMiniature version A
CLI	Command Line Interface
GUI	Graphical User Interface
VCSEL	Vertical-Cavity Surface Emitting Laser

Contents

List of Figures

List of Tables

Chapter 1

Introduction

1.1 Project introduction

Chronoptics Limited (Hamilton, New Zealand) is a company that develops Time of Flight (ToF) cameras. Their ToF camera called Kea (Figure 1.1.1) uses the iC-HG (iC-Haus GmbH, Bodenheim, Germany) Integrated Circuit (IC) to drive the laser diodes that produce modulated light that illuminates the scene. The iC-HG is a series topology light source. Chronoptics wants to improve the electrical to optical power efficiency of the light source for their Kea ToF camera. A more power efficient ToF camera light source is of value to Chronoptics because the light source can produce more optical output power for a given input power. This means that their ToF cameras could be powered from a low power source, such as Universal Serial Bus (USB) ports or battery packs, and still produce the same optical output power. Higher power efficiency means more optical output power can be produced without increasing the heat dissipation. So, the maximum light source modulation current can be increased, therefore improving ToF camera performance in high ambient light applications, such as outdoors in daylight.

Figure 1.1.1: Photo of the Kea ToF camera.

Figure 1.1.2: Photo of the TIDA-01173 ToF camera [1].

Chronoptics found that the TIDA-01173 (Texas Instruments, Dallas, Texas) ToF camera (Figure 1.1.2) uses a different ToF camera light source laser diode driving topology in their TIDA-01173 ToF camera called the shunt switching topology. TIDA-01173 claim in their Illumination Driving for Time-of-Flight (ToF) Camera System application report [2], that the shunt switching topology is more power efficient than the series topology. Chronoptics wants to know if this claim is true, and if so, they want to use the shunt switching topology to produce a more power efficient ToF camera light source. Chronoptics has done work with the TIDA-01173 camera and found that the light source does not perform as well as it promises to in theory[2].

The aim of this project is to investigate the TIDA-01173 light source design, as it has the shunt switching topology, to see if it is more power efficient than the Kea light source and investigate options for an improved ToF camera light source.

1.2 Objectives

To achieve the project aim, the electrical to optical power efficiency of the TIDA-01173 and Kea light sources must be measured. To measure the power efficiency, an apparatus must be designed to measure both the electrical input power and optical power of the light sources. To aid in the development of the light source improvements, simulation models of both the TIDA-01173 and Kea light sources must be produced. The results of the hardware efficiency measurements can also be used to confirm that the light source simulation models are representative of the real light sources.

1.3 Thesis structure

This thesis is made up of seven chapters and two appendices.

Chapter 1 is an introduction to the project, detailing the motivations, aims and project objectives.

Chapter 2 contains detailed background information and a literature review relating to the project.

Chapter 3 presents the development of a simulation model for the TIDA-01173 and Kea ToF camera light sources.

Chapter 5 shows the parameter extraction of the laser diode used in the Kea light source and the development of a SPICE model for the laser diode, so that it can be used in the simulation of the TIDA-01173 and Kea light sources.

Chapter 4 describes the apparatus that is designed to measure the electrical to optical power efficiency of the ToF camera light sources.

Chapter 6 presents the light source power efficiency results obtained from the power efficiency measurement apparatus, and simulations of the ToF light sources. The results are used to compare the light sources to each other. The light source simulations are used to identify the components that consume the most power in the light sources. These results are then used to propose and test design improvements for the light sources in simulation.

Chapter 7 summarises the project and proposed future work.

Appendix A contains specification tables of the BOB850T1000 laser diode (Bob Laser Co, Guangdong, China) and the 22045498 laser diode (Lumentum Operations, San Jose, California), from their datasheets.

Appendix B contains the simulation test to see if the TIDA-01773 can go into continuous wave mode when components are damaged, open or closed circuit. It also contains the TIDA-01173 inductor voltage waveform and a short description of its significance.

Chapter 2

Background

2.1 The Time-of-Flight camera

Time-of-Flight (ToF) cameras perform range imaging. Range imaging is a general term used to describe techniques for producing an image where each pixel holds distance values to map a three-dimensional (3D) scene. ToF cameras are used in applications such as mapping surroundings for autonomous local navigation, gesture control, motion capture, and object dimension measurements [3]. With improvements to the power efficiency and size of ToF technology, ToF cameras are now able to be incorporated into smart phones [4].

Amplitude modulated continuous wave (AMCW) ToF cameras indirectly measure distance by detecting the phase between the transmitted signal from the light source and the reflected signal received by the sensor array, after reflecting off objects in the scene [5, Sec. 2.1.3]. An image is produced that holds distance information for each pixel of the image sensor [6]. ToF cameras, like the TIDA-01173 ToF camera, include light sources that modulate the intensity of near infrared light produced by light emitting diodes (LEDs) or laser diodes, and specialised modulated sensors to detect phase change (Figure 2.1.1).

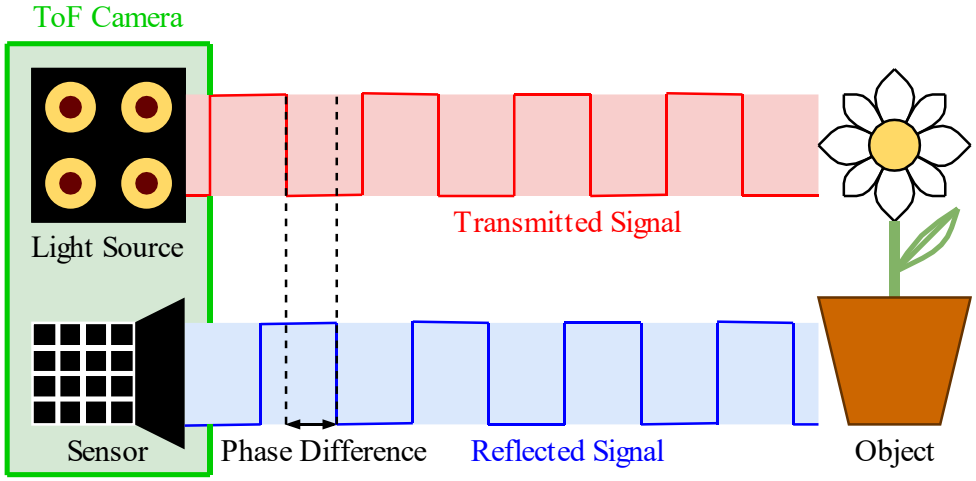

Figure 2.1.1: ToF conceptual diagram.

The light source and image sensor are modulated in phase, called homodyne. The sensor accumulates the received light over an integration period, so any phase difference in the signal received at the sensor's pixels will be observed as an intensity difference at that pixel.

As the modulation signal is periodic, the phase difference measured can only be determined within the range of 0 to 2π radians. Phase differences above 2π radians will wrap to be within this range. A maximum measurable distance (d_u), known as the ambiguity distance, arises due to the phase wrapping. The maximum distance that corresponds to the maximum determinable phase difference of 2π radians is given as,

$$d_u = \frac{c}{2f_M}, \tag{2.1.1}$$

where c is the speed of light, and f_M is the modulation frequency [7].

The lower the frequency, the longer the ambiguity distance, however, the precision of the depth measurement increases with increasing modulation frequency. Longer ambiguity distance and higher accuracy depth measurements are achieved in ToF cameras by taking a few raw frames at different modulation frequencies for each depth frame. Hence, it is preferred that the modulation frequency of the light source and sensor should be variable. The typical modulation frequency range of ToF cameras is 10 to 100 MHz but can be higher [8].

Light with wavelengths in the near-infrared range (near-infrared range defined as 700 to 2500 nm [9]), around 850 nm, is used as the illumination source for ToF cameras because it is invisible to humans, and so is unobtrusive. Both Light Emitting Diodes (LEDs) and laser diodes that emit light in the near-infrared wavelengths are used for the light sources of ToF cameras, each having associated advantages and disadvantages. Laser diodes are more sensitive to transient voltages than LEDs, and also require a more complicated driver circuitry than LEDs [10, p. 4]. LEDs have lower electrical bandwidths (slower switching abilities) than laser diodes and can only be modulated up to around 30 MHz. Some LEDs designed for communications can be modulated at up to 100 MHz [11, p. 64], however, they do not produce enough optical output power to be used for ToF cameras. Laser diodes, however, can be modulated to frequencies much higher than 100 MHz [10, p. 4].

Higher electrical bandwidth means active illumination levels can be maintained to higher frequencies, so greater precision of the depth measurement can be achieved using a laser diode, because precision increases with modulation frequency. The electrical to optical power efficiency for LEDs is up to 30% while for laser diodes it is up to 40% or 50% [11, p. 75], [10, p. 4]. So, if the light source driver circuit is 100% efficient the maximum achievable electrical to optical power efficiency of a ToF light source is only 50%. Due to the LED's beam shape, a considerable portion of the light is located in the border area of the beam, so does not fall in the field of view of the camera and is therefore wasted [10, p. 4]. However, laser diodes produce a spatially coherent beam, which can be shaped to fit the field-of-view more efficiently [10, p. 4]. The major disadvantage of laser diodes is that optical systems using laser diodes have to be designed with special considerations to skin and eye safety [12]. Eye safety is of particular importance because the eye is the only organ in the body that can focus light to a very small point (5 µm to 30 µm) [13].

The Kea and TIDA-01173 ToF camera light sources use laser diodes as the light emitting component as they provide the advantages over LEDs of higher optical output power and electrical to optical power efficiency, and the eye hazards associated with laser diodes is commonly mitigated with the use of optical diffusers.

2.2 Laser diodes

A laser diode is a semiconductor structure, comprised of a pn-junction (hence diode) and an optical resonator [14]. Laser diodes are also known in the literature as: diode lasers; semiconductor lasers; and injection lasers. Laser diodes work on the same principles of stimulated absorption, spontaneous emission, stimulated emission and population inversion, that other lasers do, but laser diodes are constructed of solid-state semiconductor materials. Lasers have the following pertinent properties:

- **Stimulated absorption** - Electron absorbs photon and rises to an excited energy state.
- **Spontaneous emission** - Photon emitted when an electron falls from excited energy state to a lower energy state.
- **Stimulated emission** - Photon interacts with an electron in an excited energy state. The electron falls back to a low energy state and emits a photon, such as in spontaneous emission, however, the emitted photon will be identical to the photon that stimulated it. So now there are two coherent (same momentum, phase, and wavelength) photons.
- **Population inversion** - The number of electrons in the excited state is larger than the number in the ground state. So, amplification of photons can occur.
- **Resonator cavity** - Fully reflective mirror on the back side off the cavity, and partially transmissive mirror on front side of cavity. Photons reflect off either side of the cavity so that more amplification of the photons by stimulated emission can occur, which perpetuates the lasing and produces a more powerful beam.

Figure 2.2.1 is a graph of the optical power output of a laser diode as a function of its forward current. For a laser diode to produce a coherent beam, it must be driven with a current above the lasing threshold current (I_q). Below this threshold, the laser diode produces non-coherent light by spontaneous emission of photons, as occurs in LEDs. Above the threshold current, the laser diode begins “lasing”, its optical power output increases by orders of magnitude, and the photons that are

produced are coherent due to stimulated emission [11, Ch. 1.4], [15, p. 159], [16, p. 74].

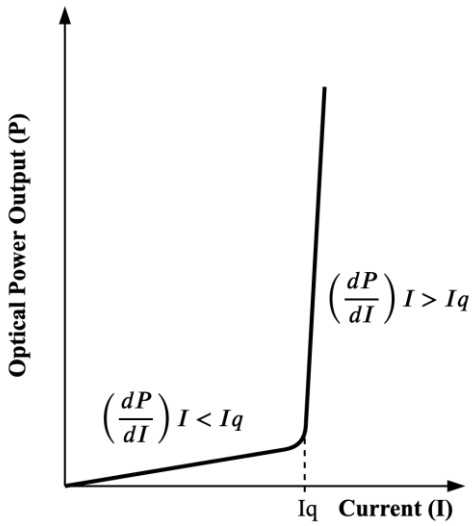

Figure 2.2.1: Graph showing laser diode output optical power to input current [17]. I_q is the current at the threshold of lasing.

2.3 Driving laser diodes

Laser diodes are negative temperature coefficient devices. This means that their resistance decreases as their temperature increases [18, Sec. 5.4.6]. If a laser diode is driven with a constant voltage, by Ohm's law, its current is free to increase with the decreasing resistance. This leads to an increased rate of heating, until the diode becomes so hot that it fails. To avoid this run away current, laser diodes have to be driven by a constant current source [19].

Diode junction temperature is a very important factor to consider when attempting to drive a laser diode in a stable manner, as the temperature of the laser diode affects its wavelength and optical output power [17]. For optimal laser diode optical output power stability, a laser diode driver has to control the bias current supplied to the laser diode by monitoring the laser diode's optical output power via a photodiode [20, p. 1211]. For this purpose, photodiodes are now commonly integrated into the laser diode package [21], [22]. This is known as constant power control. In applications where maintaining constant wavelength and optical power output of laser diodes is vital, the wavelength drift is controlled by good use of

passive heat spreading, and by adjusting the temperature of the laser diode using Peltier effect elements [23]–[25].

Laser diodes are highly vulnerable to transient voltage spikes and thermal stress, so driver circuits must be designed to protect against these. The protection methods used are the shunt Schottky diode, slow/soft start, shorting output, and voltage snubber. Due to the high current requirement for driving a laser diode at power levels required for ToF cameras, a Schottky diode is usually placed in the reverse direction and in parallel with the laser diode. This is to protect the laser diode against reverse switching transient voltages [26, p. 334]. Slow start, or soft start, is a feature of laser drivers used to increase the laser current at a slow rate. This is done to protect against excessive current, transients, and internal mechanical stresses in the laser diode, due to the changing temperature when the laser diode is initially brought up to its operating current [19], [27], [28]. To protect the laser diode from Electrostatic Discharge (ESD) damage, it is useful for the laser driver to have a shorting output. This means that the output leads of the driver are shorted while the driver is turned off [19].

The TIDA-01173 ToF camera light source uses a voltage snubber protection circuit that comprises of a PIN diode (D15) and Zener diode (D14) (Figure 2.3.1) to dampen ringing in the TIDA-01173 circuit by clamping the excess voltage across the MOSFET to protect it from over current, which would cause the laser diode catastrophic optical damage [2].

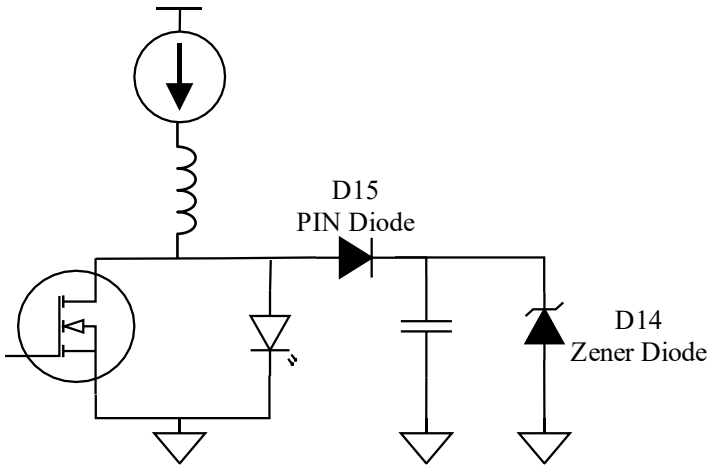

Figure 2.3.1: TIDA-01173 light source snubber circuit [2].

2.3.1 ToF laser eye safety design requirements

ToF cameras that use laser diodes as the light emitting component need to meet strict safety requirements. ToF cameras need to meet the Class 1 laser product requirements defined in [29, Sec. 3.17], so that they can be used without the need for Personal Protective Equipment (PPE), like laser safety goggles.

2.4 ToF laser diode drivers

2.4.1 Typical features

ToF camera laser diode drivers can typically set the laser diode bias current and modulation current, accept varying modulation signal duty cycle ratios and modulation frequencies, and switch on and off the light output during Integration and off times.

Laser drivers in ToF cameras are often designed to supply the laser diodes with both a bias current and a modulation current. The bias current always flows at a constant rate through the diode and the modulation current is superimposed on the bias current. The bias current sets the operating point of the laser diode to be above the threshold of lasing current so that it modulates in the linear/lasing region [30, p. 2]. Unlike the region below the threshold current, the “lasing region” above the threshold current of the laser diode is very linear, so the nonlinear part of the optical output power vs diode current curve (Figure 2.2.1) will not distort the optical waveform produced by the laser diode.

Square waveforms are typically used to modulate the light source in ToF cameras because square waves are easier and cheaper to generate than sine waves, as it only requires the current through the laser diodes to be switched on and off. However, square waves produce worse measurement linearity than sine waveforms, due to the harmonic distortion of square waveforms [31]. Square waveforms can be modified in various ways, that minimally impact the ease of generating the waveform, but produce measurement linearity that is close to the measurement linearity of sine waveform modulation [31]. A comparison of the performance of the various modulation techniques from [31] is shown in Table 2.4.1.

Table 2.4.1: Performance comparison of different modulation waveforms [31].

Light source configuration	**Ease of light source waveform generation**	**Measurement linearity**
Sine wave	Poor	Excellent
Square wave	Excellent	Poor
Optimised duty cycle	Good	Good
Harmonic cancellation with reduced duty cycle	Good	Excellent

2.4.2 Laser diode modulation driver circuit topologies in literature

Literature on the modulation of laser diodes covers a variety of applications: ToF cameras [31], data communication [32], optical storage [33], and optical beam printing [34] to name a few. Depending on the application, different methods of modulation are used in the driver circuits. So, there are many laser driver circuits used in literature. However, the literature has more focus on the applications of laser modulation, and the control circuit of laser drivers to drive the laser diode with constant current and constant power. There is less literature on the circuitry that directly drives and modulates the laser diode. By studying the literature in relation to laser driving for modulation, it was found that the laser drive methods for modulating laser diodes fit roughly into four categories: the bias-tee configuration [35]–[37], series switching [38]–[43], shunt switching [2], [32], [44]–[46], and current steering [32].

2.4.2.1 Bias-tee

A bias-tee superposes the modulation signal on to the bias current using a capacitor and inductor (Figure 2.4.1). On the bias current input, an inductor allows the DC bias current to pass to the laser diode while blocking the AC modulation signal from entering the bias current source. On the modulation current input, a capacitor allows the AC modulation signal to pass to the laser diode while blocking the DC bias current from entering the modulation source.

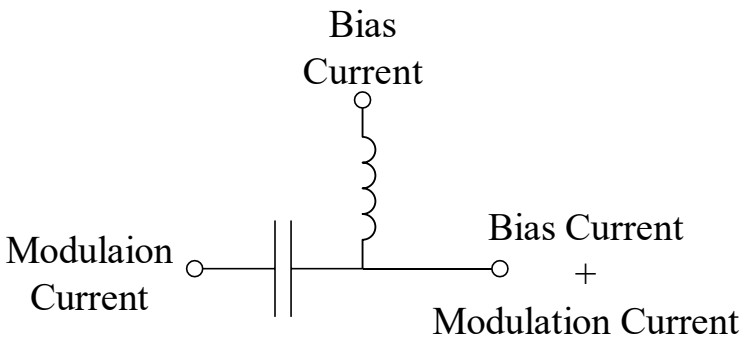

Figure 2.4.1: Equivalent circuit of a bias tee [47, p. 276], [48].

The CBTEE-01-50-6000 Redbox bias-tee (Crystek Corporation, Fort Myers, Florida) [49] is an example of a bias-tee. It has an operating frequency range of 50 MHz to 6 GHz. Bias-tees have been demonstrated in the literature for modulating laser diodes at up to 2.6 GHz [50], and 15 GHz [51]. In each of these experiments, the bandwidth limit of the laser diode was the limit of the modulation frequency.

Bias-tees have a wide modulation frequency range and can easily accept modulation waveforms of various shapes. The shunt and series switching topologies only work with square waveforms. However, Bias-tees have much lower maximum modulation current ratings than the shunt and series topologies, so are not suitable for use in ToF camera light sources.

2.4.2.2 Series switching

The iC-HK laser driver integrated circuit, made by IC-Haus, was used in ToF applications in [39]–[43].

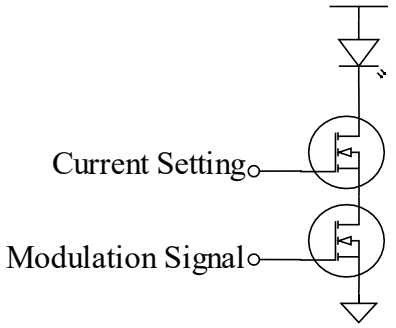

Figure 2.4.2: Series switching laser diode driver topology circuit.

The series switching laser diode driver topology (Figure 2.4.2), consists of a current setting MOSFET and a modulation switching MOSFET. The current setting MOSFET sets the modulation current, and the modulation switching MOSFET switches the laser diode current on and off according to the modulation signal. The gate voltage of the current setting MOSFET is set by a control circuit to draw the desired modulation current through the laser diode. Bias current is applied by adding another series switching topology laser driver in parallel with the first, and then setting the modulation MOSFET to be always on.

2.4.2.3 Shunt switching

The shunt switching laser driver topology (Figure 2.4.3) is the Norton equivalent of the series topology [2]. A MOSFET placed in parallel with the laser diode (or series string of laser diodes) and a current source, supplies the modulation current. The modulation signal switches the MOSFET on and off at the modulation frequency, when the MOSFET is on the drain source resistance of the MOSFET is very low (near zero), so nearly all of the current supplied by the current source flows through the MOSFET so no current flows through the laser diode so it produces no light. When the MOSFET is switched off, the current stops flowing through the MOSFET and all the current flows through the laser diode, so it produces optical output power

proportional, by a factor of the laser diode's slope efficiency, to the modulation current.

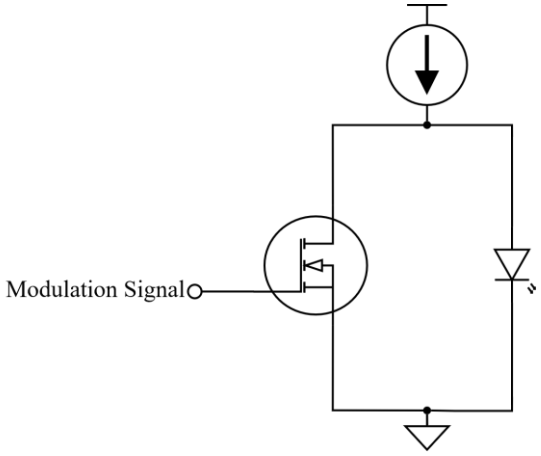

Figure 2.4.3: Simple shunt laser diode driver circuit [2].

However, the shunt switching topology is not practical as it is depicted in Figure 2.4.3 because an ideal current source is not possible. The few instances of the shunt switching topology in literature [2], [44], [46], address this problem by adding an inductor in series with a nonideal current source to store energy during the off state and supply it during the on state of the modulation signal (Figure 2.4.4). The inductor acts as a current source, changing the voltage at the node between the MOSFET and laser diode to keep the current flowing through it constant. The voltage at this node swings from IDS/RDS(on) when the MOSFET is on, which is near 0 V if the MOSFET's RDS(on) is very small, then to the forward voltage of the laser diodes when the MOSFET is off. This means that the required supply voltage can be half of the required laser diode forward voltage, when the MOSFET is off and the laser diodes are on [2].

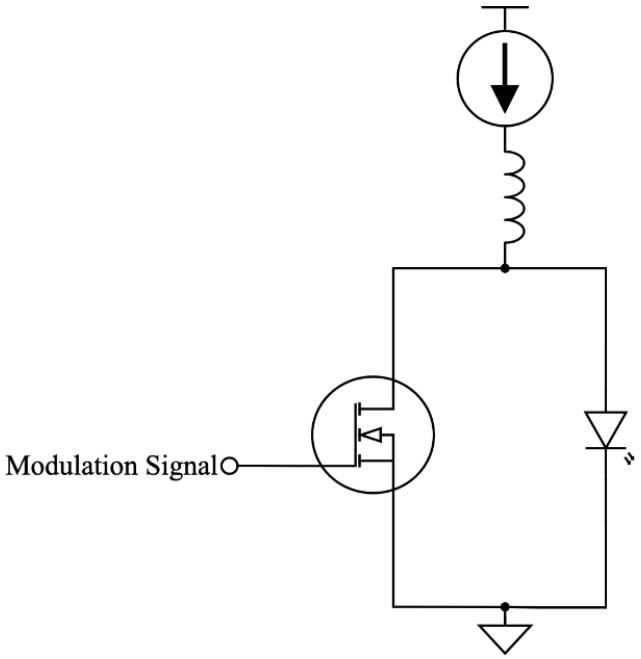

Figure 2.4.4: Simple shunt laser diode driver circuit [1].

[1] is an application report by Texas Instruments containing guidelines and examples used in the development of the TIDA-01173 ToF camera shunt switching topology based light source. This application report addresses eight aspects relating to the design of the shunt switch topology and acts as a very useful guide to design this type of laser diode driver for ToF applications. The aspects covered in this application report are:

- ToF illumination driver background information.
- A comparison of the shunt and series switching topologies.
- Explanation of the shunt switching topology.
- Analysis of the current loops in the circuit.
- Component selection guide for the:
    - Laser diode
    - Shunt MOSFET
    - Inductor
    - Snubber components
        - PIN diode
        - Zener diode
    - MOSFET gate driver

- Snubber circuit for protecting the laser diodes from transients and ringing.
- Optimal Printed Circuit Board (PCB) layout for the shunt topology using a series string of four edge emitting laser diodes.
- Power supply designs to use for the current source in the shunt switching topology.

[46] is a patent for a pulsed laser diode driver circuit that is similar to the TI design. This design has an inductor that is intended for storing energy, and a shunt switch that is connected across an array of series laser diodes. When the switch is opened, the energy stored in the inductor is suddenly released into the diode array. The patent claims that this design is more efficient than a linear current source because the switches are saturated and therefore have much lower loss. The inventor of the high-power pulsed laser diode driver is also a co-inventor on a patent for a biphase laser diode driver [44].

2.4.2.4 Current steering

[32] describes a circuit that was designed for driving laser diodes for free space laser communications for intersatellite links. This circuit is similar to the series switching topology, but bias current is set with a current source in parallel to the modulation MOSFET. The modulation current level and modulation signal are applied to the laser using a single MOSFET by using it as an adjustable current source to drive the laser diode (Figure 2.4.5). They call this current steering.

The modulation current range was from 0 to 300 mA, and the bias current range was from 0 to 100 mA, which is less than is required for the ToF camera light source. The modulation frequency range used was 10 Mbit/s to 440 Mbit/s which is similar to that required for ToF cameras (10 to 100 MHz). The overall electrical-to-light conversion efficiency achieved was 13.2% or 10.2%, and 34% electrical efficiency at full power, however, a Peltier cooling element was used for heat dissipation as the driver was intended for use in a satellite where convection cooling cannot occur.

This paper stated that “Building the current switched driver proved to be a study in circuit parasitic elements”, emphasising the importance of considering the

parasitics when designing laser drivers that modulate at frequencies in the megahertz range.

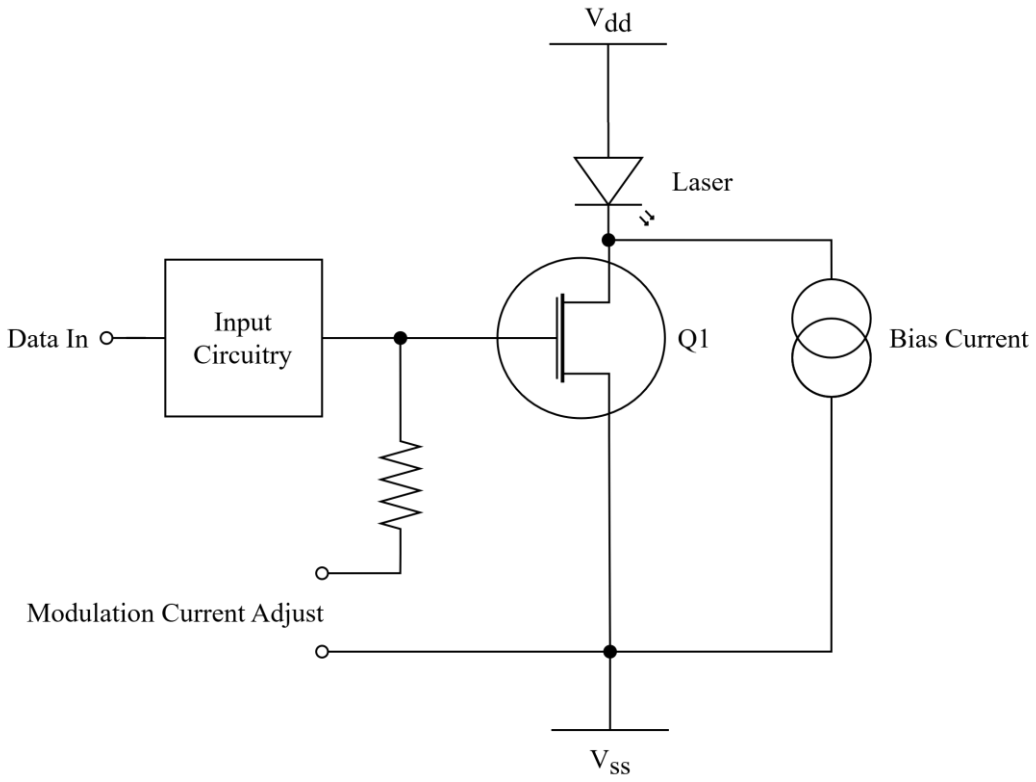

Figure 2.4.5: Laser current driver based on a single-ended switch current steering technique [32].

2.4.3 Kea ToF camera light source

The Kea ToF camera was designed by Chronoptics to be highly configurable, so it could be used in cutting edge ToF camera research and for use as a product development kit for 3D sensing. The light source for the Kea ToF camera uses the iC-HG laser diode driver IC [52]. This IC has the series switching topology. The simplified block diagram (Figure 2.4.6) shows the functional elements of the Kea light source. The Kea connector connects the light source PCB to the Kea ToF camera sensor PCB. The supply voltage for the lasers (12 V) and control circuitry (5 V and 3.3 V) come from the Kea sensor board, along with the Inter-Integrated Circuit (I^2C) bus, four modulation signals via low voltage differential signalling (LVDS), and the laser power and illumination enable signals. The 12 V laser power is converted to 5 V by the switching regulator. The modulation signals are routed

by the cross-point switch to the iC-HG laser drivers so that each laser can be controlled individually, which gives the Kea light source a wide range of configuration options. The cross-point switch is controlled via I^2C to route the modulation signals. The modulation current of each laser diode is set individually using the four channel Digital to Analogue Converter (DAC). The Bias current is set using separate DACs. The Kea light source also has an ambient light sensor.

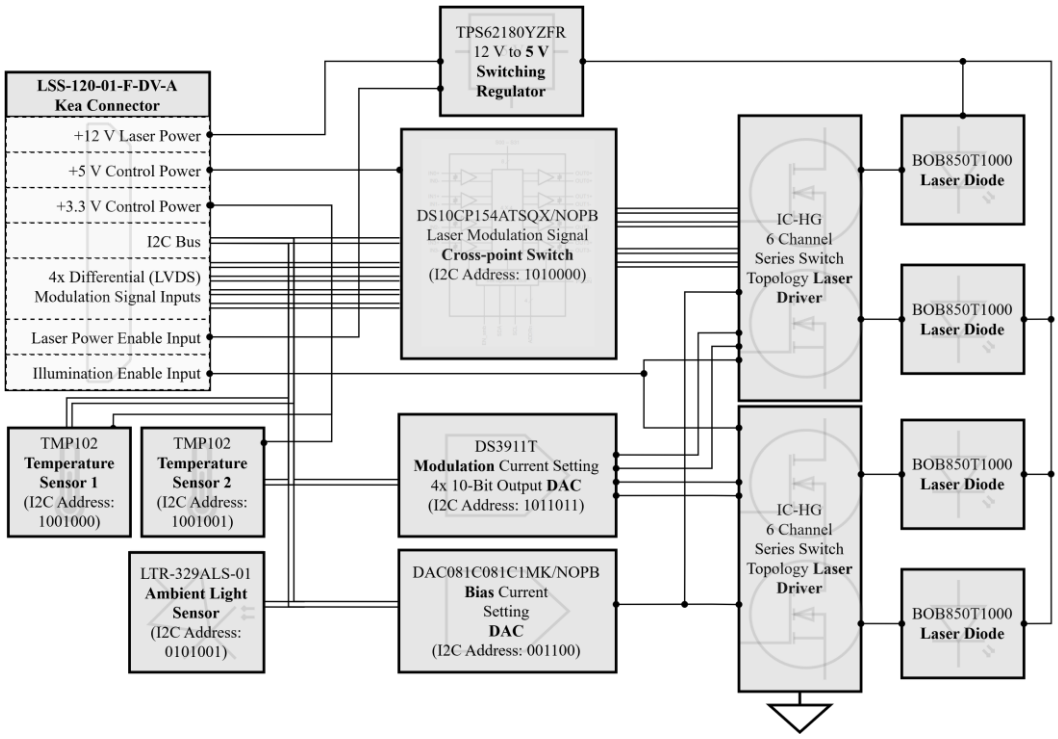

Figure 2.4.6: Functional block diagram of the Kea light source circuit.

The Kea light source has to be designed for eye safety, based on the assumption of Continuous Wave (CW) operation, because, even though Kea is designed to normally operate with the lasers modulating, it is possible for the lasers to go into CW operation if there is an error in the configuration or if components have failed (such as the modulation MOSFET failing closed). Therefore, we must guarantee that the maximum current is limited to a lower level than what would be required if the lasers were always modulated.

2.4.4 TIDA-01173 ToF camera light source

The TIDA-01173 is a reference design for a ToF camera using Texas Instrument's ToF OPT9221 controller and OPT8241 image sensor. The block diagram, Figure

2.4.7, presents the simplified functional elements of the TIDA-01173 light source. The TIDA-01173 light source PCB connects to the TIDA-01173 sensor PCB with a ribbon cable. The sensor PCB supplies, the light source PCB with the power supply lines, 5 V, 3.3 V and 1.8 V, along with the modulation signal, I^2C bus, and illumination enable signal. The 5 V line supplies the power for the laser diodes via the linear current limiter. The 3.3 V and 1.8 V lines power the control circuitry. The TIDA-01173 light source has the shunt switching topology, as the linear current limiter and inductor act as a current source. The TIDA-01173 light source has two I^2C busses for 1.8 V and a 3.3 V. The 1.8 V bus is for the temperature sensor, and the 3.3 V bus is for the digital potentiometer. The digital potentiometer sets the current limit for the linear current limiter and therefore sets the modulation current for the laser diodes. The modulation signal is a differential Complementary Metal-oxide-semiconductor (CMOS) signal that controls the modulation MOSFET via the MOSFET gate driver. The illumination enable input, controls the Integration time switching MOSFET that switches the laser current on and off, therefore enabling and disabling the lasers from producing optical output power.

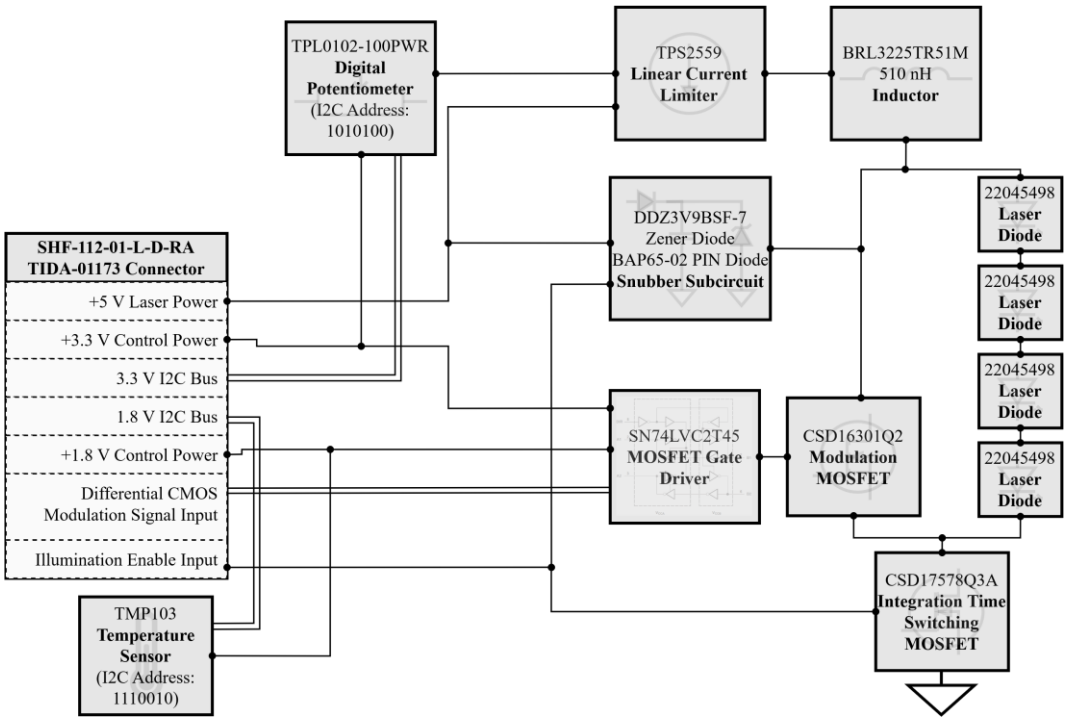

Figure 2.4.7: Functional block diagram of the TIDA-01173 light source circuit.

2.4.5 Comparison between series and shunt switching topologies

The points of comparison identified for the ToF light sources are:

- power efficiency
- waveform quality
- cost and component count
- laser safety
- configurability.

Configurability concerns the range of modulation frequencies, current settings, and duty cycle ratios.

In [2], it is stated that the only reason to use the series switching topology is to avoid using an inductor and that it has the disadvantage that the drain node of the modulation signal MOSFET goes to infinite impedance when the modulation signal is in the off state. The authors of [2], do not explain why this is a disadvantage. A possible reason is when the MOSFET goes to high impedance (open circuit), large changes in current are generated at high frequency (the modulation frequency), due to switching. This would require the voltage source to be capable of generating these high frequency load currents, and a high-performance voltage regulator being needed, which increases the cost of the circuit. Also, large changes in current at high frequencies generate radio waves that cause Electromagnetic Interference (EMI) problems [53, Ch. 8]. The shunt switching topology does not have any node with infinite impedance to ground [2]. Connecting all nodes to ground through finite impedance means that there are no large changes in current, and assuming no oscillations due to component parasitic effects, the total current from the power supply is constant. As the inductor generates the bulk of the high frequency changing voltage at the node between the laser diodes and shunt MOSFET, any power source that can maintain a constant current can be used. This reduces the cost of the circuit compared to the series switching topology, and if a high frequency shielded inductor is used, the EMI is also reduced.

In terms of efficiency, the authors of [2] state that the electrical-to-optical efficiency of the shunt switching topology is higher than the series topology,

however, they do not supply evidence nor suggest the reasoning for this claim. In [2], it is stated that the shunt topology is like the Norton equivalent of the series switching circuit. This implies that there should be no theoretical difference in power efficiency between the two topologies, assuming ideal components. So, the efficiency difference may be due to the physical implementation of the circuits because of component imperfections, such as parasitic capacitance, inductance, and resistance that causes bandwidth limits and power loss.

The series switching topology is easier to design for, as series switching topology integrated circuits, like the iC-HG laser driver [52], can be purchased. The shunt topology is more difficult, as it requires tuning of the design to achieve a consistent optical output power over the required modulation frequency range [2].

The disadvantages of the shunt switching topology is that it requires a high frequency inductor, often capable of supporting high currents, and it does not work for peak optical output powers of less than a few milliwatts [2]. The shunt switching topology does not have a mechanism for setting a bias current, the only bias current will be due to the on resistance of the MOSFET as it is in parallel to the laser diode, so some current will flow through the laser diode even when the MOSFET is in the on state. Some sort of voltage biasing has to be added to the gate of the MOSFET to set the bias current, similar to how it was done in [32] for the current steering topology.

2.5 Optical power measurements

The optical output power of many different sources of light can be measured using optical power meters. Optical power meters use photodiodes, thermopiles, and pyroelectric detectors. Photodiodes convert the photons directly to current flow, where thermopiles and pyroelectric detectors convert the photon energy to heat, which in-turn generates a voltage or current [55]. Optical power meters have a limited operating range due to limited calibration range and the sensor’s maximum optical damage threshold. Calibrated neutral-density filters can be used to reduce the optical power and extend the range that power measurements can be made.

Optical power measurement accuracy is poor in comparison to other metrics such as voltage, weight, time, and length. Absolute and relative optical power are measurable. For absolute optical power measurements, optical power meters must be tracible to standards organisations such as the National Institute of Standards and Technology (NIST) [55]. However, absolute optical power measurements are more difficult and costly than relative measurements due to the requirement of capturing and quantifying all the light emitted from the light sources that are highly diffuse or have large divergence angles. Optical elements in the path of the light from the light source to the optical power meter can reduce the accuracy of the optical power measurements due to absorption and reflection of the light. Beam alignment is critical for optical power measurements. The use of an integrating sphere allows all of the light emitted from a light source to be accounted for [56]without perfect beam alignment. [57] details the difficulties of taking optical power measurements and explains why integrating spheres (Figure 2.5.2) are better than direct coupling methods (Figure 2.5.1) for measuring the optical power of a diffuse or large divergence angle light source.

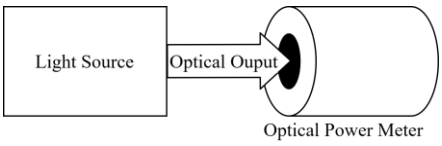

Figure 2.5.1: Direct Coupling [57].

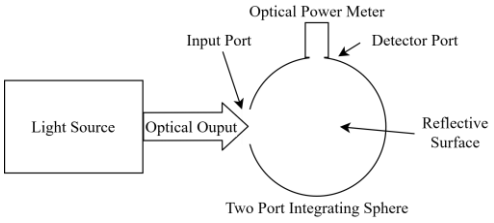

Figure 2.5.2: Integrating sphere coupling [57].

An integrating sphere is a spherical cavity with a reflective diffuse interior coating used to couple a light source to an optical power meter. The reflective diffuse coating in the sphere is designed to distribute the light evenly throughout the sphere. The optical power meter collects light from a known portion of the area of the sphere so the total optical power can be measured without perfect alignment [57]. Integrating spheres are relatively expensive, in the order of $1000 USD [58].

Absolute power measurements are required for calculating the electrical to optical power efficiency of light sources, as electrical to optical power efficiency is

the ratio of optical power in watts to electrical power in watts. In order to make comparisons between the light source efficiencies found by other researchers and those found in this research, an absolute efficiency measurement is required.

2.6 Conclusion

The literature provided good background on the operation of lasers and laser diodes, and considerations for designing circuits for driving laser diodes. The only literature that compared the series switching topology to the shunt switching topology was the Texas Instruments application report [2]. No other research could be found comparing different types of amplitude modulation techniques for driving laser diodes. The Texas Instruments application report, [26], provides a good general overview for designing the shunt topology laser diode drive, but it does not go into much detail or give reasoning for the design recommendations such as the claim that the shunt topology is more power efficient than the series topology and that the shunt topology is better for high modulation frequency than the series topology.

The literature shows that heat dissipation is very important for the efficiency of the laser driver. Efficiency is limited by the light emitter used, if laser diodes are used, then the maximum electrical to optical power efficiency of the ToF camera light source is between 40% and 50% depending on the laser model used. This maximum efficiency limit is reduced further with increasing temperature of the ToF camera light source, as the laser diode slope efficiency decreases with increasing temperature. The efficiency limit means that the laser diodes produce around 50% of the heat on the ToF camera light source, so to achieve maximum efficiency, good heat sinking is required to cool the laser diodes, regardless of the efficiency of the laser driver circuity.

The ToF camera light source electrical to optical power efficiency measurements require absolute optical power measurements, so that ToF camera light sources can be compared to other light sources in literature. Absolute optical power measurements of diffuse or large divergence angle light source are difficult, so integrating spheres should be used to couple these light sources to the optical power

meter. Integrating spheres are costly: a lower cost method of measuring the optical output power of ToF camera light sources is required.

Due to the difficulty in measuring the optical output power of the ToF light source, a simulation should be created to compare optical output power and electrical to optical power efficiency in order to assess the validity of the optical power measurements.

Chapter 3

Building the ToF light source simulation

Simulations allow rapid evaluation analysis of electronic circuits. A simulation of the TIDA-01173 ToF camera light source is required for several reasons. The validity of the hardware measurement needs to be confirmed in simulation. Losses of power in the TIDA-01173 light source can be identified using the simulation, then it can be used to develop design improvements. A simulated efficiency benchmark is required to assess design improvements. A simulation model of the Kea ToF camera light source is also required to compare Kea to TIDA-01173 as a comparison of series to shunt ToF camera light source topology.

3.1 Simulation software

The circuit simulation software selected was Texas Instrument's TINA-TI. TINA-TI was chosen because it is a SPICE (Simulation Program with Integrated Circuit Emphasis) based circuit simulator and is compatible with the component models provided by Texas Instruments. Texas Instruments encrypts their component models so that they can only be used with TINA-TI or Pspice. TINA-TI is free and simpler to use, so it was selected over Pspice. The TINA-TI version used was: Version 9.3.200.277 SF-TI Build date: Thursday, 4 October 2018, 7:41:54 p.m.

3.2 Component models

To make an accurate simulation, accurate component models are required. All the component models, apart from the BOB850T1000 laser diode (Bob Laser Co, Guangdong, China), were sourced from the manufacturer's websites. The BOB850T1000 laser diode model had to be produced manually by characterising the physical component using various analysis techniques. The components required to model the Kea and TIDA-01173 ToF camera light source circuits are shown in Table 3.2.1.

Table 3.2.1: Components required to model the Kea and TIDA-01173 ToF camera illumination circuits.

Illumination Source	**Component**	**Manufacturer Part Number**	**SPICE Model Source**
Kea	Series Laser Driver IC	iC-HG	Manufacturer's Website
	Transient protection diodes	UCLAMP1201H.TCT	Manufacturer's Datasheet
	Laser Diode	BOB850T1000	From Characterisation
TIDA-01173	Inductor	BRL3225TR51	Manufacturer's Website
	Current Limiter	TPS2559	Manufacturer's Website
	Shunt MOSFET	CSD16301Q2	Manufacturer's Website
	Series MOSFET	CSD17578Q3A	Manufacturer's Website
	Laser Diode	22045498	Not available, so will be compared to the BOB850T1000 laser diode as it is a near drop-in replacement.

3.3 Simulation component model confirmation

A simulation is only as good as the models it is based on [59]. For this reason, the component models used to form the TIDA-01173 light source simulation were confirmed as at least matching the specifications and characteristics described in their datasheets, and where possible, in hardware.

3.3.1 TIDA-01173 light source component model confirmation

The component models assessed for the TIDA-01173 light source simulation are the BRL3225TR51M inductor (Taiyo Yuden, Tokyo, Japan), TPS2559 linear current limiter (Texas Instruments, Dallas, Texas), CSD16301Q2 (Texas Instruments, Dallas, Texas) shunt MOSFET, CSD17578Q3A (Texas Instruments, Dallas, Texas) series MOSFET, and the 22045498 laser diode (Lumentum Operations, San Jose, California). The 22045498 laser diode is compared to the BOB850T1000 laser diode (Bob Laser Co, Guangdong, China) as the 22045498 laser diode SPICE model could not be sourced nor characterised, because the physical component was not available.

All the Texas Instruments component models are encrypted. This means that the SPICE parameters cannot be compared to the datasheet parameters. For this reason, each component had to be tested in simulation, then compared to the specifications in their respective datasheets.

3.3.1.1 Inductor - BRL3225TR51M

The BRL3225TR51M inductor SPICE model (Code 3.3.1) is sourced from the manufacture's website [60].

```
* BRL3225TR51     SPICE MODEL  ( General Type )
*-------------------------------------------------------------------
-------------------------------------
* Model Generated by TAIYO YUDEN Corporation (http://www.ty-
top.com)
* Version 3.0
* TAIYO YUDEN Control No. 180130NI43EB-FBB
*-------------------------------------------------------------------
-------------------------------------
*
* Products Name : Inductors
*
* Characteristics :
*     Inductance : 0.51 uH , SRF(min) : 270 MHz , DC Resistance(ma
x) : 0.0377 Ohm
*     Rated Current : Saturation :3600 mA , Temp Rise : 2550 mA
*     Case Size : 3.2 x 2.5 / 0.126 x 0.098 [mm/inch] , Thickness
: 1.7 / 0.067 [mm/inch]
*     (Conditions: Temperature = 25 degC , DC Bias Current/Voltage
 = 0A / 0V)
*
* External Node Assignments :
*
*  1  o---GGG---o  2
*
*-------------------------------------------------------------------
-------------------------------------
.SubCkt BRL3225TR51 1 2
**************************
Rdc 1 101 0.029
L0 101 111 0.39685u
L1 111 121 0.023814u
R1 111 121 0.09
L2 121 131 0.045412u
R2 121 131 2.5229
L3 131 2 0.073926u
R3 131 2 32.856
Rp 101 2 1.5k
Cp 101 2 0.289p
**************************
.ends
```

Code 3.3.1: BRL3225TR51M inductor SPICE model netlist (BRL3225TR51.cir) [60].

To confirm that the SPICE model is representative of the real component, the BRL3225TR51M's inductance is measured against frequency in hardware and simulation, and then compared against the frequency vs inductance plot presented in the BRL3225TR51M datasheet [61].

The inductor SPICE model (Code 3.3.1) is imported into TIDA-TI and a plot of the model's frequency vs inductance was produced. The data from the BRL3225TR51M datasheet frequency vs inductance plot [61] is digitised using the Engauge Digitizer software [62].

For the hardware measurements, the BRL3225TR51M inductor was desoldered from the TIDA-01173 light source PCB and wire leads were added to it, and it was soldered to the Solatron 1260A component test mount (Figure 3.3.1). The Solatron 1260A impedance analyser was used to do a frequency sweep from 100 kHz to 30 MHz and measure the inductance of the real inductor.

Figure 3.3.1: BRL3225TR51M inductor hardware test.

The frequency vs inductance plots from the hardware, simulation, and datasheet are plotted on the same plot (Figure 3.3.2). The BRL3225TR51M inductor SPICE model, provided by the manufacturer, matched the datasheet specifications up to 120 MHz. For frequencies above 120 MHz, the datasheet and simulated values diverged, so the simulation should only be used up to a maximum modulation frequency of 120 MHz. This simulation limitation is acceptable because it is within the modulation frequency operating limits of the TIDA-01173 light source (10 MHz to 100 MHz). The measured inductance values are close to the simulated and datasheet values for frequencies below 10 MHz, but for frequencies above 10 MHz, the measured inductance is more than the simulated and datasheet values. This may

be due to measurement inaccuracies, such as non-linearity near the upper limit of the impedance analyser used to measure the inductance (32 MHz), or parasitic inductance in the mounting of the inductor to the impedance analyser ports.

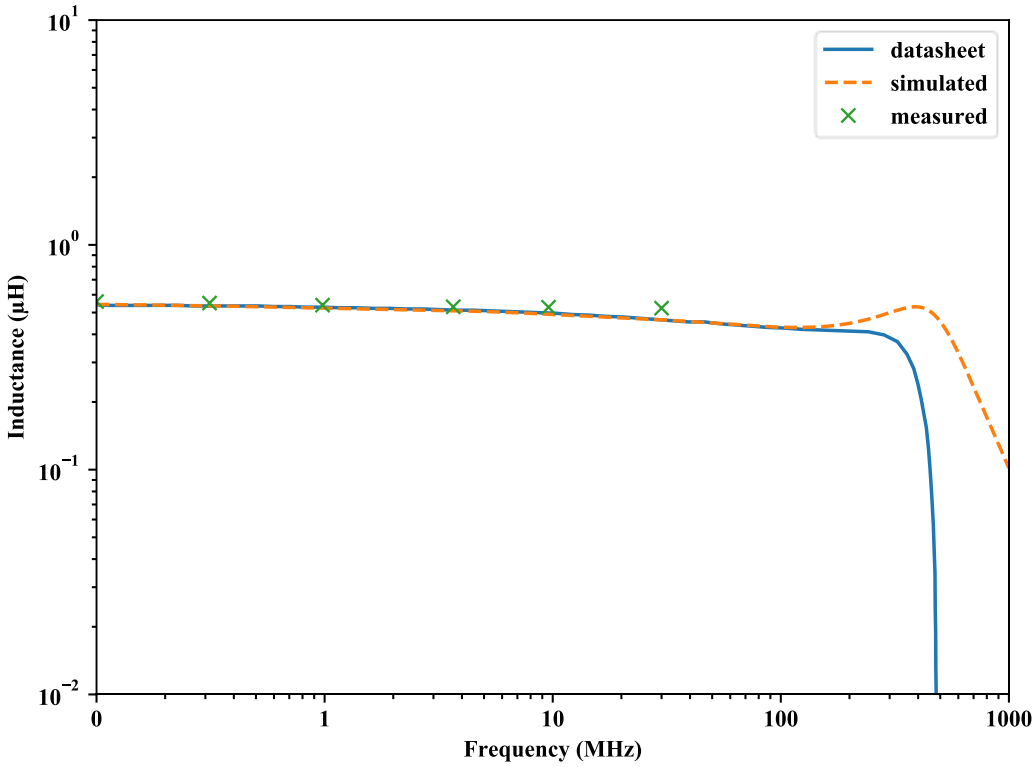

Figure 3.3.2: Plot comparing datasheet, simulated, and measured inductance as a function of frequency for the BRL3225TR51M inductor.

Considering the possible inaccuracies in the hardware measurements due to the impedance analyser being used near its maximum frequency limit of 32 MHz, and the divergence of the model and datasheet inductance values for frequencies above 120 MHz being outside of the 10 MHz to 100 MHz range of interest, it was decided that the BRL3225TR51M inductor model was acceptable to be used in the TIDA-01173 ToF camera light source simulation.

3.3.1.2 Current limiting switch - TPS2559

The TIDA-01173 light source uses the TPS2559 Precision Adjustable Current-Limited Power-Distribution Switch. There was no TINA-TI model available for the TPS2559, so the TPS2557 model, selected from the TINA-TI macro component

library, was used instead. The supporting circuitry was added into the TPS2557 circuit (Figure 3.3.3). The supporting circuitry was made up of ideal components.

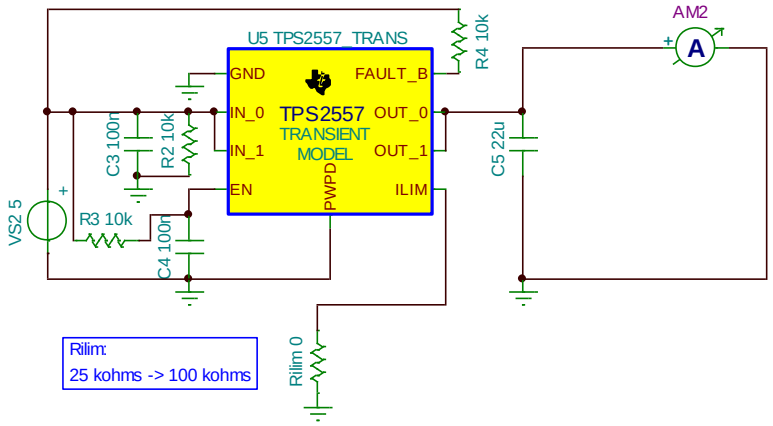

Figure 3.3.3: TINA-TI TPS2559 current limiter model confirmation circuit diagram.

A simulation was run with the current limit setting resister (RIlim) swept from 25 kΩ to 100 kΩ and the output limit current measured. The results from this simulation were plotted on the same plot as the Current-Limit vs RIlim plots from both the TPS2559 datasheet [63] and the TPS2557 datasheet [64] (Figure 3.3.4). The datasheets supplied the typical current limit vs RIlim curve as well as the maximum and minimum current limit vs RIlim curves. The datasheet curve for the TPS2559 had a narrower tolerance than the TPS2557, and the typical current limit for a given current limit setting resistor value was higher for the TPS2559 than the TPS2557.

As was expected, the simulated TPS2557 results consistently matched the typical curve from the TPS2557 datasheet. The simulated TPS2557 results matched the minimum typical current limit vs RIlim curve from the TPS2559 datasheet. So, as the TPS2557 model was used instead of the TPS2559 model, the current limit in the simulation will be expected to be lower for a given RIlim value than the real TIDA-01173 hardware results. It would have been preferable to use a TINA-TI model for the TPS2559, but as one was not available, this was not possible, and the closest linear current limiter model was used (TPS2557). The TPS2557 model could not be modified to match the TPS2559 because the TPS2557 model was encrypted.

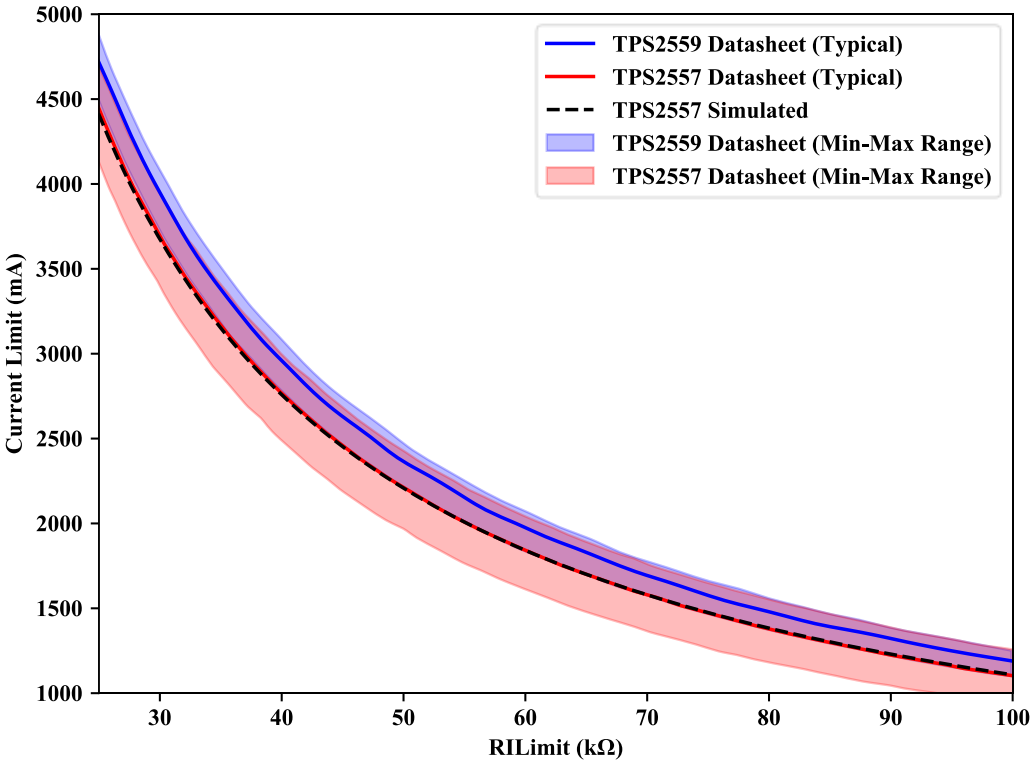

Figure 3.3.4: Plot comparing the linear current limiter Current-Limit vs $R_{(ILIM)}$ curves from the TPS2559 and TPS2557 datasheets to the simulated TPS2557 linear current limiter Current-Limit vs RIlim curve.

3.3.1.3 MOSFET models

The method described in [65] was used to verify the Shunt MOSFET - CSD16301Q2 and Series MOSFET - CSD17578Q3A models. The authors of [65] verified a MOSFET model by comparing three characteristic plots supplied in the MOSFET datasheet to ones produced in simulation. The plots they used to make the verification of the model were:

1. Drain-Source on state resistance (RDS(on)) plotted as a function of Drain-Current (IDS) at given Gate-Source voltages (VGS). The CSD16301Q2 datasheet only has RDS(on) vs VGS for ID = 4 A at given temperatures TC = 25°C and 125°C, so this plot was used instead.
2. Typical output characteristics, IDS plotted as a function of Drain-Source voltage (VDS) at given VGS, VDS vs IDS.
3. Typical transfer characteristics, VGS plotted as a function of IDS at given temperatures, VGS vs IDS.

For the verification, these plots are sourced from the Shunt MOSFET - CSD16301Q2 and Series MOSFET - CSD17578Q3A datasheets and equivalent graphs will be produced in simulation using the respective MOSFET models. The models should have been compared to real hardware measurements, however this was not done due the project's time constraints - significant time is required to produce a set of characterisation PCBs necessary to accommodate the MOSFET's surface mount packages.

3.3.1.3.1 Shunt MOSFET - CSD16301Q2

The CSD16301Q2 is an N-channel power MOSFET made by Texas Instruments. The CSD16301Q2 model was sourced from the Texas Instruments website[1].

3.3.1.3.1.1 RDS(on) vs VGS

The RDS(on) vs VGS plot collected and digitised from the CSD16301Q2 datasheet [66]. The RDS(on) vs VGS simulation plot was generated in TIDA-TI using the circuit (Figure 3.3.5): a constant current of 4 A was run through the drain pin of the CSD16301Q2 MOSFET model and a DC analysis was run to sweep VGS from 0 V to 10 V.

A circuit was constructed in TINA-TI to measure the drain-source resistance of the MOSFET as a function of gate-source voltage in simulation (Figure 3.3.5). The simulation circuit comprises of a voltage source (VGS) connected between the CSD16301Q2 MOSFET's gate pin and ground, and a current source (IS) connected between the CSD16301Q2 MOSFET's drain and source pins set the drain source current to 4 A to match the IDS used in the datasheet RDS(on) vs VGS plot. The MOSFET's drain voltage and source current (VDS and IS) were measured to calculate the MOSFET's drain source resistance (RDS) in a post process by dividing VDS by IS. A DC transfer analysis was configured to sweep VGS from 0 V to 10 V. When the plot was created, RDS(on) was plotted only for VGS from 2 V to 10 V as this was all that the datasheet showed. The simulation was run for temperatures of 25°C and 125°C to match the plots from the CSD16301Q2 datasheet.

[1] http://www.ti.com/product/CSD16301Q2/toolssoftware, accessed 25th Feb. 2020.

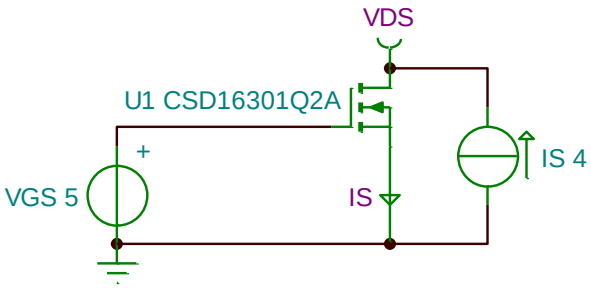

Figure 3.3.5: TINA-TI circuit diagram for the RDS(on) vs VGS simulation.

The plot (Figure 3.3.6) shows that there is a difference between the datasheet and simulation RDS(on) vs VGS curves. By observing this plot, it appears that the simulated curves (dashed lines) are shifted down and to the right compared to the datasheet curves (solid lines). The MOSFET driver sets the CSD16301Q2 shunt MOSFET VGS voltage to 3.3 V in the on state, so by drawing a vertical line where VGS is 3.3 V on the RDS vs VGS plot (Figure 3.3.6), it can be seen that it intersects the simulated and datasheet curves almost at the point where there is no difference between them. This is good because it means that the simulation model of the CSD16301Q2 MOSFET matches the datasheet where it needs to for the simulation of the TIDA-01173 ToF camera light source. So in regards to the RDS(on) vs VGS properties, the CSD16301Q2 model is acceptable.

The percentage error between the simulated and datasheet RDS(on) values, at a VGS of 3.3 V, is -3.7% for a temperature of 25°C and -1.7% for a temperature of 125°C. The minimum and maximum vs typical values in the datasheet, as an indicator that tolerances of physical devices are much wider than these errors in simulation, for example, the CSD16301Q2 datasheet specifies a RDS(on) range of 27 mΩ to 34 mΩ for VGS of 3 V and IS of 4 A. This shows that the component to component variations is quite wide, so the simulation does not need to be exact.

The reason for this difference between the simulation model and datasheet may have been because the manufacturer of the CSD16301Q2 MOSFET intended VGS to be near 3.3 V when the MOSFET model is used in switching applications. To help find the source of the differences, it would have been helpful to compare these

to measured characteristics. However, time constraints meant that it was not possible in the scope of this project.

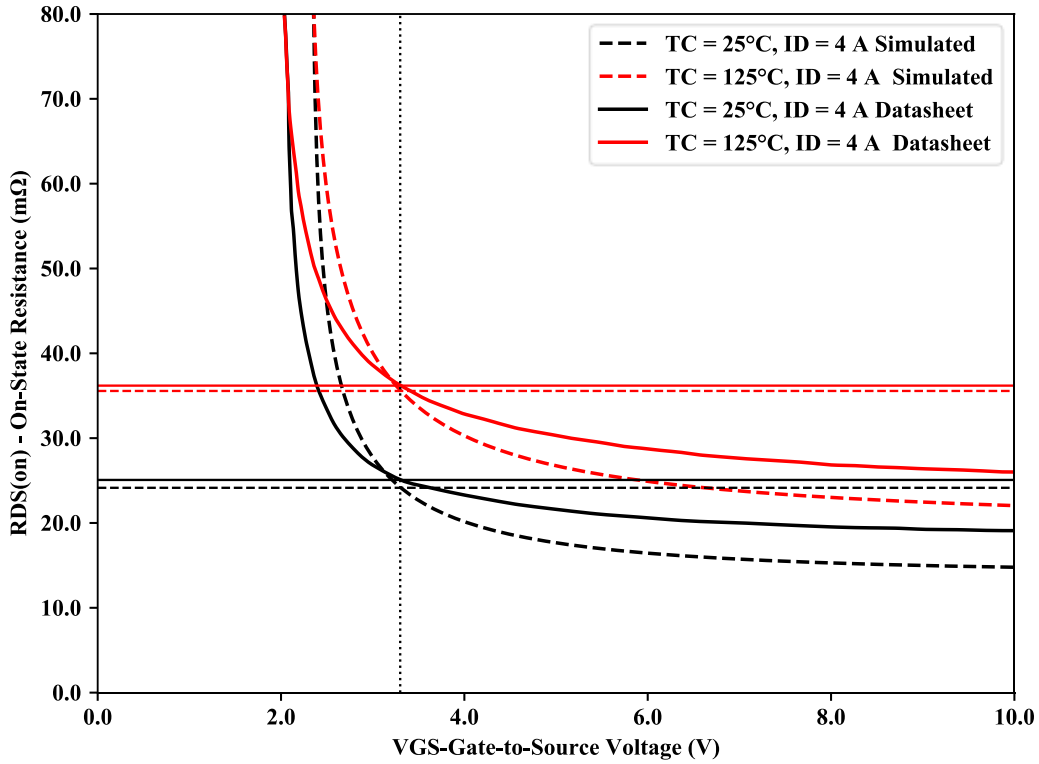

Figure 3.3.6: Plot comparing the CSD16301Q2 MOSFET RDS(on) vs VGS plots from the datasheet and simulation.

3.3.1.3.1.2 Typical output characteristics, VDS vs IDS

The circuit shown in Figure 3.3.7, was created in TINA-TI to obtain the VDS vs IDS curves for the CSD16301Q2 simulation model. A DC analysis was configured to sweep VDS from 0 to 0.5 V for VGS of 3, 4.5, and 8 V and measure IDS at a temperature of 25°C. The datasheet VDS vs IDS plot was digitised and plotted along with the simulation data (Figure 3.3.8).

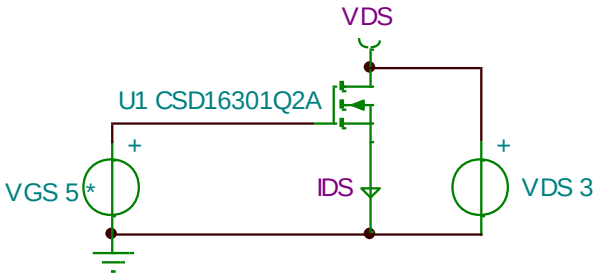

Figure 3.3.7: TINA-TI circuit diagram for the CSD16301Q2 typical output characteristics, VDS vs IDS simulation.

The CSD16301Q2 VDS vs IDS plot (Figure 3.3.8) shows that there is a difference between typical output characteristics produced by the CSD16301Q2 simulation model and the one presented in its datasheet. The IDS for a given VDS is consistently higher for the simulation model than the datasheet. However, the typical output characteristic curve of the simulation model when VGS is 3 V, is much closer to the datasheet than it is when VGS is 4.5 or 8 V. This is similar to the result of the RDS(on) vs VGS datasheet simulation comparison, where the smallest difference between the datasheet and simulation was also near a VGS of 3 V. The difference between the simulated and datasheet plots reduces for smaller IDS and VDS. The expected maximum IDS in the TIDA-01173 is near 2 A. At a VGS of 3 V, this corresponds to a simulated VDS of 0.05 V and a datasheet VDS of 0.08 V. This difference may result in a higher power dissipation in the TIDA-01173 light source simulation when the shunt MOSFET is on than is measured, if the datasheet is a good representation of the physical component. However, the component to component variation of the VDS vs IDS characteristics for the CSD16301Q2 MOSFET may be greater than the difference shown in the simulated and datasheet plots, but the component to component variation is not provided in the CSD16301Q2 datasheet.

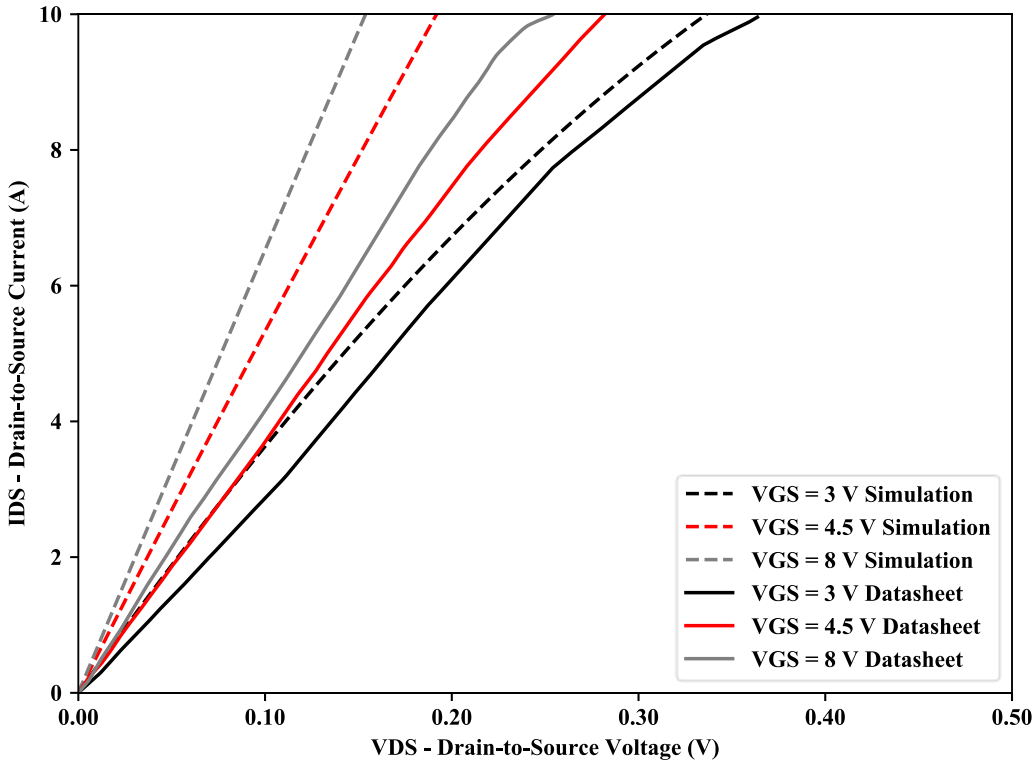

Figure 3.3.8: CSD16301Q2 shunt switch MOSFET Typical output characteristics, VDS vs IDS at 25°C.

3.3.1.3.1.3 Typical transfer characteristics, VGS vs IDS

The circuit shown in Figure 3.3.9 was created in TINA-TI. A DC analysis was configured to sweep VGS from 1.0 to 2.5 V and measure IDS for temperatures of 25, 125, and -55°C. The simulated VGS vs IDS curve was plotted along with the digitised VGS vs IDS plot from the CSD16301Q2 datasheet.

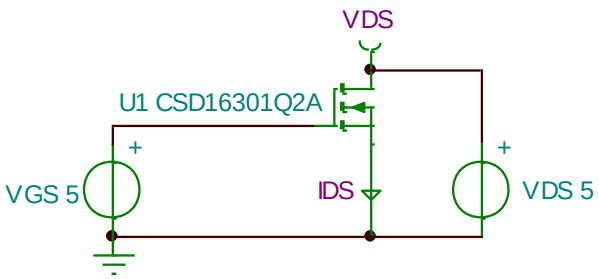

Figure 3.3.9: TINA-TI circuit diagram for the CSD16301Q2 typical output characteristics, VGS vs IDS simulation.

The VGS vs IDS plot (Figure 3.3.10) show that typical transfer characteristic curves of the MOSFET produced in simulation are different to those given in the datasheet. The simulated curves appear shifted to the right compared to the datasheet curves. This increase in VGS-threshold by about 0.3V, so the simulation may underestimate the drain source current of the CSD16301Q2 shunt switching MOSFET, therefore reducing the electrical to optical power efficiency of the TIDA-01173 calculated by the simulation.

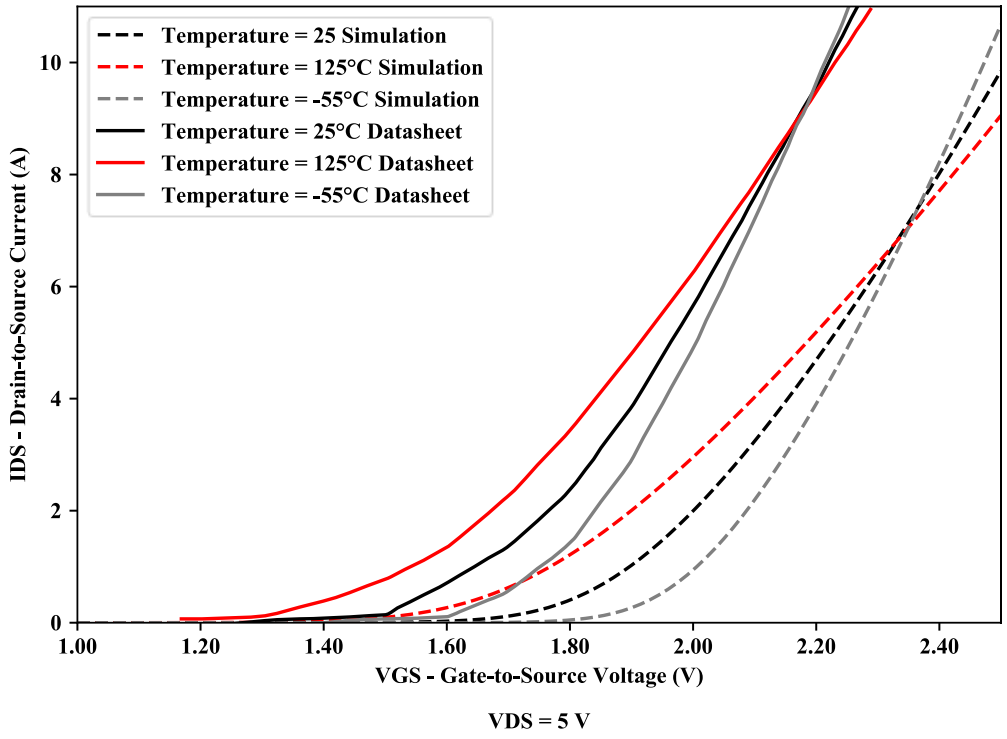

Figure 3.3.10: CSD16301Q2 shunt switch MOSFET typical transfer characteristics, VGS vs IDS.

3.3.1.3.2 Series MOSFET - CSD17578Q3A

Like the CSD16301Q2, the CSD17578Q3A is also an N-channel power MOSFET made by Texas Instruments. The same plots were produced using the same method as used for the CSD17578Q3A series MOSFET as was for the CSD16301Q2 shunt MOSFET. The results are shown in Figure 3.3.12, Figure 3.3.14, and Figure 3.3.16. None of the simulation curves in these three plots matches the datasheet curves.

The gate of the CSD17578Q3A series MOSFET is to be driven with a 0 to 5 V square wave signal and is designed to enable and disable the laser driver circuit by switching the laser driver circuit current on and off. The percentage error between the simulated and datasheet RDS(on) vs VGS curve (Figure 3.3.12) at VGS of 5 V is small: 5.4% for a temperature of 25°C and 4.6% for a temperature of 125°C. However, the RDS(on) vs VGS curves are at an IDS of 10 A, and the expected current to be switched by the MOSFET is around 2 A, so this comparison may not be valid for the TIDA-01173 simulation. The datasheet does not provide the RDS(on) vs VGS curve at an IDS of 2 A.

The difference between the simulation model and datasheet IDS vs VDS plots (Figure 3.3.14) at an IDS of 2A, as will be used in the TIDA-01173 simulation, is very small, so this part of the CSD16301Q2 MOSFET model is acceptable.

The CSD16301Q2 MOSFET IDS vs VGS plot (Figure 3.3.16) is for a VDS of 5 V which is much higher than is expected in the TIDA-01173, however, a IDS vs VGS plot at a lower VDS is not provided in the CSD16301Q2 datasheet. Assuming this plot is representative, the difference between the MOSFET IDS values gets smaller as VGS approaches the 5 V. A VGS of 5 V is the expected gate voltage of the CSD16301Q2 MOSFET in the TIDA-01173 light source, so the difference between the measured and simulated power results should be impacted minimally. However, IDS at 5 V is not provided in the datasheet IDS vs VGS plot, so the difference between the TIDA-01173 measured and simulated results caused by the CSD16301Q2 MOSFET model cannot be determined using the datasheet.

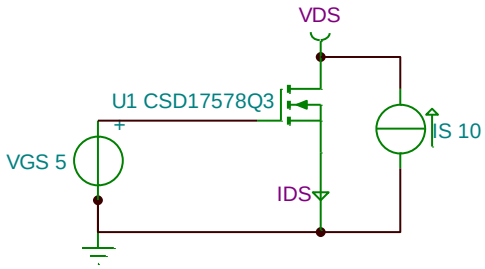

Figure 3.3.11: RDS(on) vs VGS circuit.

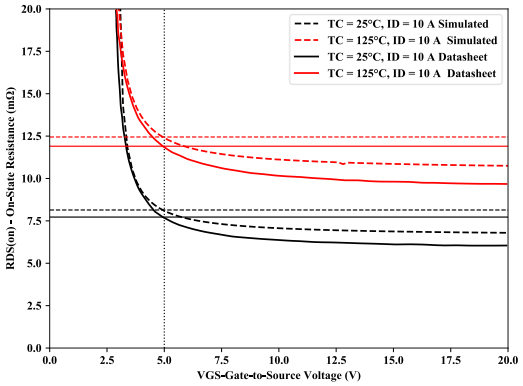

Figure 3.3.12: CSD17578Q3A RDS(on) vs VGS.

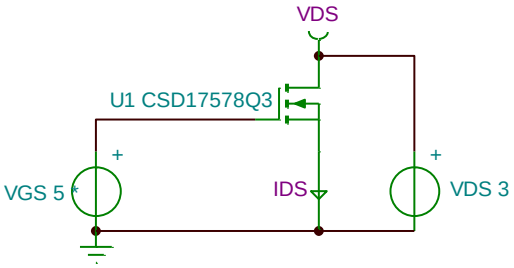

Figure 3.3.13: VDS vs IDS circuit.

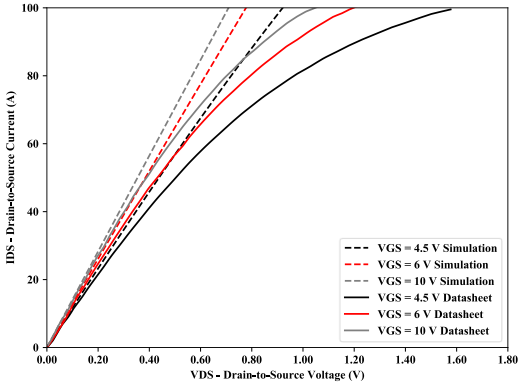

Figure 3.3.14: CSD17578Q3A VDS vs IDS.

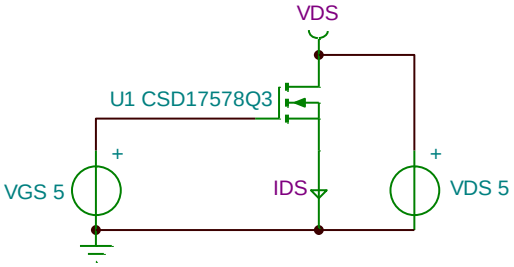

Figure 3.3.15: VGS vs IDS circuit.

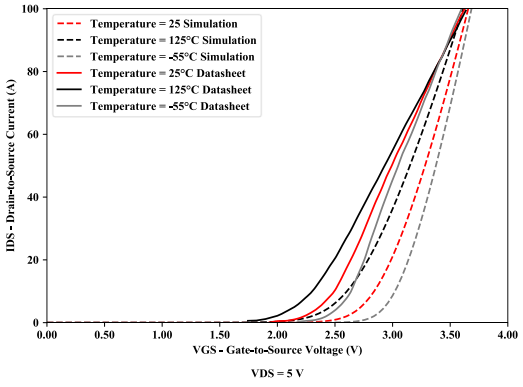

Figure 3.3.16: CSD17578Q3A VGS vs IDS.

The unexpected finding that the MOSFET models provided by Texas Instruments do not match the characteristic curves of the datasheets means that the TIDA-01173 light source simulation cannot be assumed to be representative of the physical TIDA-01173 light source. Without access to the physical MOSFETs to compare with the simulation models, the full TIDA-01173 simulation needs to be compared to real measurements to confirm that it represents the real TIDA-01173 light source and can be used to develop design improvements.

3.3.1.4 Laser diode – 22045498

The specifications supplied in the laser diode datasheets were all based on the assumption that the diode operates at a temperature of 25°C. The ToF light sources will usually operate at temperatures substantially higher than 25°C. So, it was necessary to create a model for the laser diode based on real measurements. There were no 22045498 laser diodes available, however the laser diodes used for the Kea light source, the BOB850T1000, were available. Chronoptics claimed that the laser diodes used in the Kea light source had practically the same specifications as the ones used in the TIDA-01173 (22045498), so the BOB850T1000 laser diode could be substituted for the 22045498 in the simulations of the TIDA-01173 light source.

The BOB850T1000 was sourced from Alibaba.com[2] and the only datasheet that could be found was the product description on the product's Alibaba page. The table of parameters for the BOB850T1000 extracted from the product description can be seen in Appendix A, Table A.1. The datasheet for the 22045498 contained more detail than the BOB850T1000 laser diode. The parameter table for the 22045498 can also be seen in Appendix A, Table A.2. The parameter tables from the BOB850T1000 and 22045498 laser diode datasheets did not contain all of the same parameters, Table 3.3.1 contains the subset of parameters that were specified in both datasheets. By comparing the parameter values in this table, it was determined that the claim made by Chronoptics that the laser diodes used in the Kea light source (BOB850T1000) has the same specifications as the ones used in the TIDA-01173 (22045498) was true apart from the operating voltage. The BOB850T1000 had a

[2] https://laserpointer.en.alibaba.com/product/60539297671-803473670/850nm_1000mw_laser_diode_TO_18_infrared_illumination.html Accessed: 2nd of January 2020.

typical operating voltage of 2.5V while the 22045498 had a typical operating voltage of 1.8 V and a maximum of 2.0 V. This may result in a slightly higher voltage swing at the node between the inductor, laser diodes, and shunt switching MOSFET in the TIDA-01173 light source simulation than would occur in the real TIDA-01173.

Table 3.3.1: Comparison between the datasheet parameters for the 22045498 and BOB850T1000 laser diodes.

Parameter		**22045498**			**BOB850T1000**
		Min.	Typ.	Max.	Typ.
Electrical	Optical Power CW	-	1 W		1 W
	Operating Voltage	-	2.0 V		2.5 V
	Operating Current	1.0 A	1.4 A		1.3 A
	Threshold Current	-	0.5 A		0.2 A
	Slope Efficiency	-			1.1 W/A
Mechanical/ Thermal	Operating Temperature Range	5°C	65°C		10°C to 50°C
	Non-operating Storage Temperature	- 40°C	85°C		-20°C to +80°C
Optical Performance	Wavelength Shift Over Temperature		-		~0.3 nm/°C
	Beam Divergence - fast axis	14°	21°		35°
	Beam Divergence - slow axis	6°C	7°C	9°C	7.5°

These laser diodes are suitably similar, so the BOB850T1000 laser diode model, to be created in Chapter 4, was used in the TIDA-01173 light source simulations in place of the 22045498 laser diode.

3.4 Assembling ToF camera light source simulations in TINA-TI

3.4.1 TIDA-01173 light source simulation

The TIDA-01173 and light source circuit was drawn into TINA-TI using the component models that were gathered (Figure 3.4.1). The passive supporting circuitry components such as resistors and capacitors were modelled using ideal component models. The TPL0102-100PWR digital potentiometer was modelled using the potentiometer model that is built-in to TINA-TI. The TPL0102-100PWR

datasheet states that the digital potentiometer wiper to low side resistance value (R_{WL}) is modelled with,

$$R_{WL} = R_{TOT}\frac{D}{256}, \tag{3.4.1}$$

where, R_{TOT} is the resistance of the potentiometer from the high side to low side terminals, and D is the digital value written to the wiper setting register in the digital potentiometer chip [67]. This equation was used when setting the potentiometer value in the TIDA-01173 light source simulation.

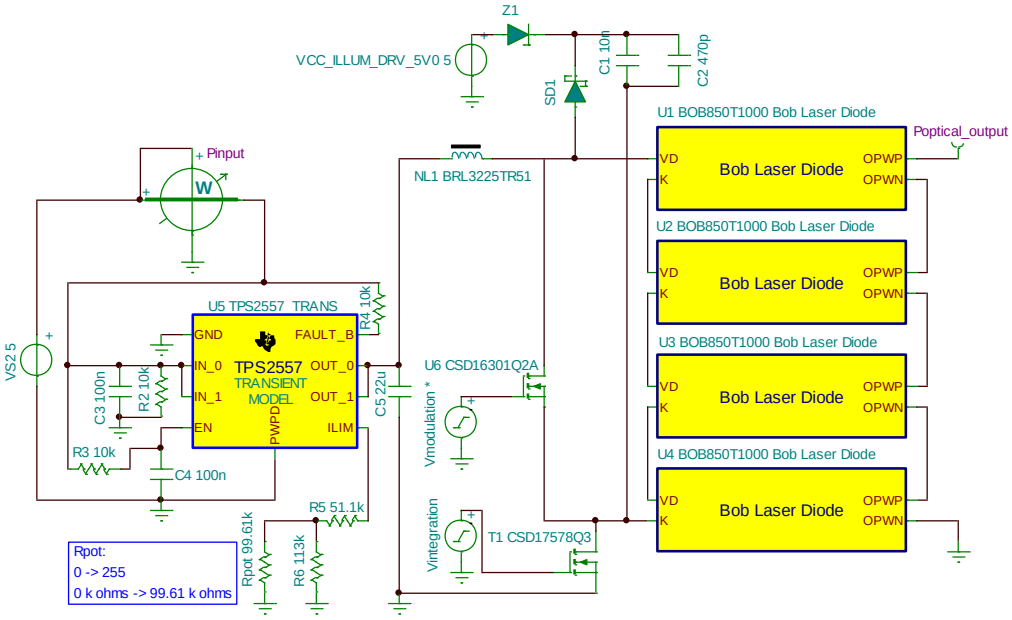

Figure 3.4.1: Circuit diagram of the TIDA-01173 light source modelled for simulation in the TINA-TI software.

3.4.2 Kea light source simulation

In addition to the TIDA-01173 light source circuit, the Kea light source circuit was also drawn into TINA-TI Figure 3.4.2. This simulation will be used to compare with the TIDA-01173 light source to determine the difference in efficiency between the series and shunt switching ToF laser driver topologies.

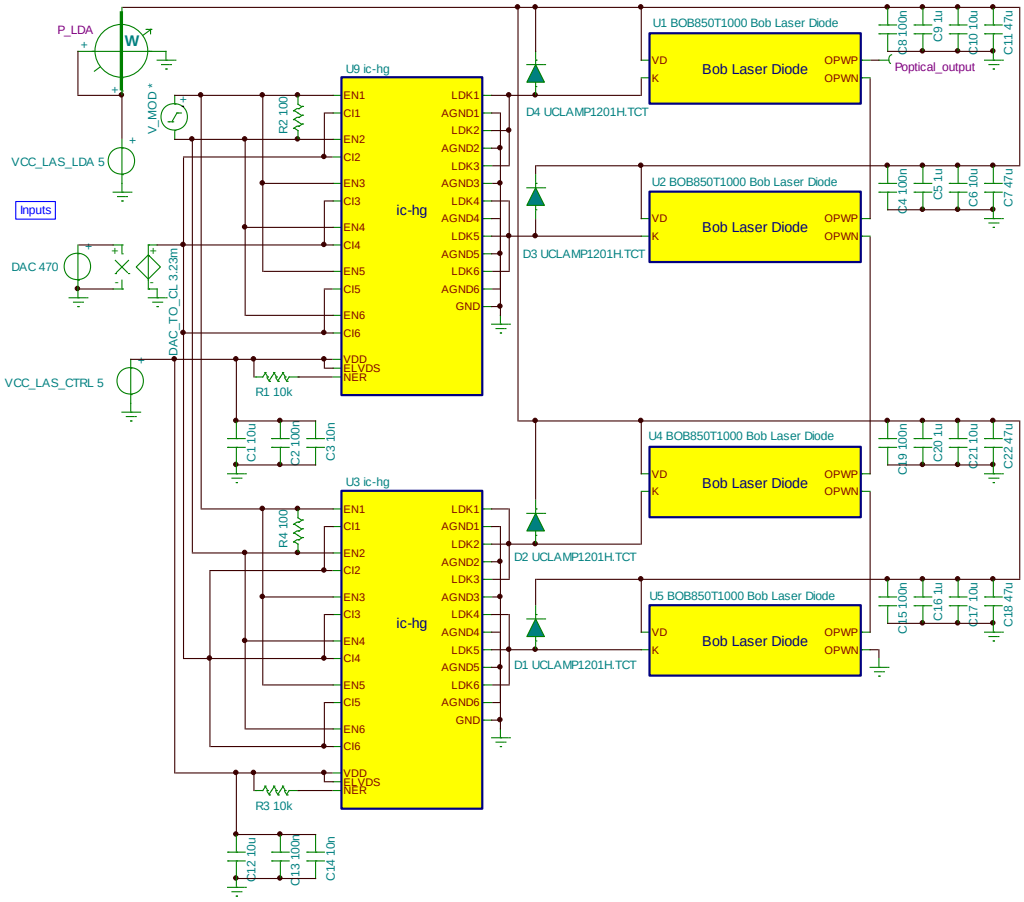

Figure 3.4.2: Circuit diagram of the Kea light source modelled for simulation in the TINA-TI software.

The SPICE model for the iC-HG [52] series switching topology laser driver IC, used in the Kea light source, was sourced from the manufacture's (iC-Haus, Bodenheim, Germany) website [68]. The SPICE model for clamp ESD protection diode, the uCLAMP1201H, was sourced from its datasheet [69].The parameters for the diode model are shown in Table 3.4.1.

Table 3.4.1: uCLAMP1201H SPICE parameters [69].

Parameter	Unit	Value
IS	A	1.48E-14
BV	V	15.33
VJ	V	0.723
RS	Ω	0.772
IBV	A	1.0E-3
CJO	F	52E-12
TT	s	2.541E-9
M	-	0.268
N	-	1.1
EG	eV	1.11

A circuit model for the BOB850T1000 laser diode was created by characterising the laser diode. The characterisation of the BOB850T1000 laser diode was a lengthy process and will be described in the next chapter (Chapter 4).

Chapter 4

Laser diode modelling

A SPICE model for the BOB850T1000 laser diode could not be found, so the diode had to be characterised, and a SPICE model created for it.

4.1 Laser Diode Electrical Properties

Laser diodes behave electrically like the usual forward biased diode [70, Ch. 11], so the electrical characteristics of a laser diode can be modelled in SPICE using the standard diode model with the appropriate parameters. The parameters can be found in the diode's datasheet, or by measurement. The datasheet for the BOB850T1000 laser diode (Appendix A, Table A.1) is of poor quality and unreliable as it could only be found on the online retailer website Alibaba.com[3]. Therefore, it was best to extract the laser diode parameters using measurements, then produce a SPICE model of the laser diode. The SPICE diode parameters to be extracted from the BOB850T1000 are shown in Table 4.1.1. A transient model of the laser diode is required, so both the SPICE DC and Charge storage parameters were extracted.

[3] https://laserpointer.en.alibaba.com/product/60539297671-803473670/850nm_1000mw_laser_diode_TO_18_infrared_illumination.html, accessed: 5/02/2020

Table 4.1.1: SPICE diode model parameters [71].

General Characteristics	Symbol	Name	Parameter	Units
DC	I_S	IS	saturation current	A
	R_S	RS	ohmic resistance	
	n	N	emission coefficient	-
Charge Storage		TT	transit-time	s
		CJO	zero-bias junction capacitance	F
		VJ	junction potential	V
		M	grading coefficient	-

The laser diode's optical parameters cannot be modelled using the standard built-in SPICE diode model, but to get a value of the optical output power, it was necessary to have them modelled in the simulation. To solve this problem, the optical properties were modelled using a SPICE sub-circuit and an arbitrary voltage source component. This will be shown in the netlist for the BOB850T1000 laser diode SPICE model shown in Code 4.3.4 later in this chapter. The optical properties to be modelled are Slope efficiency and lasing threshold current.

4.2 Laser safety considerations

The laser diodes used in the experiments are class 3B in the IEC 60825-1 standard, as the light they produce is not visible to the naked eye (near infrared wavelength of 850 nm) and cannot burn the skin. So, for all experiments involving the use of laser diodes, laser hazard control measures (engineering controls, administrative controls, and personal protective equipment) must be taken. Laser safety training and authorisation was gained before the laser testing was started. This meant that laser safety principles were studied, and an examination was passed, an eye exam was performed by an optometrist to get ocular history, visual acuity, macular function, colour vision responses, and ocular fundus baselines. A Standard Operating Procedure (SOP) was produced for the experiment setup, and a Hazard Evaluation was done. The laboratory's Laser Safety Officer (LSO) inspected the laser equipment, SOP, and the hazard evaluation, before testing was started. The

laser tests are all conducted inside a light proof optical enclosure (Figure 4.2.1). The laboratory used for the laser tests is equipped with laser safety signs, laser status warning lights (Figure 4.2.4), light locked entryway (Figure 4.2.3), an interlock system that is configured to disable the lasers when the laboratory door was opened, and the laboratory is laid out in such a way that there was no direct line of sight from the entrance door to the laser experiment. Laser safety glasses (with OD 6+ at 850 nm) (Figure 4.2.2) are worn by everyone in the laboratory when the lasers are being operated.

Figure 4.2.1: Light proof optical enclosure.

Figure 4.2.2: Laser safety glasses.

Figure 4.2.3: Photo of the entrance to optics laboratory inside the light lock.

Figure 4.2.4: Laser status warning lights.

4.3 Electrical laser diode parameter extraction

There are twelve electrical parameters that need to be extracted from the laser diode to make the SPICE model: Reverse Saturation Current (IS), Ideality Factor (N), Series Resistance (RS), Transit-Time (TT), Zero-Bias Junction Capacitance (CJO), Junction Potential (VJ), and Grading Coefficient (M).

The DC properties: RS, IS, and N are all found from the laser diode's current vs voltage (IV) curve. The AC (transient) properties: CJO, VJ, and M are found using an impedance analyser, and TT is found from measuring the transient response of the laser diode.

4.3.1 Laser diode IV curve – RS, IS, and N

4.3.1.1 Method

To extract the RS, IS, and N diode parameters from the laser diode, a plot of the voltage across the diode as a function of the diode forward current is to be measured. The equipment is set up is shown in Figure 4.3.1.

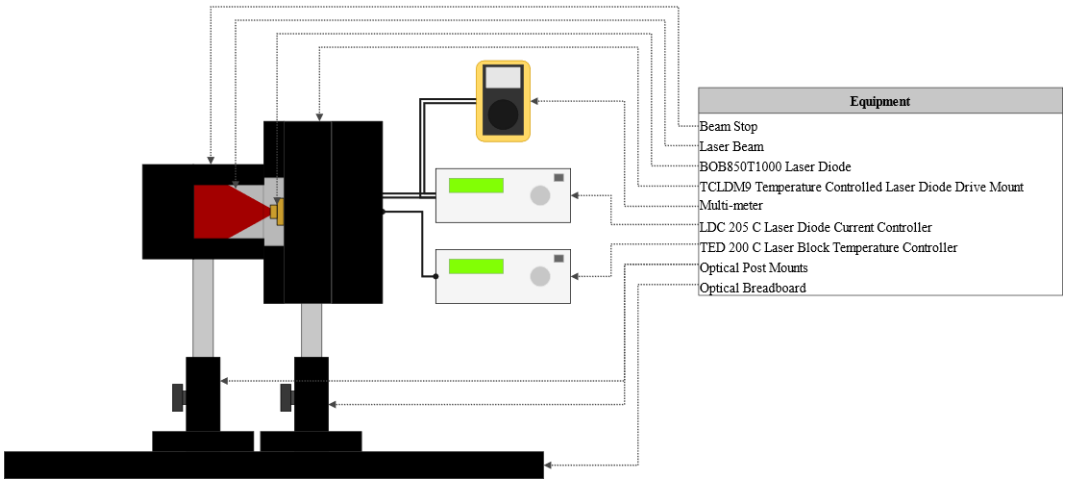

Figure 4.3.1: Diagram of IV curve experiment setup.

This experiment is set up inside the light proof optical enclosure for eye safety. The BOB850T1000 laser diode is mounted in the TCLDM9 temperature-controlled laser diode mount (Thorlabs, Newton, New Jersey) with the pins oriented as shown in Figure 4.3.2. The beam stop is placed in front of the laser diode to safely terminate the laser beam. The TED 200 C temperature controller (Thorlabs,

Newton, New Jersey) and LDC 205 C laser diode controller (Thorlabs, Newton, New Jersey) are both connected to the temperature-controlled laser diode mount.

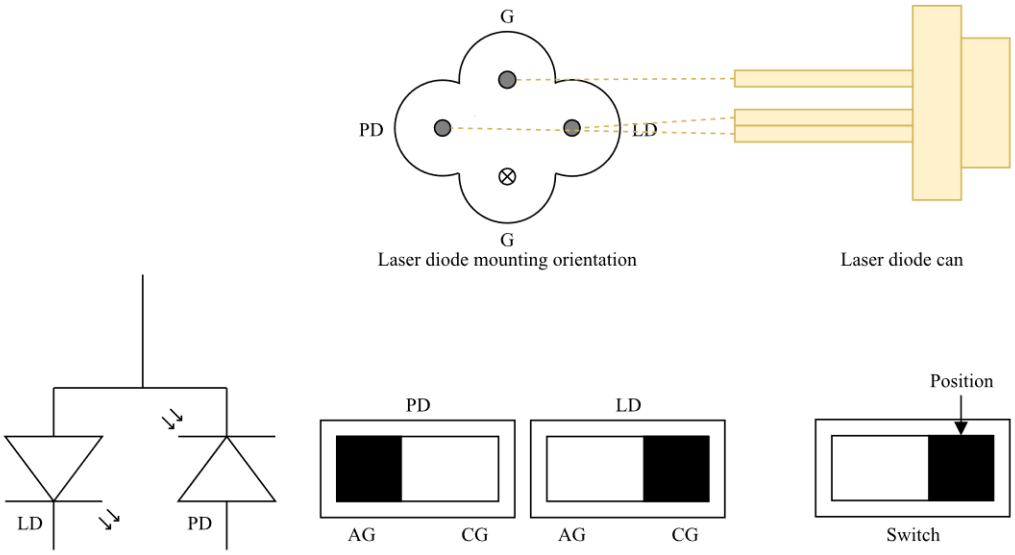

Figure 4.3.2: Thorlabs TCLDM9 mounting orientation and switch settings used for the BOB850T1000 laser diode: LD = AG, PD = CG [72].

The connection between the laser diode current controller and the laser diode mount was custom made from a ribbon cable and DB-9 connectors to expose access to the voltage across the laser diode (Figure 4.3.3). A Fluke 175 True-RMS (root mean squared) digital multimeter (Fluke, Everett, Washington) with a DC voltage measurement accuracy of ±(0.15% of reading + 2 counts) [73], set to measure voltage, is connected to the exposed laser diode wires.

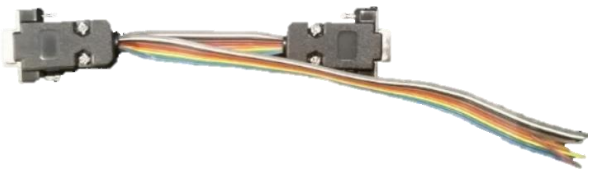

Figure 4.3.3: Custom made laser diode current controller to temperature-controlled laser diode mount cable.

The TCLDM9 temperature-controlled laser diode mount is a bias-tee type of laser modulation driver, but only the bias current input is used. The modulation input is required for the laser diode characterisation.

The temperature controller is set to 25°C and switched on. The laser diode current controller is set to 0 mA and switched on. Once the temperature had settled at 25°C, the voltage measured by the multi-meter is read and recorded in a spreadsheet against the current setting. The current settings are set roughly to the desired target setting and the actual laser diode current read from the laser diode current controller. Replicant measurement of the current settings are taken over the range of 0 mA to 500 mA (LDC 205 C laser driver's maximum current setting).

4.3.1.2 Results

The laser diode current is plotted against the laser diode voltage to form the IV curve of the BOB850T1000 laser diode (Figure 4.3.4).

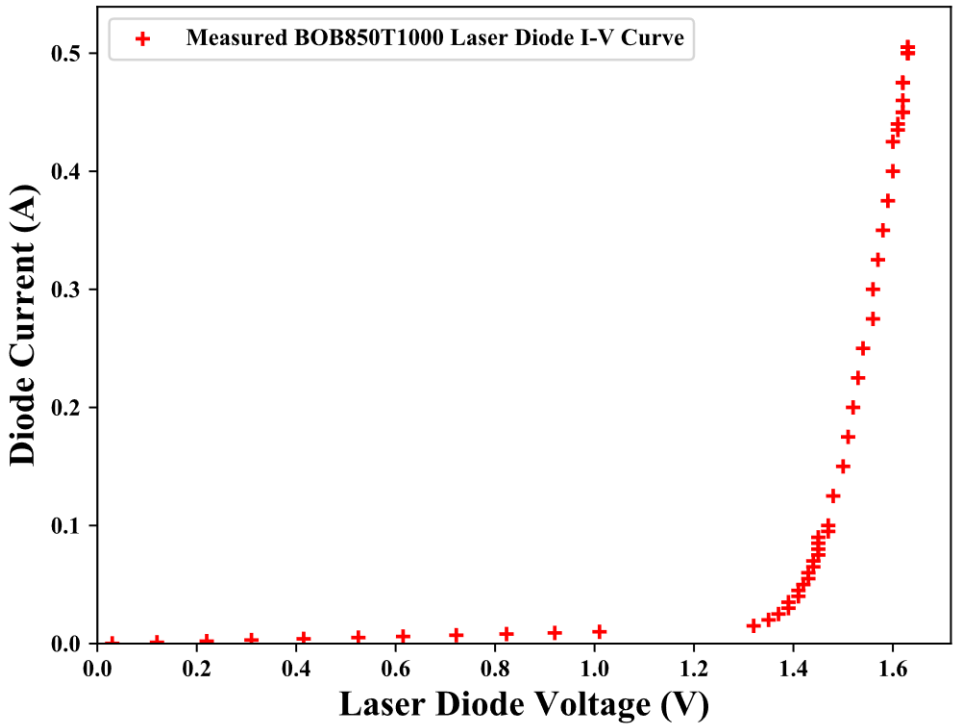

Figure 4.3.4: Measured IV curve for the BOB850T1000 laser diode.

The measured BOB850T1000 laser diode IV curve has the expected shape that is modelled by the Shockley ideal diode equation [74],

$$I_d = I_s \cdot \left(e^{\left(\frac{V_d}{nV_t}\right)} - 1 \right) \tag{4.3.1}$$

$$I_d \approx I_S \cdot \left(e^{\left(\frac{V_d}{nV_t}\right)} \right), \text{when } V_d \gg V_t \tag{4.3.2}$$

where, I_d is the current passing through the diode, I_s is the reverse saturation current, V_d is the voltage across the diode, V_t is the thermal voltage with an approximate value of 0.0259 V at 300 K, and n is the ideality factor [75].

The diode IV curve (Figure 4.3.4) must be linearised to extract the diode DC SPICE parameters IS, N, and RS. Taking the natural logarithm of both sides of the Shockley ideal diode equation (4.3.2) and rearranging, a linear relationship is formed,

$$\ln(I_d) = \frac{1}{nV_t} V_d + \ln(I_S), \text{when } V_d \gg V_t. \tag{4.3.3}$$

It can be seen that a linear plot can be formed if the natural logarithm of the diode current is plotted against the diode voltage to form a linear plot (Figure 4.3.5).

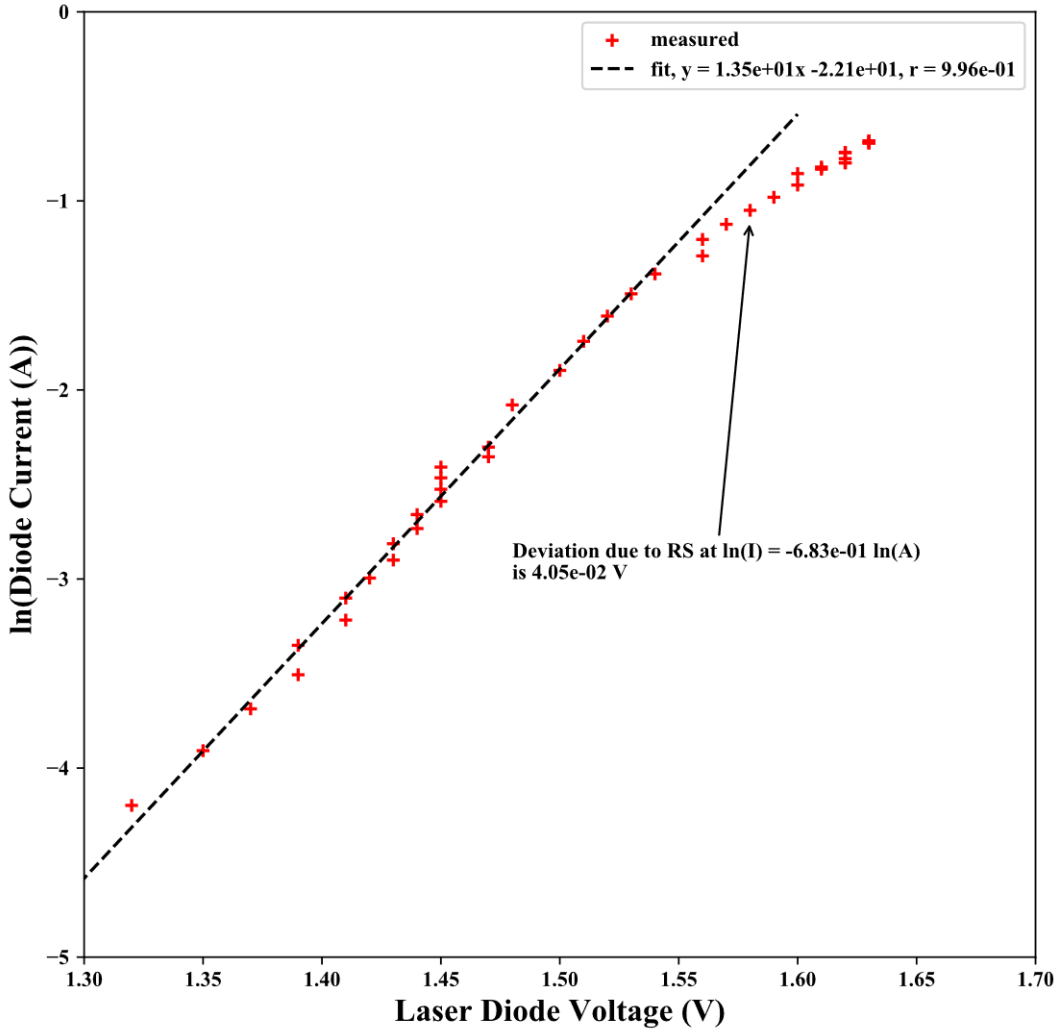

Figure 4.3.5: Measured ln(I) vs V curve for the BOB850T1000 laser diode.

Figure 4.3.5 is linear in the region where the diode voltage is greater than 1.30 V and less than 1.55 V. The r value of the fitted line is 0.996 indicating that the ln(I) vs V line has a strong linear correlation.

The procedure described in [76, Sec. 2.8.1] is used to extract the diode DC SPICE parameters IS, N, and RS. To extract these parameters, the following properties of the linearised IV curve are required, m, c, ΔV_{R_s}, $ln(I_{R_s})$, and I_{R_s}. m is the slope of the fitted line, c is the y-axis intercept of the fitted line, ΔV_{R_s}, is the deviation from the fitted line to the curve where the linearised IV curve (Figure 4.3.5) begins to diverge from the fitted line (just above the laser diode voltage of 1.55 V), $ln(I_{R_s})$ is the natural logarithm of the current at the point where ΔV_{R_s} is

taken, and I_{R_s} is the current at this point. These properties with their corresponding values taken from the linearised IV curve (Figure 4.3.5) are listed in Table 4.3.1.

Table 4.3.1: Linearised IV curve (Figure 4.3.5) BOB850T1000 laser diode properties.

Ln(I) vs V BOB850T1000 Curve Properties	**Values**
$\boldsymbol{m}$	13.5 ln(A)/V
$\boldsymbol{c}$	-22.1 A
$\boldsymbol{\Delta V_{R_s}}$	0.0405 V
$\boldsymbol{ln(I_{R_s})}$	-0.683 ln(A)
$\boldsymbol{I_{R_s}}$	0.505 A

The slope of the linearised IV curve (Figure 4.3.5) fitted line, m, corresponds to $\frac{1}{n \cdot V_t}$ in the linearised Shockley ideal diode equation (3.4.1), so the ideality factor (n) is found using the formula,

$$n = \frac{1}{m \cdot V_t}. \tag{4.3.4}$$

where, n is the diode ideality factor, m is the slope of the fitted line of the linearised diode IV curve (Figure 4.3.5), and V_t is the thermal voltage at room temperature.

The y-axis intercept of the fitted line, c, corresponds to $\ln(I_S)$, so the diode's reverse saturation current is found using,

$$I_S = e^c. \tag{4.3.5}$$

R_s is found by taking the difference in voltage between the fitted line and the measured datapoints where the fitted line deviates from the data points at voltages above about 1.55 V, ΔV_{R_s}, then dividing by the measured current at that point, I_{R_s},

$$R_s = \frac{\Delta V_{R_S}}{I_{R_S}},\ \Delta V_{R_s} = V_{Data} - V_{Fitted\ Line}. \tag{4.3.6}$$

Table 4.3.2 shows the evaluation of the IS, N, and Rs diode parameters.

Table 4.3.2: Extracted BOB850T1000 ID, N, and RS properties

SPICE DC Diode Parameters	**Values**
IS	2.53E-10 A
N	2.87
RS	0.0802 Ω

The extracted DC SPICE parameters were added to a standard SPICE diode model shown in Code 4.3.1:

```
.model BOB850T1000 D(IS=2.53E-10  N=2.87 RS=0.0802)
```

Code 4.3.1: Electrical SPICE parameters extracted from the BOB850T1000 IS, N, and RS in the standard SPICE diode model.

An IV diode curve is plotted using this model to compare the measured IV curve to the Simulated one. A calculated IV curve is also generated using the Shockley ideal diode equation (4.3.7) modified to incorporate the diode's ohmic resistance (RS, R_s),

$$I = I_S\left(e^{\left(\frac{V_d-(I_dR_s)}{nV_t}\right)} - 1\right) \tag{4.3.7}$$

$$\Longrightarrow V_d = nV_t\left(ln\left(\frac{I_d}{I_S} + 1\right)\right) + I_dR_s, \tag{4.3.8}$$

Figure 4.3.6 shows the plot comparing the measured, calculated, and simulated BOB850T1000 IV curve.

The calculated and simulated IV curves (Figure 4.3.6) were the same, showing that the SPICE model uses the Shockley ideal diode equation (4.3.1). The measured IV curve matched the simulated and calculated curves closely. The most obvious difference between the measured IV curve and simulated is between laser diode voltages of 0.25 and 1.00 V, where the diode current deviates from the simulation curve. This is only a small difference and at a diode voltage that is below the expected drive levels anticipated in the ToF light sources.

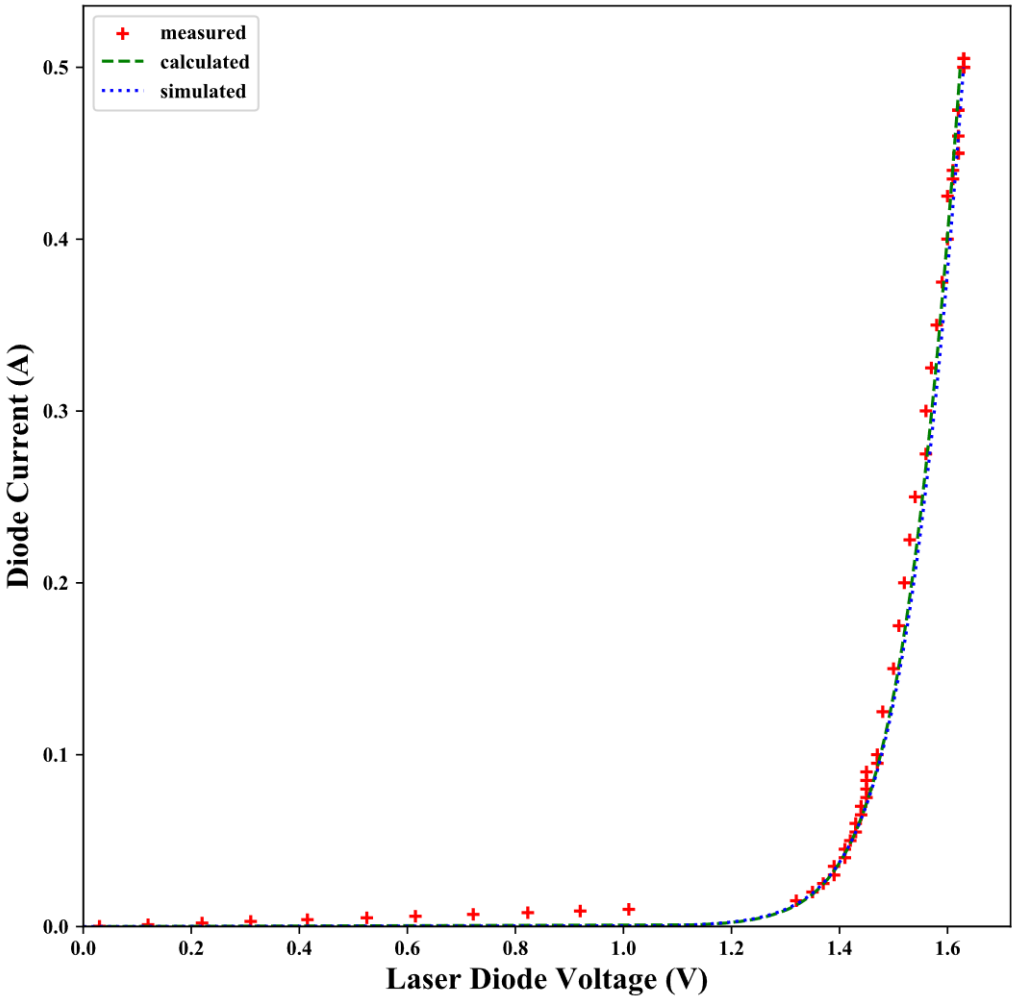

Figure 4.3.6: Plot showing comparison between measured, calculated, and simulated BOB850T1000 IV curve.

The relative error between the measured and simulated IV curve and the expected IV curve cannot be obtained because the expected IV curve is unknown as it is not provided in the BOB850T1000 datasheet.

4.3.2 Laser diode CV curve – CJO, VJ, and M

4.3.2.1 Method

To extract the CJO, VJ, and M diode parameters from the laser diode, a plot of the diode capacitance, as a function of bias voltage, must be measured.

The Solartron 1260A [77] impedance analyser is used to measure the capacitance of the BOB850T1000 laser diode over a range of bias voltages. The Solatron 1260A component mount, shown in Figure 4.3.7, is used to connect the BOB850T1000 to the Solatron 1260A. The component mount consists of two copper strips that connect opposite pairs of four BNC connectors. The BNC connectors are designed to fit onto the Solatron 1260A front panel connectors. To connect the BOB850T1000 to the component mount, a TO-18 laser diode connector is soldered to the component mount. This is done to keep the cable length short, as long cable lengths may degrade measurement accuracy at high frequency [77, Sec. 6.5.1].

For eye safety, a cover is made for the laser diode (Figure 4.3.7) to block the laser light if it is produced when connected to the Solatron 1260A. The cover is wrapped in aluminium foil tape to ensure that no light can escape.

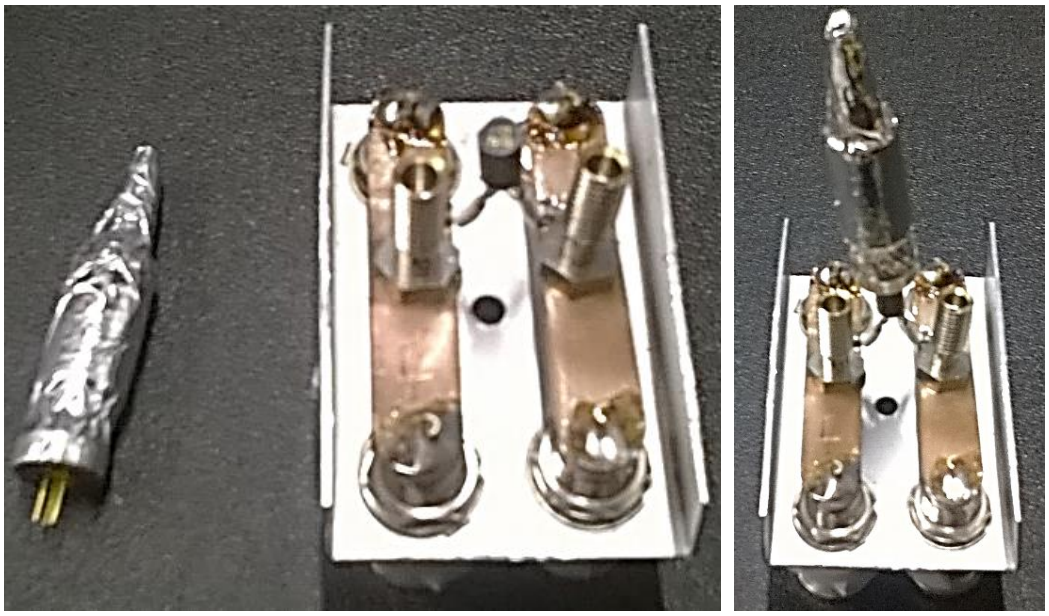

Figure 4.3.7: The custom laser diode beam cover on the laser diode (left), and the custom Solation component mount (right).

The beam cover is fixed to the laser diode, then the laser diode is inserted into the laser diode connector on the custom Solatron 1260A component mount (Figure 4.3.7) and the component mount is fixed to the top four BNC (current, gen output, and voltage 1 lo and hi) connectors on the Solatron 1260A (Figure 4.3.8).

Figure 4.3.8: BOB850T1000 CV curve setup showing the component mount connected to the Solatron 1260A.

The Solatron 1260A is configured to produce a 32 MHz signal with an amplitude of 20 mV. This frequency was selected as it is the highest measurement frequency that the Solatron 1260A is capable of and is near to the middle range required for the TIDA-01173 light source (10 to 100 MHz). The amplitude of 20 mV is chosen as it is a small signal and therefore unlikely to affect the bias voltage in the measurements. The Solatron 1260A is set to read out measurements in capacitance. The Solatron 1260A's sweep facility is used to sweep the bias voltage from -0.5V to 1.4 V and save the measured capacitance values.

4.3.2.2 Results

The CV curve for the BOB850T1000 laser diode produced from the collected data is shown in Figure 4.3.9.

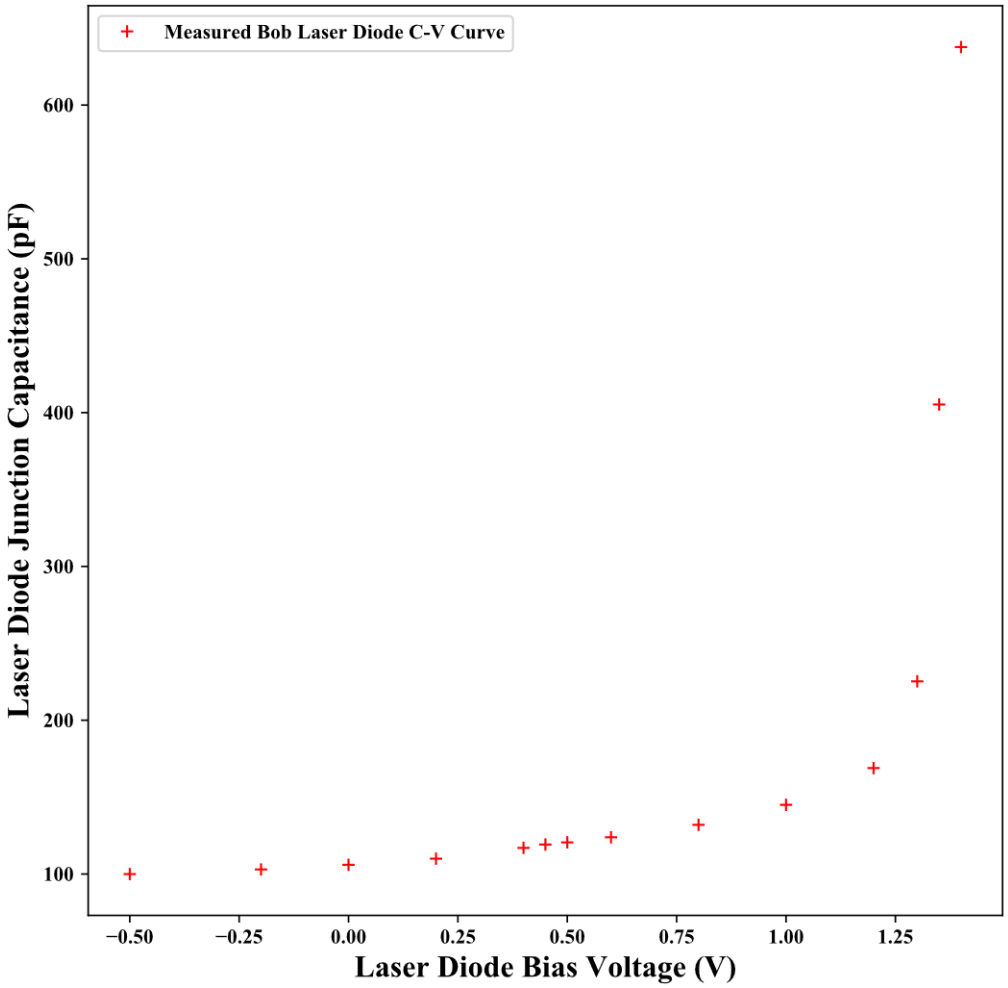

Figure 4.3.9: BOB850T1000 CV curve at 32 MHz.

The CJO SPICE parameter is the zero-junction voltage bias capacitance, that is the capacitance measured at zero bias voltage on the CV curve (Figure 4.3.9). From this plot, CJO was found to be 106 pF.

To find the SPICE parameters VJ and M, the CV curve is linearised using the diode junction capacitance equation [74],

$$CJ = \frac{CJO}{\left(1 - \frac{V}{VJ}\right)^{M}} \tag{4.3.9}$$

$$\Rightarrow \sqrt[M]{\frac{CJO}{CJ}} = \frac{-1}{VJ}V + 1 \tag{4.3.10}$$

and adjusting M until the line appeared linear. This occurred when M was set to 0.25.

The linearised plot (Figure 4.3.10) has a fitted slope, m, of -0.644 V^{-1} and y axis intercept, c, of 0.976. The r value of the fitted line is -0.998, showing a strong linear fit. The y axis intercept, c, should be 1 as CJO and CJ at 0 V bias, should be equal. The reason the c value is less than 1 is the fitted line happens to be fitted below that data point.

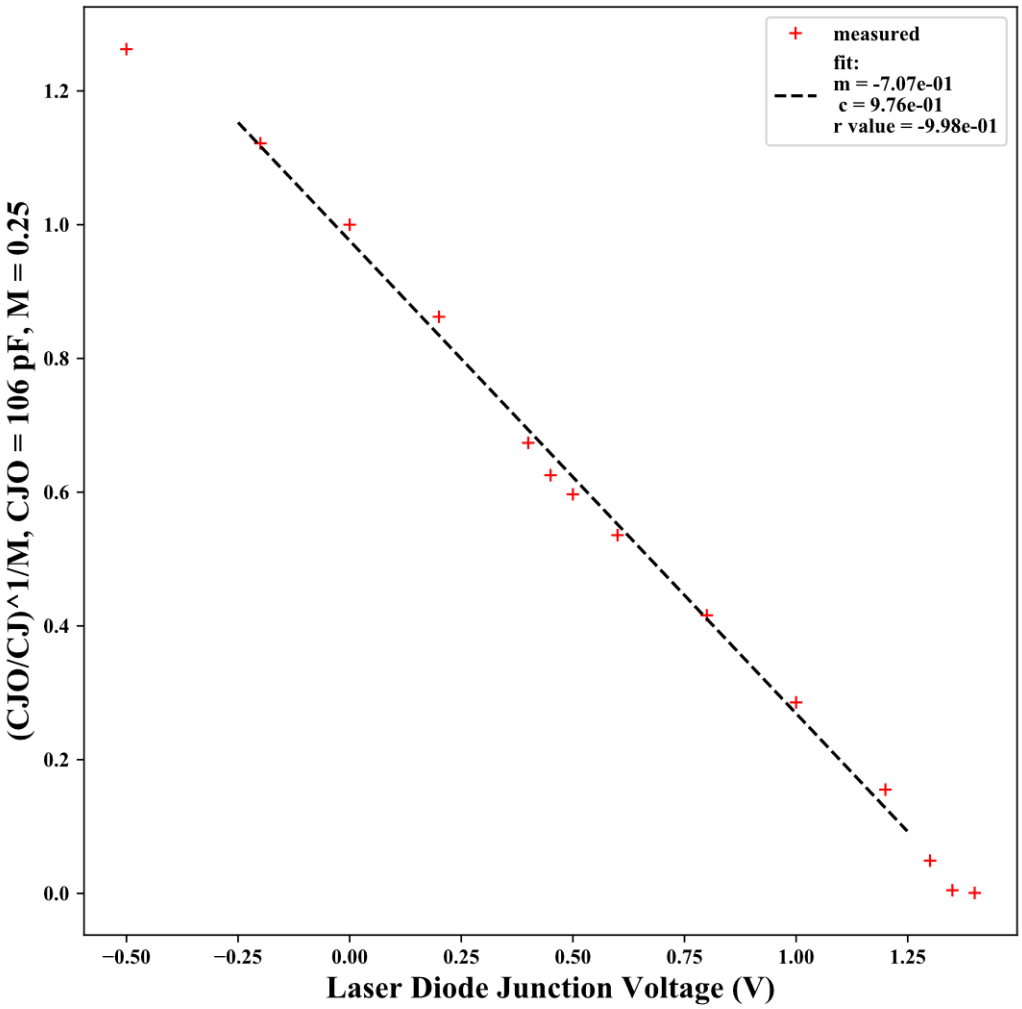

Figure 4.3.10: Linearised BOB850T1000 CV curve at 32 MHz.

Table 4.3.3: Linearised BOB850T1000 laser diode CV curve (Figure 4.3.10) properties.

Ln(I) vs V Bob Curve Properties:	Values:
$\boldsymbol{m}$	-0.707 V^{-1}
$\boldsymbol{c}$	0.976

VJ is calculated by taking the negative inverse of the slope of the linearised CV curve (Figure 4.3.10),

$$\mathrm{VJ} = \frac{-1}{m}, \tag{4.3.11}$$

where, VJ is the diode junction voltage, and m is the slope of the linearised CV curve (Figure 4.3.10). VJ is found to be 1.41 V.

Table 4.3.4 shows a summary of the extracted CJO, M, and VJ diode parameters.

Table 4.3.4: Extracted BOB850T1000 CJO, M, and VJ properties.

SPICE Charge Storage Diode Parameters Extracted from CV Curve	Values
CJO	106 pF
M	0.250
VJ	1.41 V

The extracted CJO, M, and VJ SPICE parameters are added to the BOB850T1000 model (Code 4.3.2):

```
.model BOB850T1000 D(IS=2.53E-10 N=2.87 RS=0.0802 CJO=106E-12
M=0.25 VJ=1.41)
```

Code 4.3.2: Electrical SPICE parameters extracted from the BOB850T1000 IS, N, RS, CJO, M, and VJ in the standard SPICE diode model.

The CJO, M, and VJ parameters, extracted from the BOB850T1000 laser diode, are substituted into the diode junction capacitance equation (4.3.9) to create a calculated CV curve. This curve is plotted over the measured CV curve (Figure 4.3.11). The calculated and measured CV curves matches for all but two points at just above a bias voltage of 1.25 V. This confirms the CJO, M, and VJ parameter extraction at 32 MHz. So the characteristics of the BOB850T1000 laser diode simulation model are expected to match well with the real BOB850T1000 laser diode characteristics.

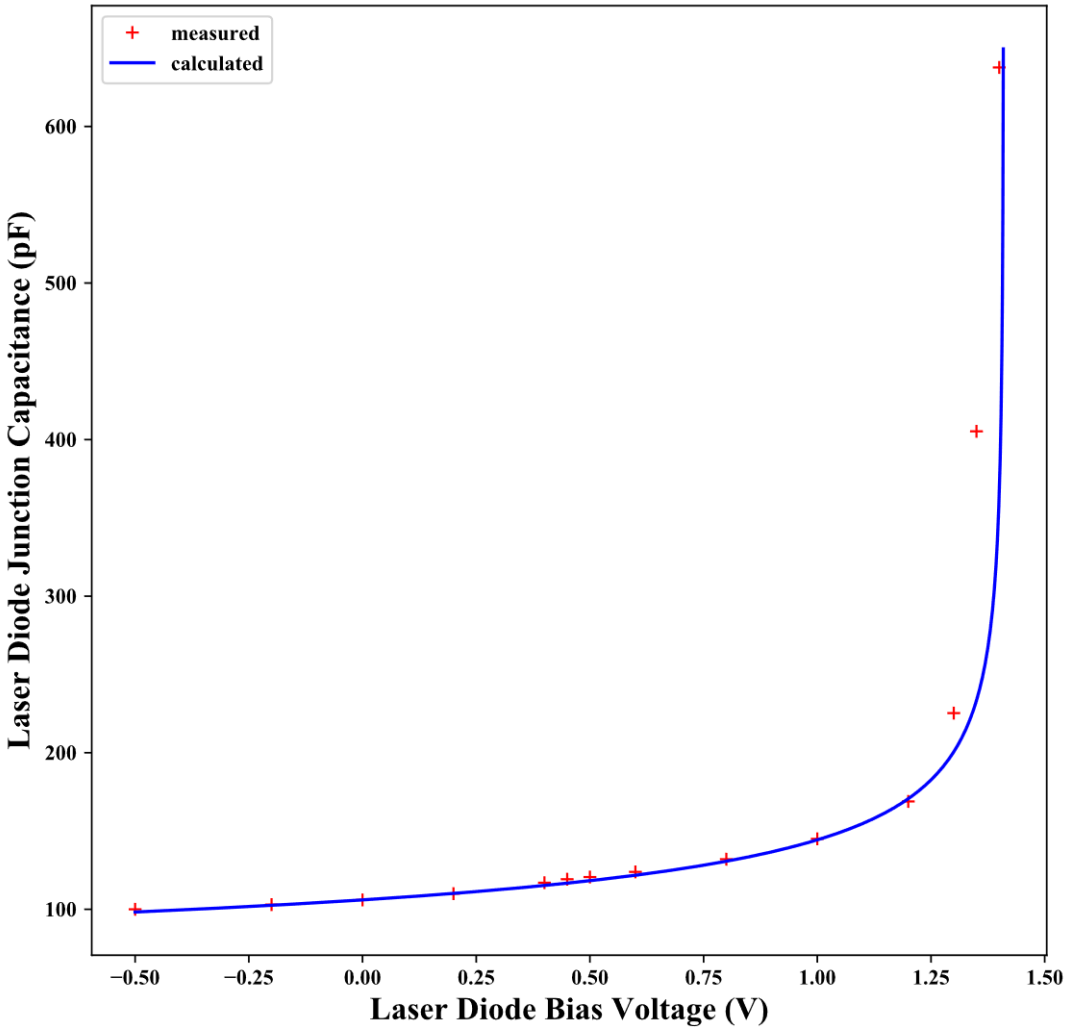

Figure 4.3.11: Plot showing measured and calculated BOB850T1000 laser diode CV curve.

The parameter extraction of the CV curve can be improved by taking repeated measurements to gain a measure of the variance of the parameters due to measurement uncertainties. These repetitions were attempted using a Python script

to automate the measurements, however, the measurements recorded using the script were incorrect. The reason for this could not be resolved. An impedance analyser with a higher maximum frequency (more than 100 MHz) should have been used, as testing at the limits of an equipment's range can be less accurate, however, one was not available. It would have been useful to take measurements over the full modulation range of the TIDA-01173, 10 to 100 MHz, to see how the CV parameters change over frequency. However, it would have been impractical to incorporate this into the TIDA-01173 simulation, as a separate BOB850T1000 model would have been required for each frequency. The 32 MHz measurement is an acceptable compromise, as it is the nearest possible measurement to the centre of the TIDA-01173 modulation frequency range.

4.3.3 Laser diode reverse recovery – TT

When a diode is switched from forward bias to reverse, the ideal response is for the diode to immediately become open circuit, therefore stopping the flow of current. However, in real diodes, the current does not immediately become open circuit, but instead reverses for a time before the current stops. This reversal of current is due to the time that it takes for excess minority carrier charges to leave the diode when it is reverse biased. The time taken for the reverse current to stop flowing is known as the reverse recovery time. The reverse recovery current waveform is illustrated in Figure 4.3.12.

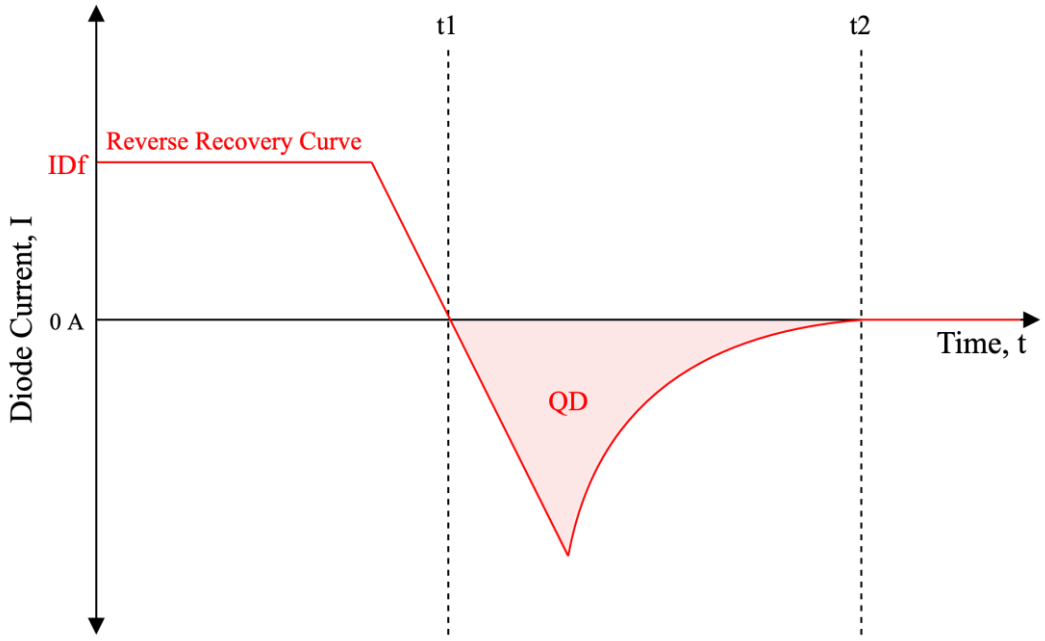

Figure 4.3.12: Depiction of reverse recovery current waveform in a non-ideal diode [78], where QD is the amount of charge stored in the diode, and ID is the diode forward current.

The SPICE parameter transit time (TT) is used in the diode model to set the reverse recovery characteristic. Transit time is a proportionality constant relating reverse current to reverse storage time and is calculated as,

$$Q_D = I_{Df}TT, \tag{4.3.12}$$

where, Q_D is the amount of charge stored in the diode, I_{Df} is the current passing through the diode when it is in forward bias, and TT is the transit time [74, Sec. 3.7.2]. So, to find the transit time parameter (TT), Q_D must be obtained. Q_D is

measured from the diode's reverse recovery current curve by integrating the reverse diode current over the reverse recovery time,

$$Q_D = \int_{t_1}^{t_2} I_D(t)\, dt, \tag{4.3.13}$$

where, $I_D(t)$ is the diode current as a function of time, t, t_1 is time when the diode current falls below 0 A, and t_2 is the time when then current returns to 0 A [79, p. 208].

The reverse recovery waveform is found by switching the diode from forward bias to reverse bias and capturing the waveform of the diode current at this transition. To capture this waveform, the circuit shown in Figure 4.3.13 is used. The function generator is set to generate a square waveform and the diode current waveform is captured using an oscilloscope to measure the voltage across the 10 Ω resistor.

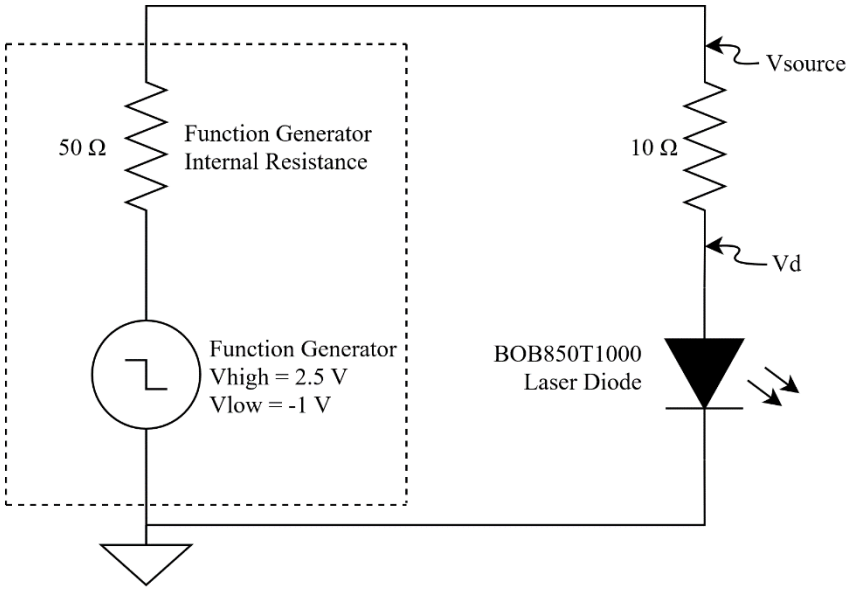

Figure 4.3.13: Circuit diagram of the reverse recovery measurement setup.

The function generator is set to a 1 kHz 50% duty cycle square waveform with a high voltage of 2.5 V and a low voltage of -0.5 V. These voltages were selected to put the diode into forward and reverse bias. Considering the 50 Ω internal resistance of the function generator and 10 Ω resistor used to measure the diode current, the diode forward current is expected to be about 20 mA with a forward voltage of about 1.3 V, according to the BOB850T1000 IV curve (Figure 4.3.4).

The circuit shown in Figure 4.3.13 is constructed using a Rigol DG1022 function generator, and a Keysight DSOS604A digital oscilloscope (Figure 4.3.14).

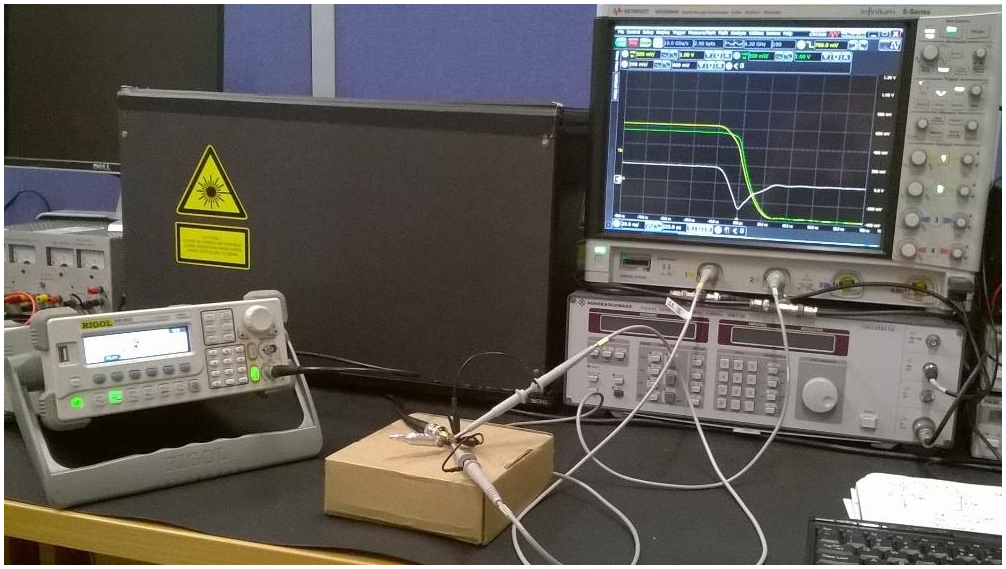

Figure 4.3.14: Photo of the BOB850T1000 laser diode transit time (TT) SPICE parameter

A SubMiniature version A (SMA) connector is soldered to a TO-18 laser diode connector and the 10 Ω resistor to connect the function generator via a 50 Ω impedance coaxial cable. The length of the wire connections between the function generator connector, laser diode, and resistor are kept as short as possible to minimise parasitic inductance (Figure 4.3.15). There will be parasitic inductance in the resistor, however, this could not easily be avoided with the available resource. The light cover for the laser diode that is used in the laser diode CV curve measurements (section 4.3.2), is put on the laser diode to prevent laser light escaping if it is produced during the experiment. The laser diode is inserted into the TO-18 laser diode connector. The oscilloscope measured the voltage across the 10 Ω resistor using two voltage probes connected to the nodes *Vsource* (source voltage) and *Vdiode* (diode voltage), as is shown in Figure 4.3.13.

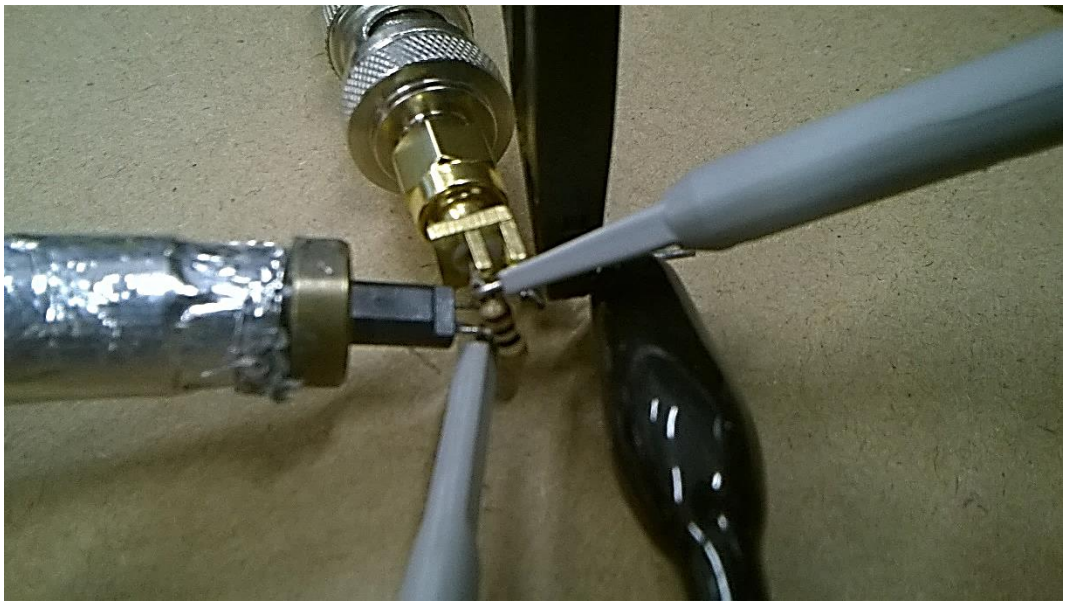

Figure 4.3.15: TT BOB850T1000 laser diode parameter extraction circuit hardware.

The resulting waveforms are shown in Figure 4.3.16.

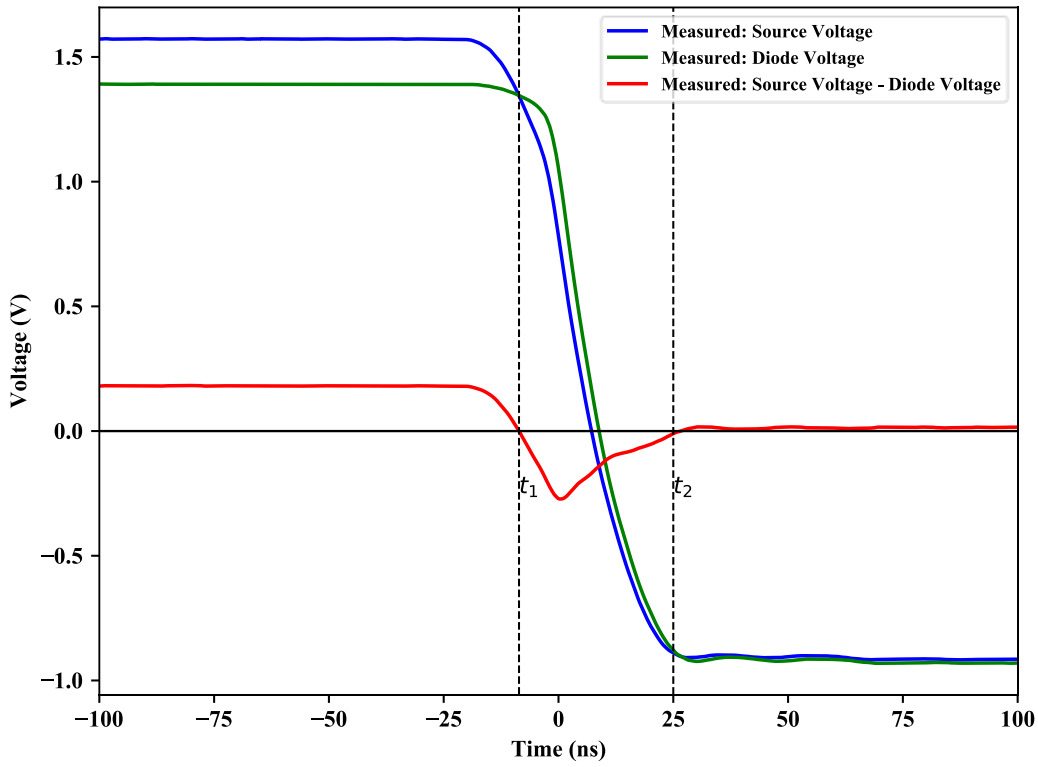

Figure 4.3.16: Measured reverse recovery waveform for the BOB850T1000 laser diode.

The BOB850T1000 laser diode's reverse recovery waveforms are plotted using a Python script. The Python script is also used to integrate the difference between

Source Voltage and Diode Voltage between the times -8.6 and 25 ns, as indicated by the black dotted lines in Figure 3.3.16. The composite trapezoidal rule [80] was used for this integration. As the difference between the Source Voltage and Diode Voltage waveform is the voltage across the 10 Ω resistor, it is also the diode current waveform. So, by dividing the result of the integration by 10 Ω, the diode charge, Q_D is found. The transit time of the BOB850T1000 laser diode is found to be 24 ns by dividing Q_D by the measured forward diode current (I_{Df}):

$$TT = \frac{Q_D}{I_{Df}}. \qquad (4.3.14)$$

The calculations and measurements taken from the reverse recovery curve to find TT are shown in Table 4.3.5. The measured value of transit time is within the expected range of transit times for diodes, less than 10 ns for small signal or switching diodes to 250 ns for fast rectifier diodes[10] [81].

Table 4.3.5: Summary of measurements and calculations made to extract the transit time (TT) SPICE diode model parameter for the BOB850T1000 laser diode.

Measurements /Calculations	Results
$\int_{t_1}^{t_2} \left(\boldsymbol{V_{Source}(t)} - \boldsymbol{V_{Diode}(t)}\right) \boldsymbol{dt}$	4.3 E^{-9} Vs (2 sf)
$\boldsymbol{Q_D} = \frac{\int_{t_1}^{t_2} \left(\boldsymbol{V_{Source}(t)} - \boldsymbol{V_{Diode}(t)}\right) \boldsymbol{dt}}{\boldsymbol{10\ \Omega}}$	4.3 E^{-10} C (2 sf)
$\boldsymbol{I_{Df}}$	0.018 A (2 sf)
$\boldsymbol{TT} = \frac{\boldsymbol{Q_D}}{\boldsymbol{I_{Df}}}$	24 ns (2 sf)

The extracted TT SPICE parameter was added to the BOB850T1000 model (Code 4.3.3):

```
.model  BOB850T1000  D(IS=2.53E-10    N=2.87  RS=0.0802  CJO=106E-12
M=0.25 VJ=1.41 TT=24E-9)
```

Code 4.3.3: Electrical SPICE parameters extracted from the BOB850T1000 IS, N, RS, CJO, M, VJ, and TT in the standard SPICE diode model.

The circuit used to extract the TT parameter (Figure 4.3.13) is created in TINA TI using the BOB850T1000 model containing the newly extracted TT parameter (Code 4.3.3). The simulation and measured recovery waveforms are plotted together (Figure 4.3.17).

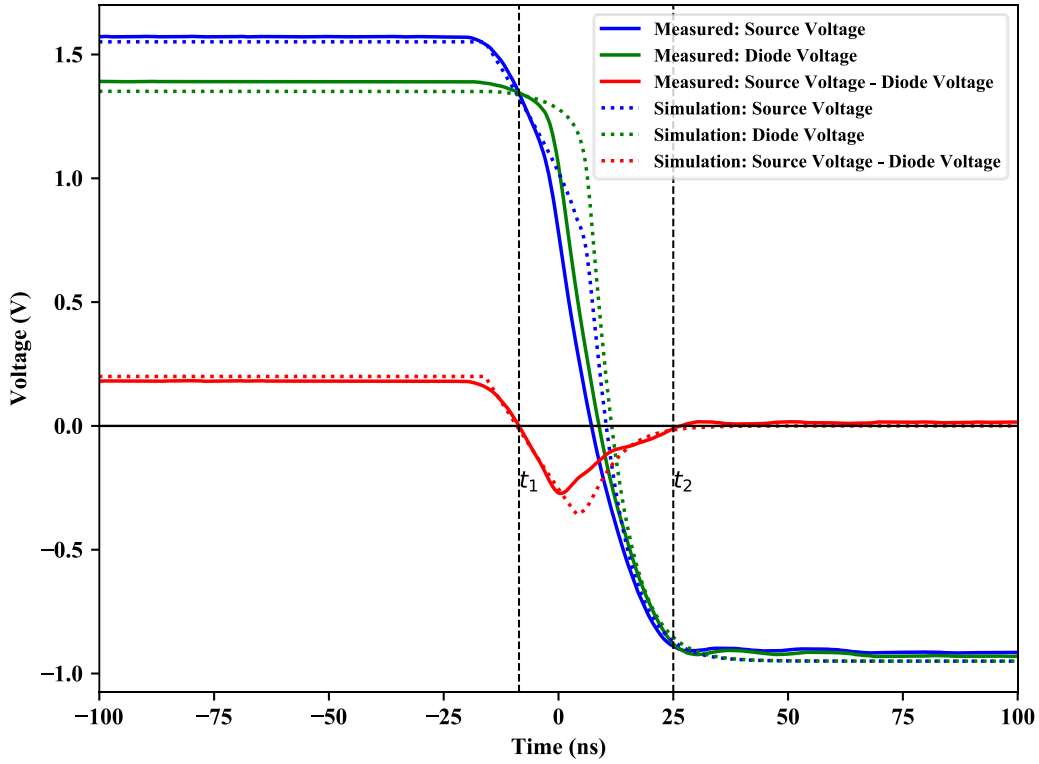

Figure 4.3.17: Measured (solid lines) and simulated (dotted lines) BOB850T1000 laser diode reverse recovery waveform.

The simulated difference between Source Voltage and Diode Voltage waveform, which is just a scale factor of 10 Ω in amplitude from the diode current waveform, has the same recovery time as that of the measured waveform. However, the maximum reverse current of the simulated waveform is greater than that of the measured waveform. The reason for this may be that the forward current for the simulated waveform was slightly more than the measured waveform, or that the waveform hardware measurements were affected by parasitic components.

The transit time is calculated using the simulated reverse recovery waveform (Figure 4.3.6) and found to be 27 ns. This represents a 12.5% error compared to the measured transit time of 24 ns. This is an acceptable difference, as the reverse recovery time is the same for the measured and simulated diodes and both values of TT are within the expected range for diodes, between 10 and 250 ns [81].

Literature on methods for measuring the transit time (TT) SPICE diode parameter is difficult to find. No explicit method for measuring TT could be found. Information from textbooks, [74, Sec. 3.7.2], [78], and [79, p. 208] were used, along with consultation with Professor Jonathan B. Scott, to produce the method presented here. Given that no method could be found in literature to measure TT, it was a good result to find that the method used here extracted a TT that, when used in the SPICE diode model, produced a reverse recovery waveform with only 12.5% error in TT.

4.3.4 Laser diode optical parameter extraction, I-Op curve

The slope efficiency and lasing threshold current optical properties of the BOB850T1000 laser diode are extracted by measuring the output power of the laser diode as a function of current. A PM100D optical power meter (Thorlabs, Newton, New Jersey) with an S302C thermal power sensor head (Thorlabs, Newton, New Jersey) are used to measure the total optical output power of the laser diode.

To measure the BOB850T1000's optical output power vs current curve, the laser diode is mounted in the TCLDM9 temperature-controlled laser diode mount in the same way that it is in the IV curve measurements (section 4.3.1), with the pins oriented as shown in Figure 4.3.2. The TED 200 C temperature controller and LDC 205 C laser diode controller are both connected to the temperature-controlled laser diode mount. The Thorlabs S302C thermal power sensor head is mounted in front of the laser diode. The front cover of the laser diode mounting block is removed permitting the positioning of the laser diode closer to the power meter sensor therefore allowing all the laser beam to be measured (Figure 4.3.18). The measurements were taken inside the Thorlabs optical enclosure for eye safety, as explained in section 4.2.

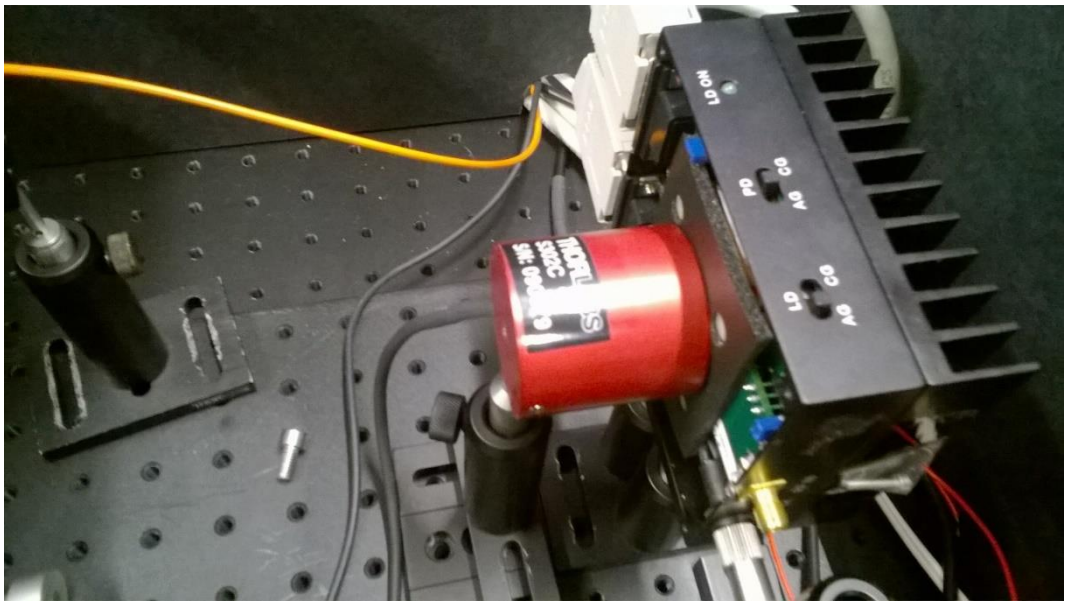

Figure 4.3.18: Photo of the slope efficiency experiment setup, showing how the optical power meter thermal power head was positioned in front of the laser diode mount with the front face plate removed, so that all of the light emitted from the laser diode was captured by the power meter head sensor.

The temperature controller is set to 25°C and switched on. The laser diode controller is connected to the laser diode mounting block, and just enough current was supplied to the laser diode so the power meter displayed a reading. The beam is aligned to the sensor by moving the sensor's height and angle position until the reading on the optical power meter is maximised. A diagram of the setup is shown in Figure 4.3.19.

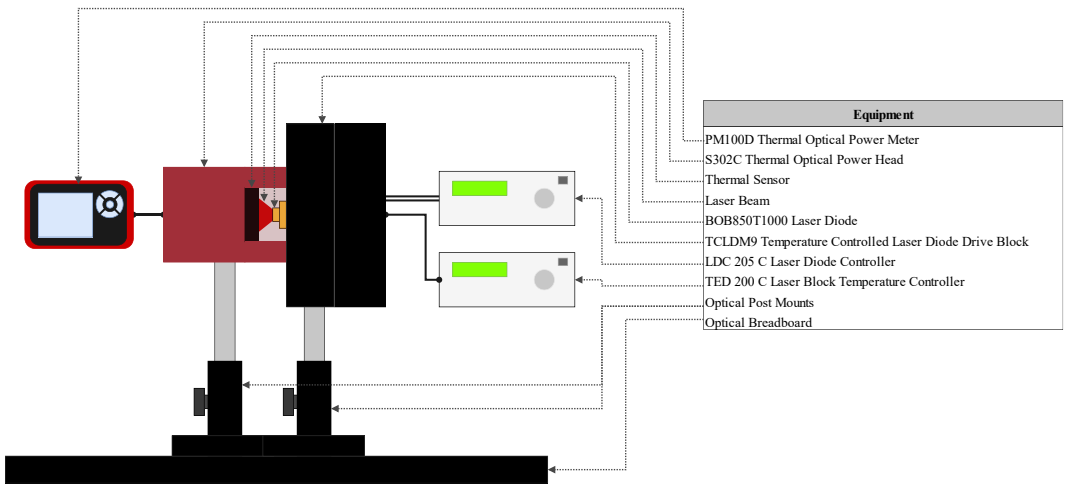

Figure 4.3.19: Diagram of the slope efficiency experiment setup.

Once the laser is aligned with the optical power sensor, the laser diode current controller is set to 0 mA and switched on. Once the temperature settles at 25°C, the optical output power is measured using the optical power meter and recorded against the current settings. The current settings are set roughly to the desired current and the actual laser diode current is read from the laser diode current controller. The optical power measurements are repeated for current settings in the range of 0 mA to 500 mA (LDC 205 C laser diode controller's maximum current setting). The resulting I-Op curve is shown in Figure 4.3.20.

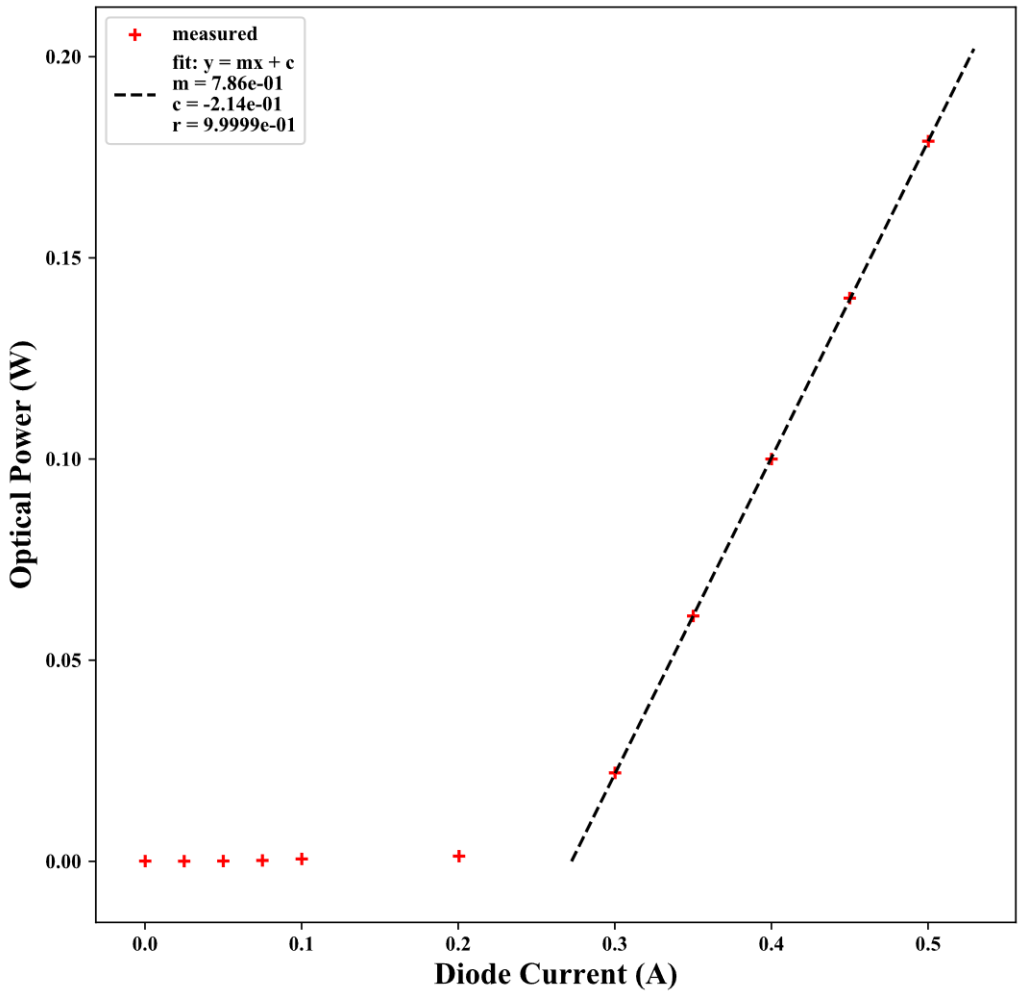

Figure 4.3.20: Measured Op-I curve for the BOB850T1000 laser diode at 25°C.

A line is fitted to the I-Op curve (Figure 4.3.20) for the region of the plot where the laser is lasing. The slope of the plot, m, is the slope efficiency of the laser diode. So, the equation of the I-Op curve is:

$$P_{op}(I_d) = \mathrm{SE}I_d + c, \tag{4.3.15}$$

where P_{op} is the optical output power of the laser diode, I_d is the laser diode current, SE is the slope efficiency of the laser diode, and c is the y-axis intercept of the I-Op curve.

The parameters of the fitted line are shown in Table 4.3.6.

Table 4.3.6: I-Op curve fitted line parameters.

Fitted line of BOB850T1000 I-Op curve parameters	Values
$\boldsymbol{m}$	0.786 W/A
$\boldsymbol{c}$	-0.214 W

The threshold current of the laser diode is found by rearranging (4.3.15) and solving for I_d when P_{op} is 0 W:

$$I_{\mathrm{TH}} = \frac{-c}{\mathrm{SE}} \tag{4.3.16}$$

where, I_{TH} is the laser diode threshold current, SE is the slope efficiency of the laser diode, and c is the y-axis intercept of the I-Op curve.

By evaluating (4.3.16) with a slope efficiency of 0.786 W/A and a I-Op curve y-axis intercept of -0.214 W, the threshold current of the BOB850T1000 laser diode is found to be 0.272 A. The extracted optical properties are summarised in Table 4.3.7.

Table 4.3.7: Measured and datasheet (at 25°C) optical properties of the BOB850T1000 laser diode.

Optical Parameters	Measured values	Datasheet Values
$\boldsymbol{SE}$	0.786 W/A	1.1 W/A
$\boldsymbol{I_{TH}}$	0.272 A	0.200 A

The datasheet values for the BOB850T1000 laser diode slope efficiency and threshold current are also shown in Table 4.3.7. The measured and datasheet values for slope efficiency and threshold current do not match. There is a 28.5% error in

the slope efficiency and 36.0% error in threshold current between the measured and simulated values. So, there is a substantial difference between the measured and datasheet optical properties.

The difference between the measured and datasheet slope efficiency and threshold current could be due to not all the light being captured by the optical power meter. An integrating sphere is used in [82] to measure the optical output power of the laser diodes being characterised. An integrating sphere would have been a much better option to use for the optical power measurements taken in the BOB850T1000 laser diode characterisation, instead of the direct coupled power meter that was used. This is because all the light is accounted for when an integration sphere is used: it cannot be guaranteed that all the light emitted from the laser diode was captured in the direct coupled thermal optical power meter. It was also very difficult to align the power meter to capture all the light emitted from the laser diode; this would have been easier if an integration sphere was used as the alignment of the beam in the integrating sphere is not crucial. Unfortunately, an integrating sphere was not available.

Another reason for the differences between the laser diode extracted and datasheet optical parameters is that these properties are temperature dependent and the BOB850T1000 laser diode datasheet (Appendix A, Table A.1) only provides property values for a constant diode junction temperature of 25°C. With increasing diode temperature, the slope efficiency decreases and threshold current increases [82]. The measured slope efficiency is less than the datasheet value, and the measured threshold current was more than the datasheet value. So, if the temperature dependency of the slope efficiency and threshold current is the cause of the difference between the datasheet and measurements, the diode temperature must have been more than the 25°C that the temperature controller was set to.

In the optical parameter extraction, the TCLDM9 temperature-controlled laser diode mount and temperature controller is set to keep the temperature at a steady 25°C. However, the junction temperature of the BOB850T1000 laser diode may have been higher than this due to thermal resistance between the diode junction and temperature feedback sensor. In order to check if this temperature differential is

substantial, the difference in temperature between the diode junction and temperature-controlled laser diode mount, due to thermal resistance, was calculated. The expected diode junction temperature at the maximum measured optical power of 0.179 W, measured at a current of 0.500 mA, and assuming the laser diode mount and temperature was 25°C, is calculated using the equivalent thermal circuit diagram (Figure 4.3.21).

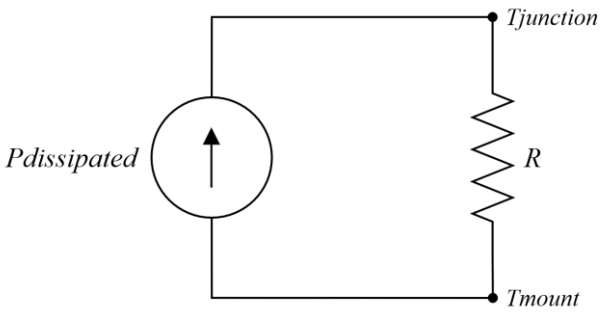

Figure 4.3.21: Equivalent thermal circuit for the BOB850T1000 laser diode optical property extraction. *Pdissipated* is the power dissipated by the laser diode, *R* is the thermal resistance of the laser diode case, *Tjunction* is the temperature of the laser diode junction, and *Tmount* is the temperature of the temperature-controlled laser diode mount.

When operating the laser diode with an optical output power ($P_{optcial}$) of 0.179 W, and with an electric to optical conversion efficiency (η) of 35%, as given in the BOB850T1000 datasheet (Appendix A, Table A.1), the power dissipated as heat ($P_{dissipated}$) is found to be 0.347 W:

$$\begin{aligned} P_{optcial} &= \eta P_{total} \\ \Rightarrow P_{total} &= \frac{P_{optcial}}{\eta}, \end{aligned} \tag{4.3.17}$$

$$\begin{aligned} P_{dissipated} &= P_{total} - P_{optical} \\ \Rightarrow P_{dissipated} &= \frac{P_{optcial}}{\eta} - P_{optical} \\ \Rightarrow P_{dissipated} &= P_{optcial}\left(\frac{1}{\eta} - 1\right). \end{aligned} \tag{4.3.18}$$

With the laser diode dissipated power of 0.347 W, and the laser diode temperature-controlled mount temperature (T_{mount}) set to 25°C, the laser diode

junction temperature ($T_{junction}$) is found to be 29.9°C. So, the temperature of the laser diode junction was about 5°C higher than what the temperature controller is set to. The thermal resistance (R) used in the calculation is the BOB850T1000 laser diode case thermal resistance, 14°C/W (Appendix A, Table A.1):

$$\Delta T = T_{junction} - T_{mount}$$

$$\Rightarrow T_{junction} = T_{mount} + \Delta T \quad (4.3.19)$$

$$\Delta T = P_{dissipated} \times R \quad (4.3.20)$$

$$T_{junction} = T_{mount} + \left(P_{dissipated} \times R\right) \quad (4.3.21)$$

The temperature difference between the laser diode junction and temperature-controlled mount was evident when the optical power measurements were taken. It was observed that the optical output power decreased immediately after the current setting was increased, then eventually settling at a lower optical power. It is likely that the increase in temperature due to increasing the current setting caused a decrease in slope efficiency that resulted in a decrease in optical output power.

In [82], the temperature drift of the laser diode during characterisation is controlled by measuring the emitted light spectrum using a spectrometer. The output power wavelength is a function of the temperature of the diode junction, so the wavelength measurement provides the temperature of the diode junction. This avoids the problem of the thermal resistance between the laser diode and temperature sensor. The temperature dependence of the laser diode measured in [82] was found to be linear for the slope efficiency, and exponential for the threshold current.

To improve the accuracy of the laser diode parameter extraction and model, the temperature dependence of the slope efficiency and threshold current temperature must be measured using a method like the one described in [82]. This was outside the scope of this project due to time constraints.

4.3.4.1 BOB850T1000 Netlist

To incorporate the laser diode optical properties, a sub circuit model is created for the BOB850T1000 (Code 4.3.4). The sub circuit model contains the standard SPICE diode model of the BOB850T1000 created in sections 4.3.1, 4.3.2, and 4.3.3, and a voltage dependent voltage source, EB1, where the output voltage between the opWp and opWn nodes was directly proportional to the optical output power,

$$V(\mathrm{opWp} - \mathrm{opWn}) \propto P_{op} = \mathrm{SE}(I_d - I_{\mathrm{TH}}). \qquad (4.3.22)$$

The diode current in the model is measured using the voltage of a very small, 1 nΩ, series resistor (RCS). The model is made to only consider the lasing output power and lasing threshold current, not the light output below the lasing threshold. This is because the only useful light, for the ToF light source simulation, occurs in the lasing region (current values above the lasing threshold current).

```
* BOB850T1000 Laser Diode Model, Electrical and Optical:

.SUBCKT  Bob_LaserDiode vd k opWp opWn PARAMS:
+ oSE=0.786
+ oTH=0.272
+ eIS=2.53e-10
+ eN=2.87
+ eRS=0.0802
+ eCJO=106p
+ eM=0.25
+ eTT=24n
+ eVJ=1.41
+ RCS=1n

* Electrical (Diode) Model:
D1 vd dc Bob
* to measure diode current
RD1 dc k {RCS}

.model Bob D
+ IS={eIS}
+ N={eN}
+ RS={eRS}
+ CJO={eCJO}
+ M={eM}
+ VJ={eVJ}
+ TT={eTT}

* Optical (Laser) Model:

* Get the diode current:
* Id is V(D1C,k)
ED1C D1C k Value={V(dc,k)/{RCS}}

* Apply Slope efficiency and threshold current to simulate optical
output power:
* If the diode current is higher than the thrshold current, then
produce light acording to the slope efficiency and threshold curent,
else produce no light:
EB1 opWp opWn Value={IF( V(D1C,k)>{oTH},  {oSE}*(V(D1C,k)-{oTH}),
0) }

.ENDS
```

Code 4.3.4: The complete BOB850T1000 SPICE model netlist with electrical and optical characteristics.

A simulated I-Op curve is produced using the BOB850T1000 model. This plot is plotted on the same plot as the measured I-Op curve to check that the simulation model is correct (Figure 4.3.22).

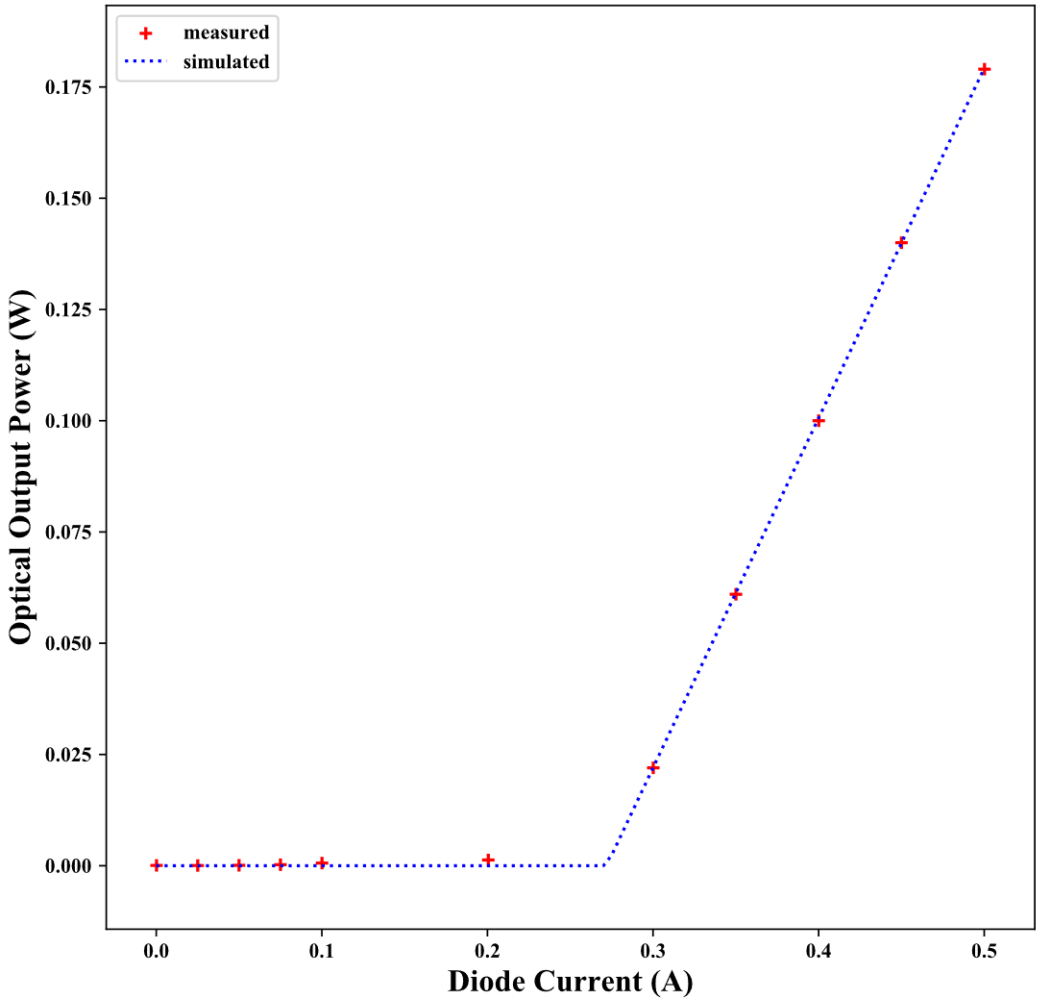

Figure 4.3.22: Plot showing comparison between measured and simulated BOB850T1000 I-OP curve.

The only difference between the measured and simulated plot is at the diode currents below the threshold current. The discrepancy between the simulation and measurements is expected, because in the simulation, the optical power is set to 0 W for current less than the threshold current. This is done to simplify the model, as the light output from a laser below threshold current is very small and not useful in the ToF camera light source. The light output below threshold current in real laser diodes is due to spontaneous emission of photons.

4.4 Conclusion

In this chapter, the electrical and optical properties of the BOB850T1000 laser diode were measured. A SPICE sub-circuit model was created for the BOB850T1000 that contained the standard SPICE diode model and a dependent voltage source that modelled the optical output power as a function of the diode current. Each of the laser diode model parameters extracted in this section were tested in simulation and confirmed to match what was measured.

The BOB850T1000 laser diode is the last component required to model the TIDA-01173 and Kea ToF camera light sources. The simulation model produced in Chapter 3 can be completed and used to compare to hardware measurements. Now an apparatus for measuring electrical to optical power efficiency of the ToF camera light sources in hardware must be produced.

Chapter 5

Electrical to Optical Power Efficiency Measurement Apparatus

5.1 Electrical to optical power efficiency

To measure the power efficiency of the ToF camera light sources in hardware, the electrical input power and optical output power of the light sources must be measured. Power efficiency (η) is defined as the useful output power ($P_{useful\ output}$) divided by the input power (P_{input}),

$$\eta = \frac{P_{useful\ output}}{P_{input}} = \frac{P_{optical}}{P_{electrical}}. \quad (5.1.1)$$

For the purpose of measuring the electrical to optical power efficiency of the ToF camera light sources, the input power (P_{input}) is the electrical power supplied to the laser driver circuit ($P_{electrical}$), and the useful output power ($P_{useful\ output}$) is the optical output power of the laser diodes ($P_{optical}$). The power consumed by the control part of the light source circuits is not the focus of this investigation so is not included in the efficiency measurements.

Power efficiency is important for ToF light sources. ToF light sources with high power efficiency produce more optical output power for their given input power, and less heat. This allows for a number of advantages, such as: the ability to be powered from low power sources like USB, heat sinks can be smaller allowing ToF cameras to be made smaller, high optical power laser pulses can be used to improve ToF performance in high ambient light conditions such as day light. Less heat sinking requirement is also beneficial for applications where ToF cameras need to be installed in enclosures with low airflow.

Texas Instruments claims in [2] that the shunt switching type of light source, as is used in TIDA-01773, should be more power efficient than the series type, as is used in Kea. To test this claim, and to set a benchmark for any improvements to be made to these light sources, the power efficiencies of these light sources must be measured. This is done in both simulation and hardware so that a theoretical power efficiency can be compared to the real results.

In this chapter we present the apparatus developed to test efficiency. A large number of measurements are required to evaluate the light source efficiency over a broad range of operating conditions. Furthermore, lasers require a settling time of several minutes to reach steady state operation. In order to undertake multiple measurements and allow for steady state conditions the system operation and data capture is fully automated.

5.1.1 Integration time considerations

Integration time is the length of time over which a ToF camera sensor accumulates light for each raw frame. The light source must emit light for at least this period of time. So, for the work described here, we define Integration time as the length of time that modulated light is emitted from the lasers and Off time as the length of time that it takes to read data from the image sensor (readout time) and dead time. The raw frame period is made up of the Integration time plus the Off time. These times are depicted in Figure 5.1.1. Integration time switching is the switching that occurs to enable modulation of the lasers during the Integration time and to turn off the lasers during the off time. In both the TIDA-01173 and Kea light sources, the Integration time switching is performed by a series switching MOSFET.

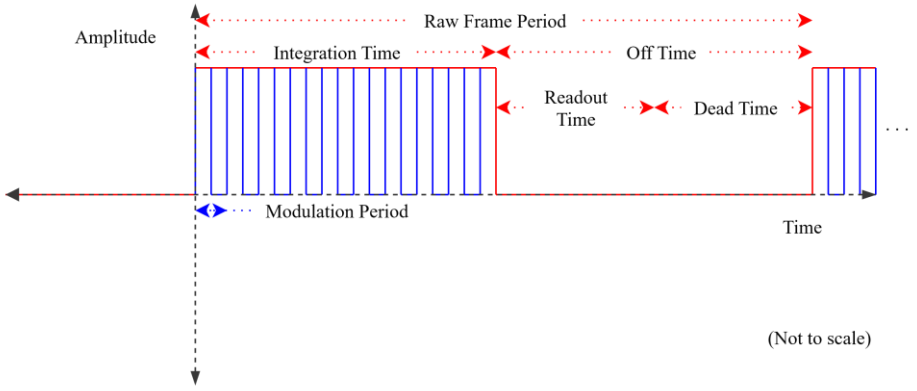

Figure 5.1.1: Diagram showing the concept of the Integration time switching waveform.

A typical Integration time and Off time for the Kea light source is approximately 2 ms for each, hence a 50% duty cycle ratio. During the Integration time, the lasers are modulated with a 50% duty cycle at a frequency of around 50 MHz (10 MHz to 100 MHz) (Dr Refael Whyte, Chronoptics Ltd, personal communication, July 8, 2019).

In hardware, the light source electrical input and optical output power is measured as average power over a number Integration and Off times. For the light source simulation, the time period of the data capture must be near the same order of magnitude as the light source modulation frequency. Otherwise, the time divisions of the simulations will be too large to produce good resolution in the simulation results, or the simulation will take too long to run. There are six orders of magnitude between the typical Integration and Off time period of 4 ms (2 ms Integration plus 2 ms Off time) and the 10 ns modulation period for the maximum light source modulation frequency of 100 MHz. So, the simulation cannot be run for the full Integration and Off time. To solve this problem, the simulation is run without the Off time, for ten periods of the modulation signal. The lack of Off time in the simulation is accounted for by halving the average if the instantaneous simulated electrical input and optical output power. The average is halved as 50% duty cycle ratio is used for the Integration switching in the hardware measurements. Initially, it was decided that Integration time switching would not be used to simplify the experiment. However, the Kea light source PCB became too hot (greater than 90°C) when Integration time switching was not used. So, it is necessary to enable Integration time switching in the hardware measurements.

5.2 Electrical input power measurement

5.2.1 Light source operating range considerations

The TIDA-01173 and Kea light sources have different current and modulation frequency operating ranges (Table 5.2.1). Modulation frequency range is the range of modulation frequencies that the light source driver can switch the laser diodes on and off. Current setting range is the range of digital values configured in software to set the modulation current driven through the laser diodes. Modulation current range is the range of average currents that is expected to be driven through the laser diodes given the current setting range.

Table 5.2.1: Table showing the TIDA-01173 and Kea light sources typical operating ranges. Modulation current range is the theoretic peak current expected and is calculated from typical operating values obtained from the component datasheets used in the light sources.

Light Source	Modulation Frequency Range	Modulation Current Setting Range	Modulation Current Range (peak)
TIDA-01173	10 to 100 MHz [1]	255/255 to 0/255	1.12 to 2.29 A
Kea	DC to 200 MHz [52]	0/1023 to 470/1023	0 to 1.48 A

Chronoptics has limited the modulation current setting DAC value in the Kea ToF camera to a maximum of 470. The maximum DAC value of 470 produces 2.30 V on the output of the modulation current DAC,

$$V_{\mathrm{DAC}} = \frac{V_{\mathrm{DD}}}{1023} \cdot \mathrm{DAC}$$

$$V_{\mathrm{DAC}} = \frac{5\,V}{1023} \cdot 470 = 2.30\,V, \tag{5.2.1}$$

where DAC is the DAC register value, V_{DAC} is the voltage of the output of the DAC, and V_{DD} is the supply voltage of the DAC. The DAC output voltage sets the iC-HG modulation current setting voltage, V(CIx), to 2.30 V. The V(CIx) input voltage corresponds to a continuous laser current of 0.74 A for each laser diode driver channel input (LDKx) of the iC-HG, according to the iC-HG datasheet at a V_{DD} of 5 V (Figure 5.2.1). Each laser diode in the Kea light source has two LDKx channels, so the modulation current per laser diode is 1.48 A (double 0.74 A).

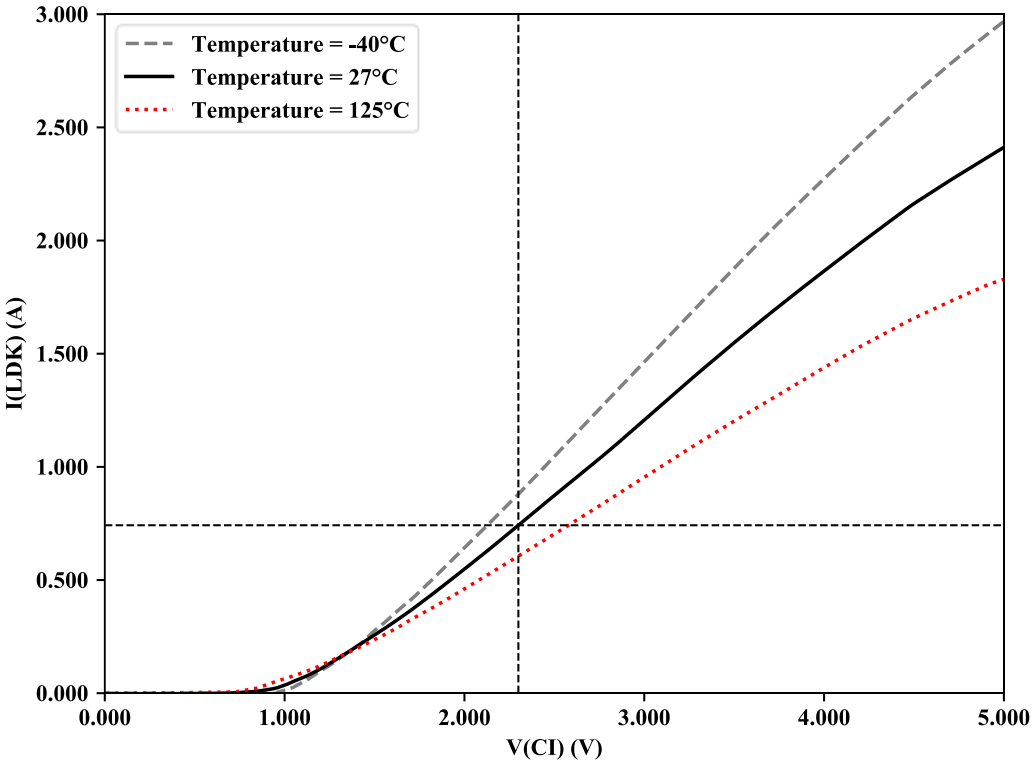

Figure 5.2.1: iC-HG LDKx channel current, I(LDKx), as a function of current setting voltage, V(CIx), at a VDD of 5V (data obtained from the iC-HG datasheet [3]).

To compare the efficiency of the two light sources, the operating range of the efficiency measurements of the two light sources must be the same. The Kea light source has a much wider operating range of modulation frequencies than the TIDA-01173 light source. The operating frequency range of the Kea light source includes the operating range of the TIDA-01173 (10 to 100 MHz), so the modulation setting range of the experiment was set to between 10 to 100 MHz. However, the Kea light source has a much lower maximum modulation current than the TIDA-01173 light source's maximum modulation current, so their modulation current ranges only overlap within a small range of modulation currents (1.12 to 1.48 A) in comparison to the full operating range of the light sources. It is possible to extend this overlap in the operating ranges by increasing the maximum DAC limit on the Kea light source to a value above 470. However, doing so risks damaging the iC-HG laser driver IC in the Kea light source due to exceeding the maximum power dissipation, so this is not attempted. An alternative to increasing the maximum Kea modulation

current is to decrease the TIDA-01173 minimum modulation current. However, this cannot be done without modifying the physical current limiting circuit of the TIDA-01173 light source, so this will also not be attempted. The modulation current range of the power efficiency benchmark will be measured for the full range for each of the Kea and TIDA-01173 light sources, and the comparison of the power efficiencies of the light sources will have to acknowledge that the modulation current overlap range is small in comparison to the full operating range of each of the light sources.

5.3 Input power meter

An Input Power Meter (IPM) is designed to control both the TIDA-01173 and the Kea light sources, measure their electrical input power, and interface the light source controls and measurements with a desk top Personal Computer (PC) to automate the power efficiency measurements. An Arduino Uno microprocessor development board controls the IPM, so the IPM Printed Circuit Board (PCB) is designed with the standard Arduino Uno Shield form factor [83], [84] (Figure 5.3.1).

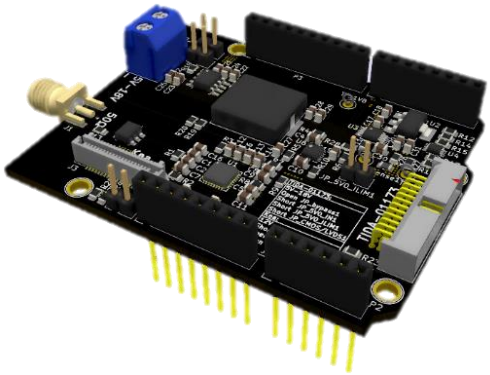

Figure 5.3.1: Computer generated image of the Input Power Meter PCB Arduino Uno Shield.

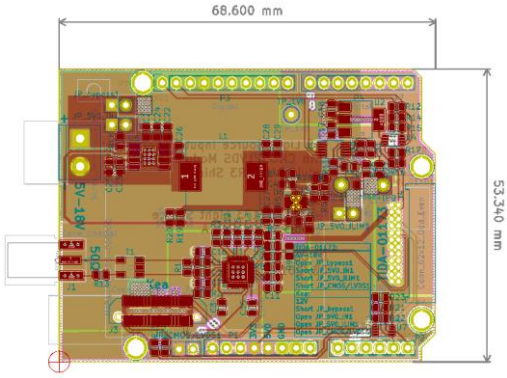

Figure 5.3.2: Input power meter PCB layout.

The diagram of the IPM circuit is shown in Figure 5.3.3. The main functions of the IMP are input power measurement, control of the TIDA-01173 and Kea light source boards, and interface to desktop computer for automated measurements.

Arduino Uno Rev3 Connector

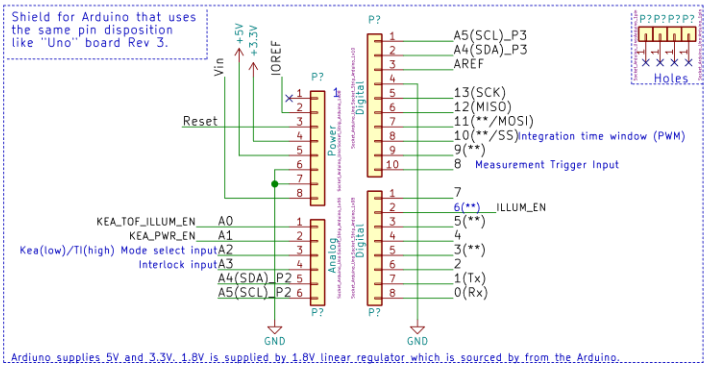

KEA Light Source Connector

TI Light Source Connector

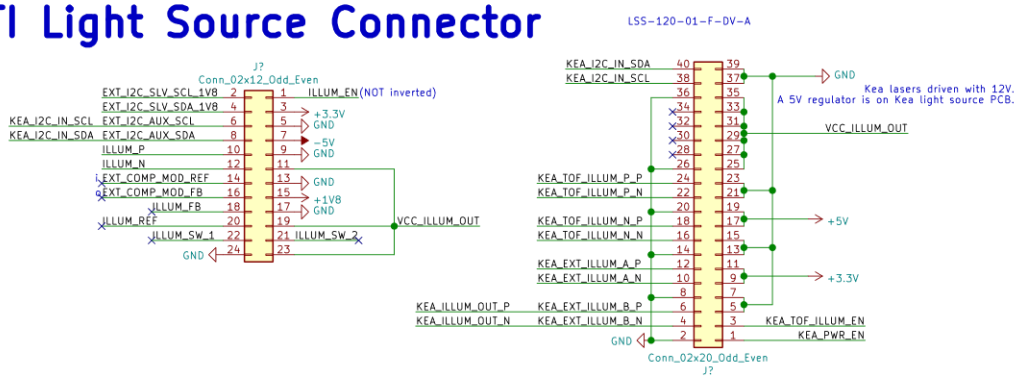

I2C 5V to 1.8V

I2C 5V to 3.3V

I2C Level Shifters

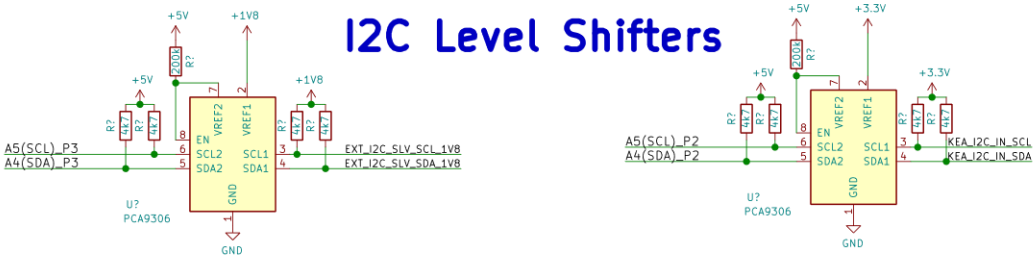

1.8V Regulator

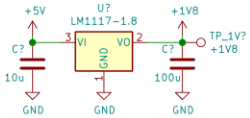

a)

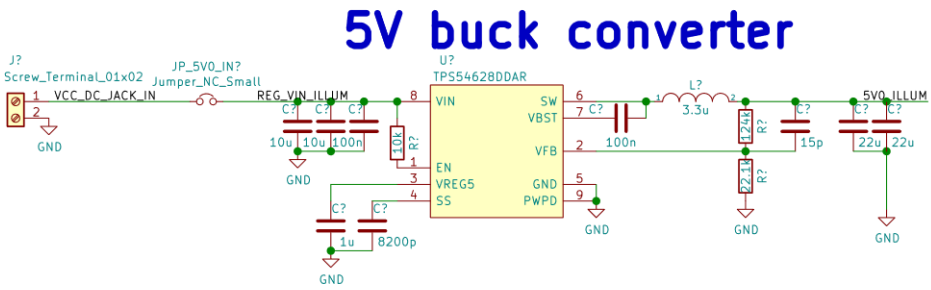
5V buck converter
J?
Screw_Terminal_01x02
VCC_DC_JACK_IN
GND
JP_5V0_IN?
Jumper_NC_Small
REG_VIN_ILLUM
U?
TPS54628DDAR
VIN
SW
VBST
VFB
EN
VREG5
SS
GND
PWPD
L?
3.3u
100n
10u
10u
100n
10k
124k
22.1k
15p
22u
22u
1u
8200p
5V0_ILLUM

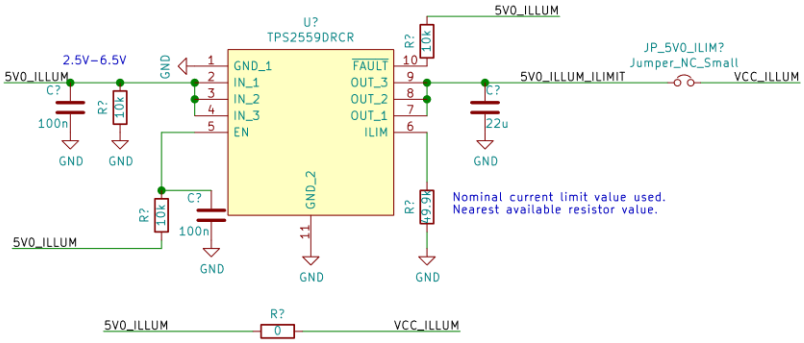
TI Current limiter
U?
TPS2559DRCR
2.5V-6.5V
5V0_ILLUM
GND_1
IN_1
IN_2
IN_3
EN
FAULT
OUT_3
OUT_2
OUT_1
ILIM
GND_2
JP_5V0_ILIM?
Jumper_NC_Small
5V0_ILLUM_ILIMIT
VCC_ILLUM
100n
10k
22u
10k
10k
100n
49.9k
Nominal current limit value used.
Nearest available resistor value.
R?
0

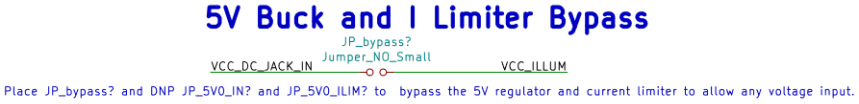
5V Buck and I Limiter Bypass
JP_bypass?
Jumper_NO_Small
VCC_DC_JACK_IN
VCC_ILLUM
Place JP_bypass? and DNP JP_5V0_IN? and JP_5V0_ILIM? to bypass the 5V regulator and current limiter to allow any voltage input.

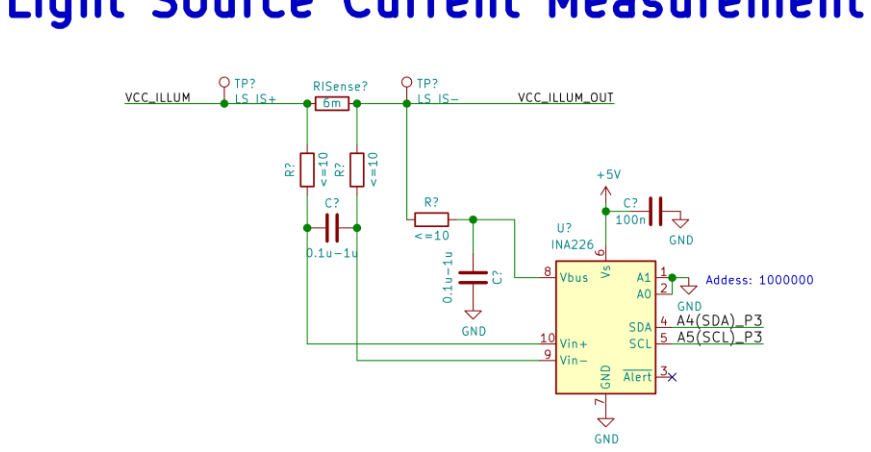
Light Source Current Measurement
VCC_ILLUM
TP?
LS IS+
RISense?
6m
TP?
LS IS-
VCC_ILLUM_OUT
<=10
<=10
0.1u-1u
<=10
0.1u-1u
+5V
100n
U?
INA226
Vbus
Vs
Vin+
Vin-
GND
Alert
A1
A0
SDA
SCL
Addess: 1000000
A4(SDA)_P3
A5(SCL)_P3

b)

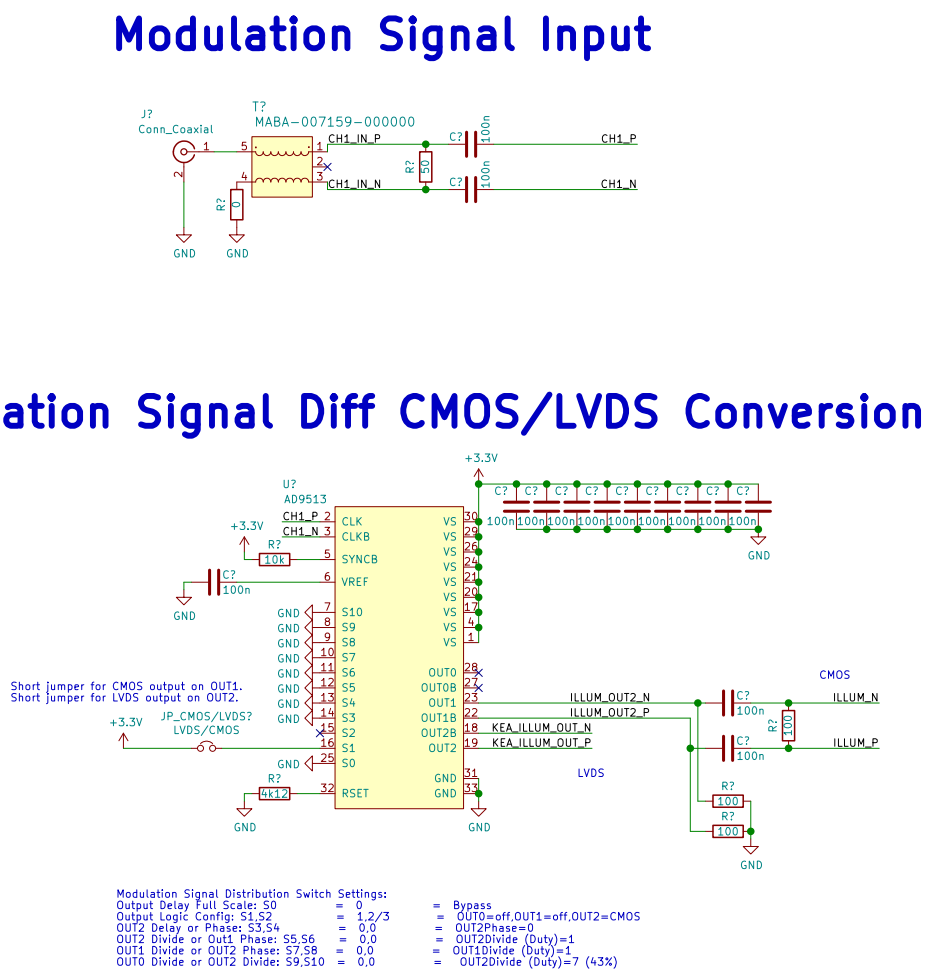

c)

Figure 5.3.3: Input power meter circuit PCB schematic broken into parts: a) interface input output (IO), b) power, and c) modulation signal.

The IPM measured the electrical input power of the connected ToF camera light source, either the TIDA-01173 or Kea light source, using an INA226 current and power monitor (Texas Instruments, Dallas, Texas). The INA226 measures the input voltage and the voltage across a series current sense resistor. The voltage across the current sense resistor supplies the INA226 with a measurement for the input current. The input power is calculated in the INA226 by multiplying the measured input current with the input voltage. The Arduino Uno is programmed to read the power measurement from the INA226 IC via the I^2C bus. The INA226 was set to take a measurement every 140 µs and average over 1024 measurements for each input power reading. The shortest measurement time and largest number of measurements used in the averaging is selected to maximise the accuracy of the electrical input power measurements [85].

The IPM is designed to interface with the TIDA-01173 and Kea light sources, so the TIDA-01173 and Kea circuits were used as the basis of the IPM circuit. An SHF-112-01-L-D-RA connector (Samtec Incorporated, New Albany, Indiana) is used to connect the TIDA-01173 light source board to the IPM via a ribbon connector (Figure 5.3.4: Input power meter in the TIDA-01173 light source configuration.). While a separate LSS-120-01-F-DV-A mezzanine (board to board) connector (Samtec Incorporated, New Albany, Indiana) is used to directly mount the Kea light source board onto the IPM (Figure 5.3.5).

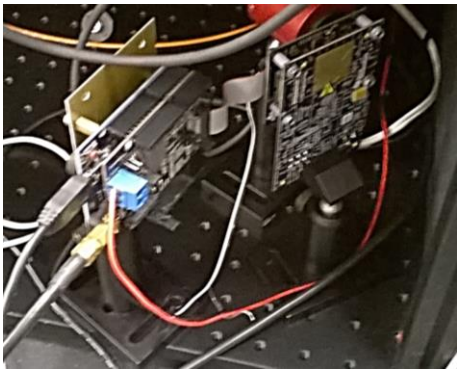

Figure 5.3.4: Input power meter in the TIDA-01173 light source configuration.

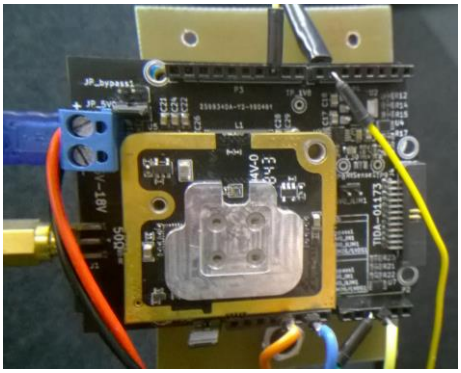

Figure 5.3.5: Input power meter in the Kea light source configuration.

The TIDA-01173 light source requires a supply voltage of 5 V to drive the lasers. A 5 V buck regulator on the IPM supplied this 5 V to the TIDA-01173 light source board. The 5 V regulator was supplied with 12 V from an external power supply connected to the terminal connector on the IPM. The Kea light source also required a 5 V supply to drive the lasers, but the Kea light source board had a 5 V buck regulator built in, so 12 V was supplied to Kea's 5 V regulator by bypassing the 5 V regulator on the IPM using a jumper (JP_bypass1).

The TIDA-01173 and Kea light source boards are not designed to be connected to the IPM at the same time. The IPM must be configured appropriately, depending on what light source board is connected to the IPM. To change the configuration of the IPM for each light source board, jumper connectors on the IPM must be set to either short or open circuit as shown in Table 5.3.1. Due to design errors in the IPM, some changes were made to the IPM circuit board during the bring up process of the PCB that meant that the jumper settings had to be changed from their originally intended use. The original jumper settings are shown in Appendix A, Table A.3.

Table 5.3.1: Modified input power meter PCB jumper settings for use with the TIDA-01173 or Kea light sources.

IPM Jumper Label	**IPM Jumper Settings**	
	TIDA-01173	Kea
JP_bypass1	Open	Shorted
JP_5V0_IN1	Shorted	Open
JP_5V0_ILIM1	Open	Open
JP_CMOS/LVDS1	Shorted	Shorted
Arduino Uno Pin A2	High	Low

The interlock input was connected to one of the Arduino Uno's General-Purpose Input Output (GPIO) pins so that if the laboratory door is opened when the light source lasers were on, they would automatically be disabled as a safety feature.

The Integration switching time signal (Section 5.1.1) is produced by the software on the Arduino Uno connected to the IPM. This Integration switching time signal is emitted from the Arduino Uno GPIO pin A3 which is connected to the illumination enable input pin of the TIDA-01173 light source connector. In the benchmark tests, the SMY02 signal generator (Rohde & Schwarz GmbH & Co KG, Munich, Germany) that is used to produce the modulation signal, mixes the

Integration time signal with the modulation signal so that the Kea light source also has the Integration time switching.

The integrated circuits on both the TIDA-01173 and Kea light sources have I^2C bus capability, but they use different voltage levels (1.8, and 3.3 V). The IPM has I^2C level shifters to accommodate these different I^2C voltage levels and enable the Arduino Uno to control the light sources via its 5 V I^2C bus.

The modulation current for the TIDA-01173 light source was controlled using the TPL0102-100PWR digital potentiometer (Texas Instruments, Dallas, Texas) located on the TIDA-01173 light source. The Arduino Uno connected to the IPM controlled the digital potentiometer, and therefore the modulation current via the I^2C bus. The modulation current for the Kea light source was also controlled via I^2C, but the DS3911T DAC (Maxim Integrated, San Jose, California) on the Kea light source board was used instead.

The External modulation signal can be sine or square wave and is sourced from a signal generator. The modulation signal from the signal generator enters the IPM via an SMA connector. The modulation signal is converted using the AD9513 clock distribution IC (Analog Devices, Norwood, Massachusetts) in the IPM to a Low Voltage Differential Signal (LVDS) for the Kea light source, and a differential CMOS voltage level signal for the TIDA-01173 light source. The frequency and duty cycle ratio of the modulation signal is set by the external signal generator, for these experiments the SMY02 signal generator was used.

Both the TIDA-01173 and Kea light sources contain temperature sensor ICs. The IPM receives the temperature data from the light sources via I^2C. Temperature measurements of the light sources is required for the power efficiency benchmark as the power measurements are taken only when the light source reaches a steady state temperature.

The Arduino Uno, connected to the IPM, connects to a desktop PC via a USB interface. A serial Command Line Interface (CLI), programmed into the Arduino Uno, is used to control and receive data from the IPM and light sources so that the input power measurements of the light sources can be taken.

5.4 Optical output power measurement

5.4.1 Beam splitter direct coupled method

In the absence of an integrating sphere (as described in section 4.3.4), the measurement of the light source optical output power was originally attempted using an apparatus created to directly couple the light source laser beam into an optical power meter. The apparatus, shown in Figure 5.4.1 and Figure 5.4.2, is constructed. This apparatus uses a beam splitter to direct part of the beam to the S302C thermal power sensor head (Thorlabs, Newton, New Jersey) and the other part to a DET01CFC high-speed fibre-coupled photodiode (Thorlabs, Newton, New Jersey) so that the average optical power and the waveform could be measured at the same time. The beam is shaped using two 1-inch diameter lenses. The first is a Fresnel lens, and the second a bi-convex lens, with focal lengths of 25 mm and 300 mm respectively. The lenses are selected and positioned to form the light emitted from the light source laser diode into a beam with a Full Width at Half Maximum (FWHM) diameter of 12 mm on the thermal optical power meter sensor. The Fresnel lens had to be used because no other type of lens could be sourced with 1-inch diameter and a focal length short enough to collimate the laser FWHM beam to a diameter of less than 1-inch. The distortion in the beam created by the Fresnel lens is not a problem because the only result required from this setup was the measurement of optical power.

The beam splitter direct coupled method did not work because it was too difficult to align the light source into the apparatus ensuring that the laser beam was centred on the thermal optical power meter sensor head. Additionally, only one of the four laser diodes on the light sources could be measured at any one time. This was a problem as each laser diode produced a different optical output power. So, each laser on each light source would have had to be individually tested, this would have taken four times longer to measure efficiency of the light sources. Individually testing each laser diode may have also introduced other problems, such as, different light source temperatures for each test.

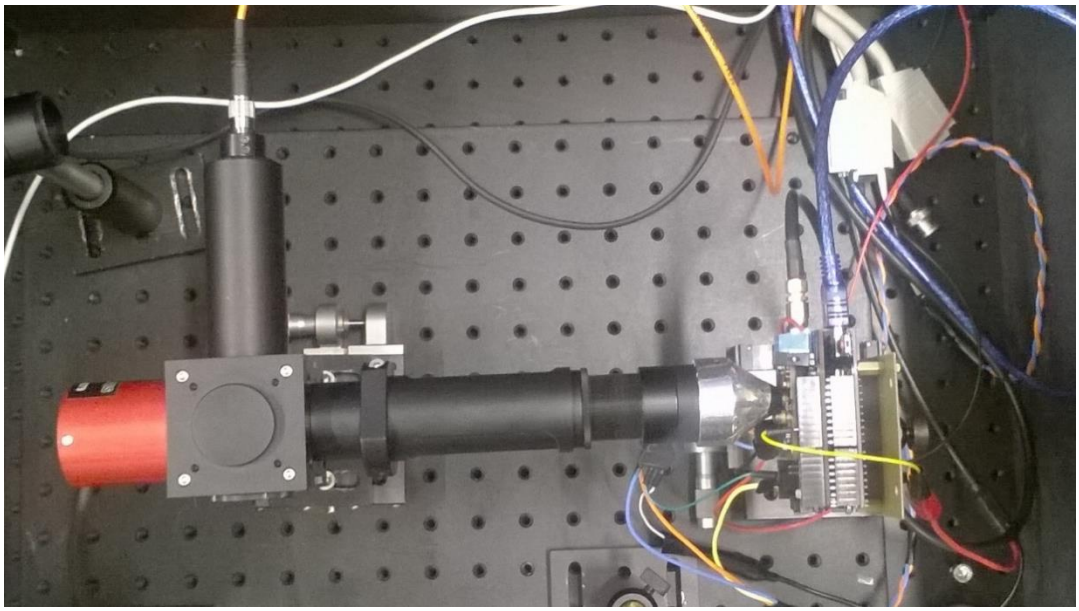

Figure 5.4.1: The beam splitter optical power measurement apparatus.

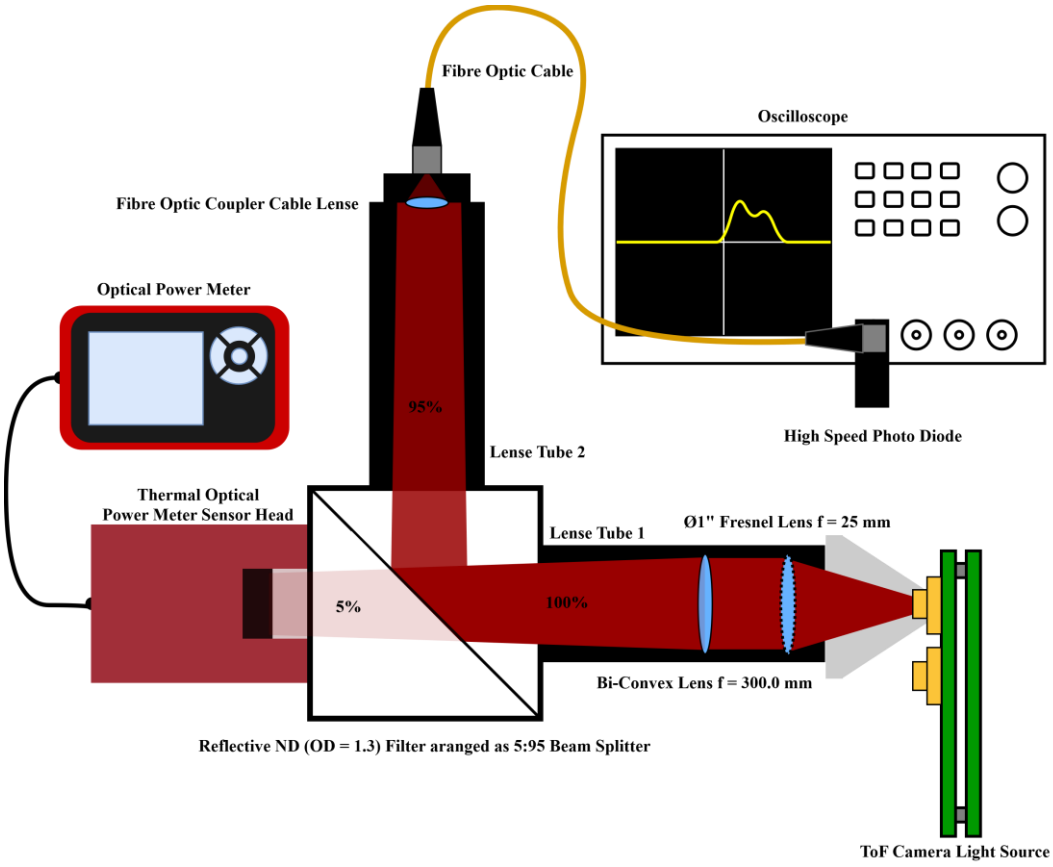

Figure 5.4.2: Diagram of the beam splitter optical power measurement apparatus showing the laser beam path.

5.4.2 Beam cross-section image method

Another optical output power measurement method was designed to avoid the problems of alignment and the single laser diode measurement, identified with the beam splitter direct coupled optical power measurement method (section 5.4.1). This new method uses a camera instead of the optical power meter to capture an image of the cross-section of the light source laser beams projected onto an optical diffusor (Figure 5.4.3). The laser beams from the light source being tested is projected through opal diffusing glass and the image captured using a DMK 23GP031 GigE monochrome industrial camera (The Imaging Source, Bremen, Germany).

The camera software is set to capture an image with a resolution of 1600×1600 pixels, so the whole laser beam cross-section for both the TIDA-01173 and Kea light sources is imaged. The laser diodes used in the TIDA-01173 and Kea light sources produce an elliptical beam, as they are edge emitting lasers. The laser diodes in the TIDA-01173 light source PCB are mounted at an orientation that is 90° to the orientation that they are mounted on the Kea light source PCB. So, the fast axis of the elliptical beams for the TIDA-01173 light source is horizontal, while for Kea, it is vertical. This elliptical beam shape is shown in the cross-section beam examples in Figure 5.4.4, Figure 5.4.5, Figure 5.4.6, and Figure 5.4.7. The aperture on the camera lens is set and locked so that the image is not saturated at the 0.008 s exposure for the TIDA-01173 light source. The maximum pixel values are around 130 to 140 out of 255 for the maximum expected light output. The current setting was set to maximum current and the modulation frequency was set to 10 MHz which produces the maximum optical output power of the TIDA-01173 light source. So, the TIDA-01173 light source (which, from previous experience was shown to have an optical output power that is higher than the Kea light source) did not saturate the image at its maximum output power for the shortest exposure time. Therefore, the Kea light source will also not saturate the image.

The DMK 23GP031 GigE camera is hardware frame synchronised to the Integration time switching signal of the light source to ensure that full periods of the Integration switching time is captured.

Once the cross-section image is captured, pixels in the image are summed to produce a value that is proportional to the average optical output power of the light source. A calibration is then applied to the sum of the cross-section image to produce the absolute average optical output power of the light source with units of Watts. The imaging method is easier to align than the beam splitter direct coupled method (section 5.4.1) and allows the light source diffusor to be left on during the measurement, potentially providing a measurement of power that is representative of when the light source is used as part of the camera system. In the imaging method, the light source must be aligned at right angles to the face of the diffusor between changing light sources. The alignment of the camera and diffusor is kept the same for all light source measurements. The ToF camera light source diffusors do not have to be removed, but they were removed for the benchmark measurements so that possible differences in efficiency between the TIDA-01173 and Kea diffusors could not affect the results. The safety precautions developed to manage the hazards associated with lasers, described in section 4.2, were strictly adhered to, as removing the diffusors creates an increased risk.

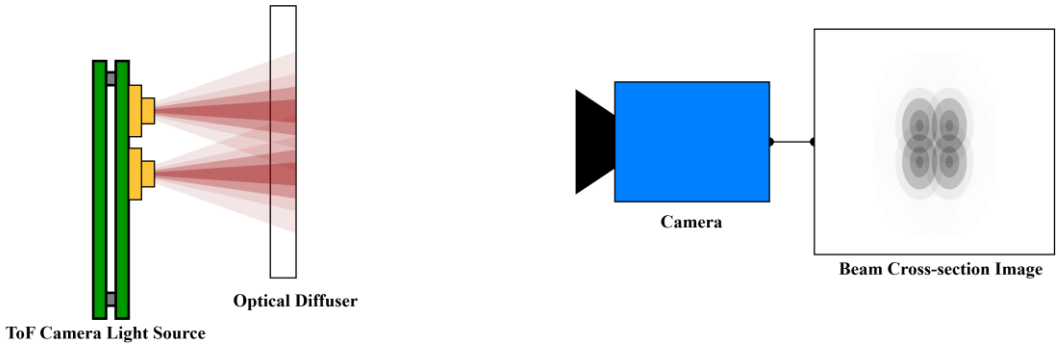

Figure 5.4.3: Diagram of the cross-section image optical power measurement apparatus and an example of the beam cross-section image.

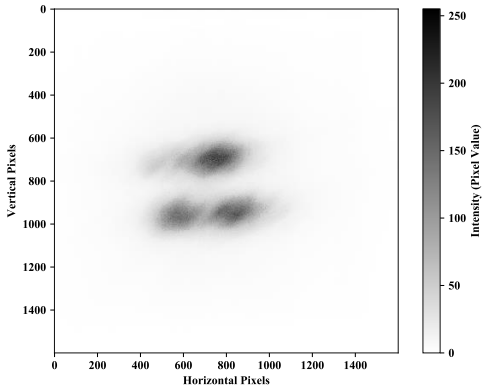

Figure 5.4.4: TIDA-01173 light source beam cross-section image with modulation frequency of 10 MHz and Current setting digital potentiometer set to 0.

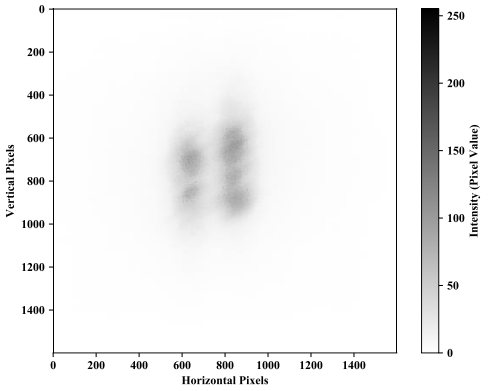

Figure 5.4.5: Kea light source beam cross-section image with modulation frequency of 10 MHz and Current setting DAC set to 470.

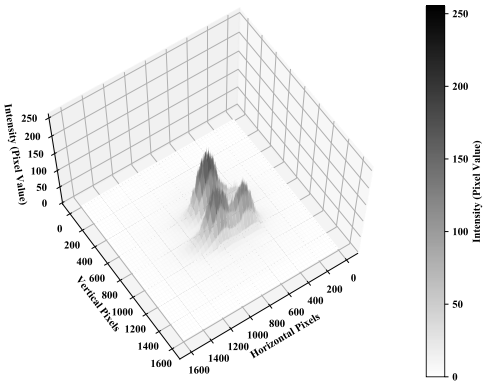

Figure 5.4.6: TIDA-01173 light source beam cross-section image (Figure 5.4.4) surface plot.

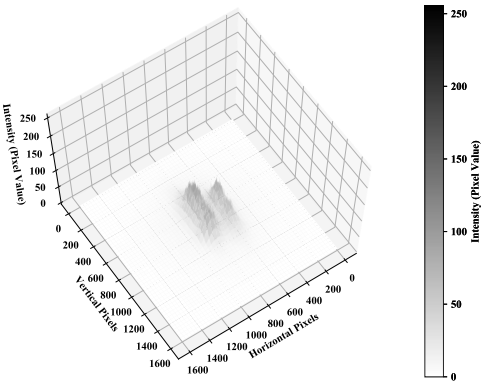

Figure 5.4.7: Kea light source beam cross-section image (Figure 5.4.5) surface plot.

The TIDA-01173 light source example cross-section image has higher optical output power than that of the Kea light source. This is simply because both light sources were configured to their maximum modulation current, and TIDA-01173 has a substantially higher modulation current than the Kea light source (Table 5.2.1). The light source beam cross-section images of the light sources show that the optical output power is not evenly distributed between all the laser diodes. This uneven distribution is more pronounced in the TIDA-01173 example. The uneven distribution of optical output power between the laser diodes is likely due to manufacturer variability of the laser diodes. The greater uneven distribution of

optical output power in the TIDA-01173 light source example is because one of the laser diodes has a substantially reduced optical output power. This may be due to manufacture variability, or the laser diode may be damaged. It will be assumed to be manufacture variability as another TIDA-01173 light source was not available to provide a comparison.

5.4.3 Optical power measurement calibration

A calibration apparatus is constructed to generate the optical output power calibration function for the beam cross-section image optical output power measurement method (section 5.4.2). The calibration apparatus has a similar setup to that of the cross-section image optical power measurement apparatus (Figure 5.4.3), but a light blocking screen with an aperture was placed between the light source and diffusor. The light blocking screen was constructed by fixing a 1-inch lens tube to the thermal optical power meter sensor head adapter through a hole in a sheet of cardboard (Figure 5.4.8).

Figure 5.4.8: Light blocking screen with thermal optical power meter sensor head adapter mounted, acting as an aperture.

For the power meter measurements, the power meter sensor head is mounted to the adapter (Figure 5.4.9). For the camera measurements, the power meter head is swapped for the opal glass diffuser (Figure 5.4.10). The adapter acts as the aperture, so the power meter sensor and camera collect the same amount of light. Photos of the setup are shown in Figure 5.4.11, Figure 5.4.12, Figure 5.4.13, and Figure 5.4.14.

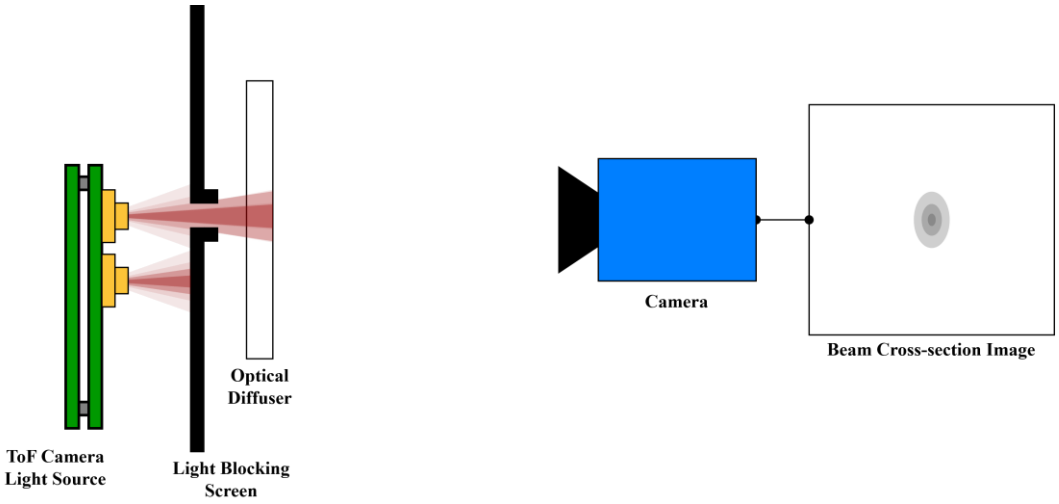

Figure 5.4.9: Beam cross-section optical power measurement apparatus calibration setup diagram showing measurement with optical diffusor and camera.

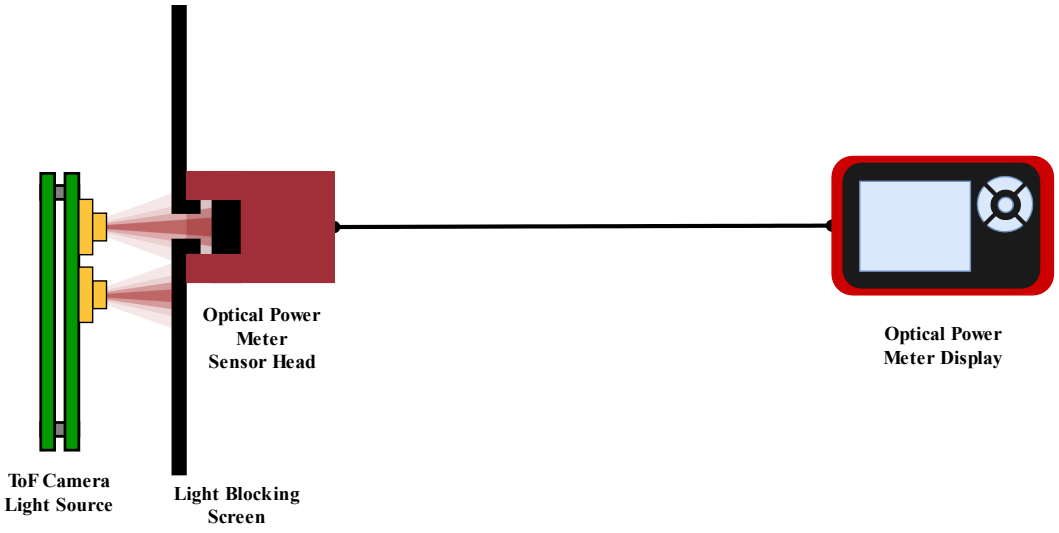

Figure 5.4.10: Beam Cross-section optical power measurement apparatus calibration setup diagram showing optical measurement with optical power meter.

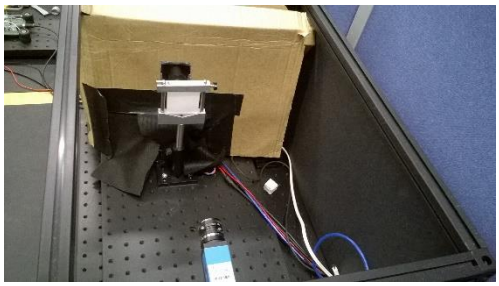

Figure 5.4.11: Front view photo of the calibration apparatus set up for cross-section image.

Figure 5.4.12: Front view photo of the calibration apparatus set up for optical power measurement.

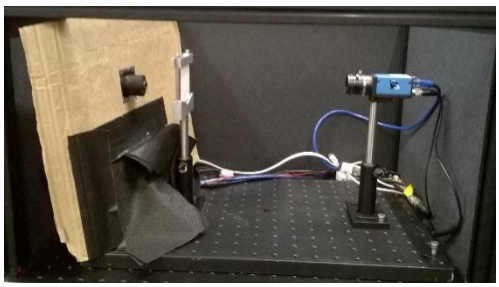

Figure 5.4.13: Side view photo of the calibration apparatus set up for cross-section image.

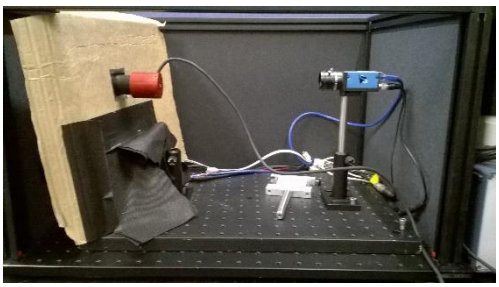

Figure 5.4.14: Side view photo of the calibration apparatus set up for optical power measurement.

The Thorlabs S302C thermal power sensor contains the National Institute of Standards and Technology (NIST, USA) and Physikalisch-Technische Bundesanstalt (PTB, Germany) traceable calibration data in non-volatile memory in the sensor connector [86]. If the calibration is accurate, then the optical power measurements using the cross-section image method will provide an absolute optical power measurement. This allows an absolute power efficiency measurement to be made for the electrical to optical power efficiency benchmark.

The Kea light source was used in the calibration. Kea was used instead of the TIDA-01173 because Kea has a greater range of modulation current settings than the TIDA-01173, therefore a greater range of optical output powers, and thus providing a greater range of datapoints for the calibration plot.

The data collection for the calibration plot is automated using a Python script. This allows for many samples to be easily taken and eliminates possible transcription errors. The optical output power of the light that passed through the

aperture of the mount is measured with the thermal optical power meter from modulation current DAC settings of 320 to 470. The modulation frequency of the Kea light source is set to 10 MHz, as this modulation frequency is suspected to have the highest optical output power. These measurements are repeated using the cross-section image method by removing the optical power meter from the mount, so the mount remains and acts as an aperture through which the light from the light source passes and projects on to the diffusor. The sum of pixel values produced from these measurements is plotted against the optical power meter measurements to produce the calibration plot (Figure 5.4.15).

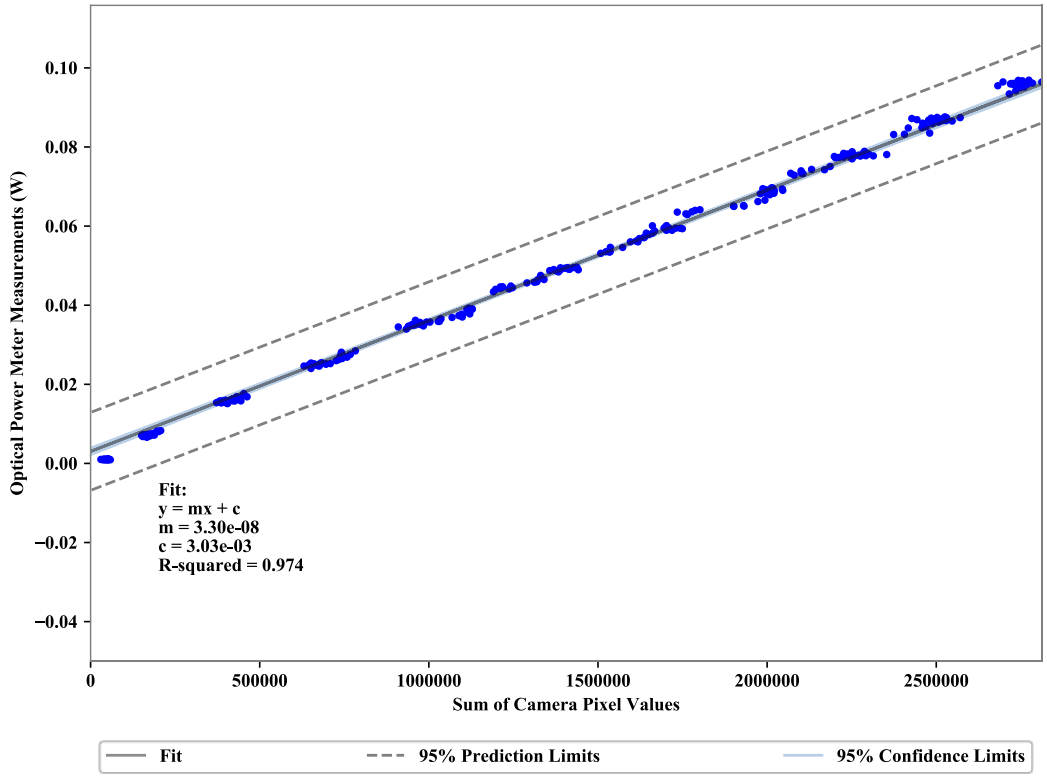

Figure 5.4.15: Beam cross-section image ToF camera light source optical power measurement calibration plot.

A fitted line is added to the calibration plot along with 95% prediction and confidence limits. The calibration plot has a good linear fit with an R-squared value of 0.974. The calibration function fit was made using the Python NumPy polyfit function [87] with the degree variable set to 1 so that it produces a linear fit. The polyfit function uses the least squares polynomial fit method [88, Ch. 2]. The

method used for the 95% prediction and confidence limits is described in [88, Ch. 2].

The fit is extrapolated out to the optical output powers that are expected to be produced by the TIDA-01173 and Kea light sources (Figure 5.4.16). This is an extrapolation of 10 times the range of measured values. At the extent of this extrapolation (at the sum of camera pixel values of 30,000,000), the 95% confidence limits approach the 95% prediction limits which are ±0.02 W from the fitted calibration line.

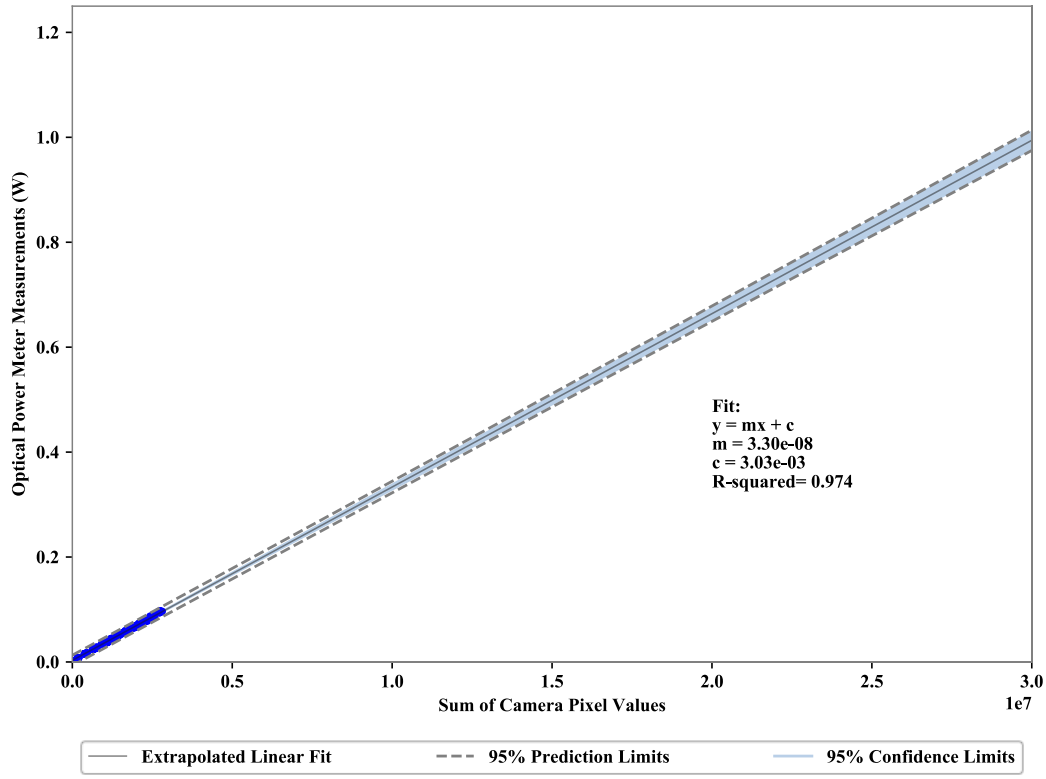

Figure 5.4.16: Extrapolated calibration plot.

The 95% prediction limits are shown as the dashed lines in the calibration plots (Figure 5.4.15 and Figure 5.4.16). Away from the endpoints of the light sensor range limits, we may assume that observed linearity in the relationship holds over the extrapolated range, and 95% of the optical power measurements will be within the 95% prediction limits. The 95% confidence interval is shown as the filled region in the calibration plots (Figure 5.4.15 and Figure 5.4.16). There is 95% probability that the true best fit line of the measurements for the calibration function lies within

the 95% confidence limits. The prediction and confidence limits show that the uncertainty associated with the calibration function gets worse the further it is extrapolated from the measured data. When the calibration function is applied to the light source optical output power measurements in the hardware benchmark, these uncertainties must be considered.

Extrapolating 10 times is a large extrapolation. It is better to collect datapoints nearer to the expected ToF camera light source optical output power range, so that the fit does not need to be extrapolated. However, the light source must be substantially more powerful and must be measurable with the thermal optical power meter. For this purpose, a collimated laser with computer controllable optical output power up to 1 W is required, however one was not available.

5.5 Automated ToF light source efficiency measurements (Python script)

The temperature settling time for the light sources between random samples of modulation current and frequency settings is four minutes on average. Hundreds of samples (at different modulation laser current settings and frequencies) are required for the benchmark measurements, so with an average of four minutes per sample, the total time for each light source benchmark will be several hours to days long. It is not practical for measurements of the light source benchmark to be taken manually, so automation is required. To automate the light source power efficiency benchmarks, the hardware is assembled as shown in the block diagram in Figure 5.5.1.

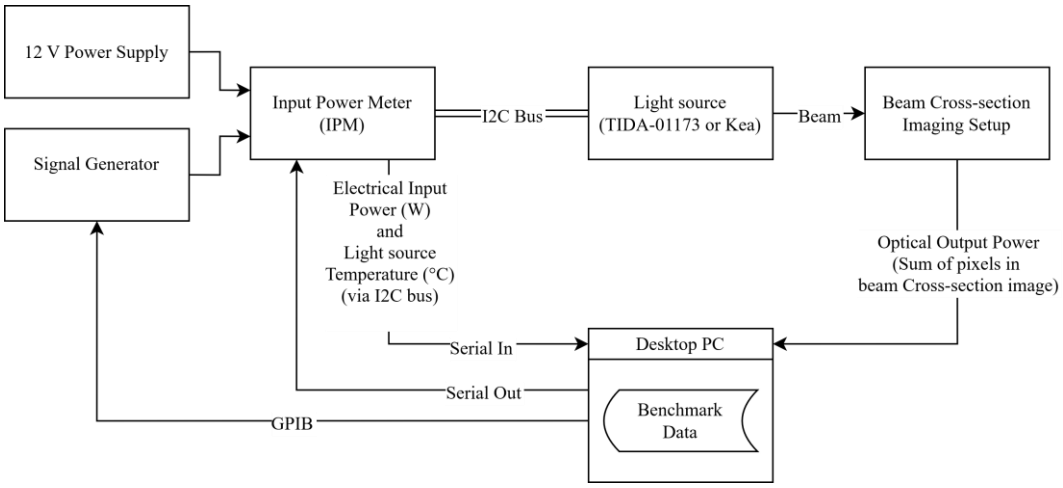

Figure 5.5.1: ToF camera light source electrical input power to optical output power efficiency benchmark automation apparatus block diagram.

A Python script generates a randomised table of the sample current values and controls the automated measurement process automatically. The simplified flow diagram of the Python automation script designed for the ToF camera light source power efficiency benchmarks is shown in Figure 5.5.2.

This automation script begins by connecting to the light source via a serial interface. The light source connected to the IPM is automatically detected. Each light source has a different interface Python library, so once the light source is detected, the appropriate light source Python library is loaded. A sample table of randomised modulation current settings and frequencies within the operating range of the light sources is generated. The script then enters a loop where it sets the light source's modulation current and frequency settings for each value in the sample table. For each of these samples, the temperature of the light source is monitored to detect when the temperature has reached a steady state. Once the light source reaches a steady state, the average electrical input and optical output power measurements are taken.

A High Dynamic Range (HDR) routine is used when capturing the beam cross-section images, to increase the intensity resolution of the image. HDR allows both very low and high intensity parts of the beam to be imaged without saturating the camera image sensor for high intensity measurements. The HDR routine captures three cross-section images with exposures of 8 ms in multiples of three: 8 ms, 24 ms, and 72 ms. These three cross-section images are rescaled by multiplying by 9, 3, and 1 respectively. Starting with the longest exposure time image and sequentially working to the shortest exposure image, pixel values approaching saturation are replaced with the rescaled values for the next shortest exposure image, forming the HDR image. Another HDR image is taken with the light source turned off. This image is subtracted from the initial HDR image to account for background light, and dark noise. The optical output power is calculated by summing the values of pixels in the HDR cross section image.

The time that it takes to run each sample is measured and used to estimate the end time of the benchmark which is a useful feature when planning the times that the benchmark is run. Each sample is recorded to a file on the desktop PC's hard drive so that the measurements are not lost if the benchmark is interrupted. The script has the ability to restart the benchmark in the case that it is interrupted. The optical output power values recorded are just the sum of the HDR beam cross-section images, so the calibration must be applied in post processing.

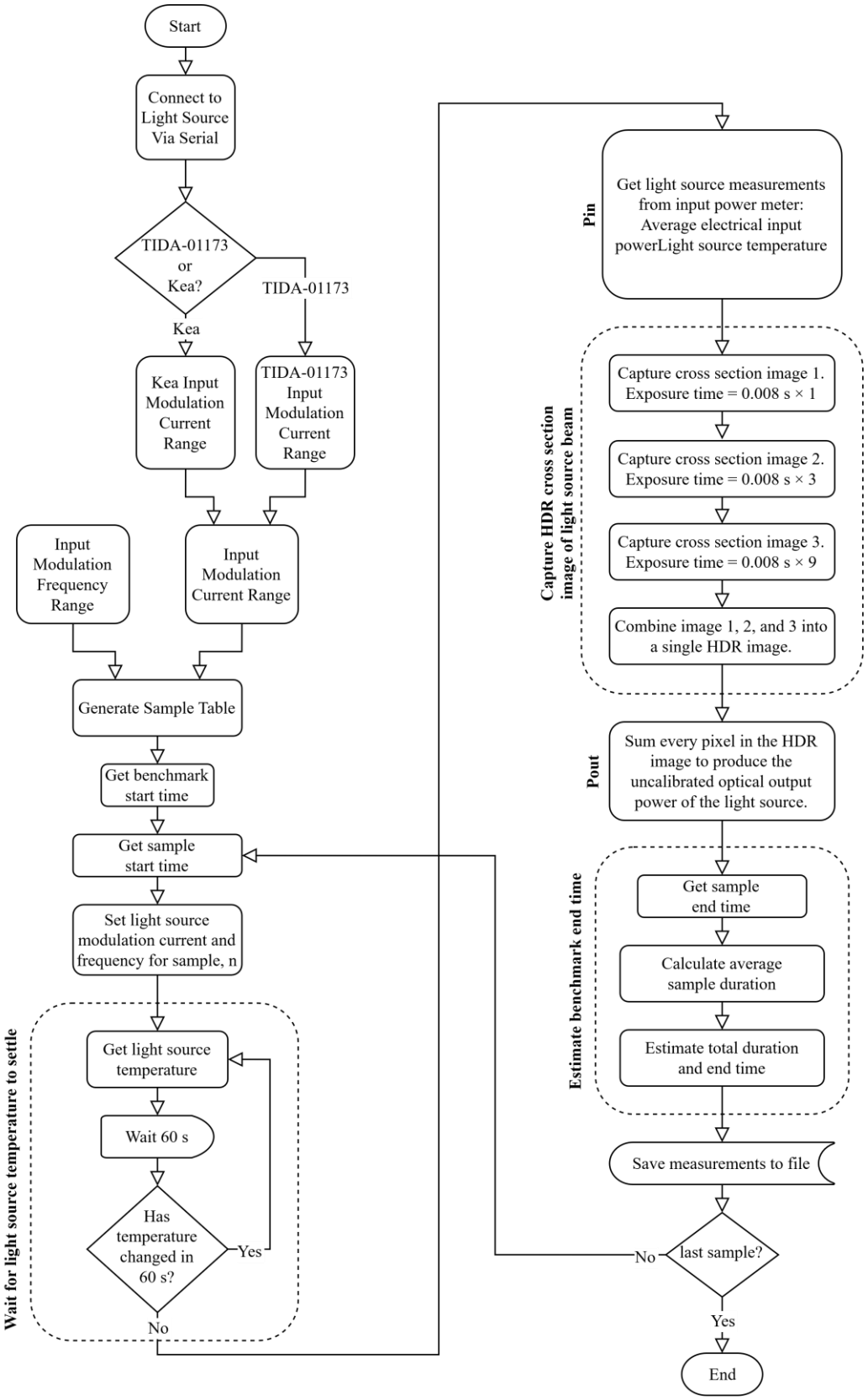

Figure 5.5.2: Simplified flow diagram of the Python script used to automate the light source power efficiency measurements.

If the ToF camera light source benchmark apparatus is going to be used for future work, such as for automated quality control testing for Chronoptics, some improvements need to be made to the automation script. The Python script was modified many times throughout the development of the benchmark automation, so it needs to be refactored. A user interface needs to be created in the form of either a Command Line Interface (CLI) or Graphical User Interface (GUI), to make it easier to use.

5.6 Conclusion

An IPM was created to measure the electrical input power of both the TIDA-01173 and Kea ToF camera light sources. The IPM also acts as the interface to the light sources so that their modulation current settings can be configured, and their temperature measured. The IPM was used in an automated ToF camera light source electrical input to optical output power efficiency benchmarking apparatus. A Python script was created to control the apparatus. Standard methods for measuring the optical output power of the ToF camera light sources were not possible because an integrating sphere was not available, therefore the beam cross-section method was developed.

The beam cross-section method for measuring optical power we develop here is advantageous as it does not require an expensive integrating sphere and provides more information than just the optical output power, such as the distribution of the light emitted from the light source. However, the accuracy of optical power measurements of the beam cross-section method, relied on an extrapolated calibration plot. To improve the accuracy of the calibration, the calibration needs to be redone with higher optical output power values. The higher optical output power values need to be in the same region as the expected light source optical output power so that extrapolation is not required. To obtain these higher optical power measurements, a collimated laser beam with computer controllable optical output power, up to at least 1 W, is required. The accuracy of the beam cross-section method also needs to be measured by comparing it to a standardised optical power measurement method, such as a method that uses an integrating sphere. The uncertainty of the optical power measurements needs to be considered when the hardware benchmark results are compared to the simulation results in the next chapter.

Chapter 6

ToF Camera Light Source Electrical Input to Optical Output Power Efficiency Benchmarking

In this chapter, the apparatus presented in Chapter 5, is used to measure the electrical input power and optical output power of the TIDA-01173 and Kea ToF camera light sources. The electrical input power to optical output power efficiency of these light sources are used to compare between the shunt and series switching topology light sources. The TIDA-01173 and Kea ToF camera light source simulations presented in Chapter 3, are used to obtain theoretical results for electrical input to optical output power efficiency to compare to the hardware results. The simulation is also used to identify the components that consume the most power in the light source circuits, therefore accounting for the efficiency. The results of the power efficiency accounting are used to propose design improvements which are tested using the light source simulations.

6.1 Electrical input to optical output power benchmark

The electrical input and optical output power measurement apparatus, from Chapter 5, is used to measure the electrical input and optical output power of the TIDA-01173 and Kea ToF camera light sources. The input and output power are measured as a function of light source modulation frequency from 10 MHz to 130 MHz. This range of modulation frequencies is selected as it contains the full operating range of modulation frequencies for the TIDA-01173 light source of 10 MHz to 100 MHz. The additional 30 MHz was measured to observe what happens when the TIDA-01173 light source operating range is exceeded. The modulation current setting ranges of the TIDA-01173 and Kea light sources do not have much overlap. The efficiency is dependent on modulation current setting, so for the measurements to be comparable, they are taken for the most similar light source modulation current settings. This is the minimum modulation current setting of the TIDA-01173 light source and the maximum of the Kea light source. Each measurement is repeated five times.

The Electrical input power and optical output power plots are shown in Figure 6.1.1 and Figure 6.1.2 respectively. Five repetitions of each modulation frequency measurements are recorded, the mean of these repetitions is plotted along with error bars that show the 95% confidence intervals. The electrical input power 95% confidence intervals are calculated from the repeated measurements. The optical output power 95% confidence intervals show the uncertainty in the optical output power measurement due to the calibration and measurement variation by combining the 95% prediction interval from the calibrating plot (Figure 5.4.16) with the 95% confidence interval of the repeated measurements. The combination was done by the square root of the sum of the square of the uncertainties. The electrical input to optical output power efficiency plot (Figure 6.1.6) is produced by dividing the optical output power by the electrical input power, as is shown in Eq. (5.1.1).

The results from the simulation models of the TIDA-01173 and Kea ToF camera light sources, developed in Chapter 3, are plotted along with the measured benchmark results (Figure 6.1.1, Figure 6.1.2, and Figure 6.1.6) so comparisons can be made between them. The instantaneous electrical input and optical output power

results from the light source simulations are measured using the method described in [89]. The hardware power is measured as average power and includes the 50% duty cycle Integration and Off times, so cannot be directly compared to the instantaneous power values produced by the simulation. To allow comparison between the hardware and simulation results, the average of simulation results is calculated in post. The average simulation results also must be halved to account for the Integration and Off times. This is because the simulation is only run for a simulation time of 0.5 µs to shorten calculation time.

6.1.1 Electrical input power

The electrical input power plot (Figure 6.1.1) shows that the Kea light source has a substantially higher electrical input power than the TIDA-01173 light source for all modulation frequencies tested. The electrical input power decreases as modulation frequency increases for the Kea light source but remains relatively constant for the TIDA-01173 light source up to a modulation frequency of 100 MHz. For modulation frequencies above 100 MHz, the electrical input power of the TIDA-01173 light source dips substantially. This is expected as 100 MHz is the maximum of the TIDA-01173 light source's modulation frequency operating range (Table 5.2.1), as the inductor's inductance drops off at frequencies above 100 MHz (Figure 3.3.2)

Like the hardware measurements, the electrical input power results for the Kea light source simulation are also substantially higher than the TIDA-01173 light source simulation. However, the Kea light source simulation has a slightly decreasing trend for the electrical input power as with increasing modulation frequency, but it does not show the same rate of decrease as the hardware measurements. The electrical input power of the TIDA-01173 light source simulation remains constant over the full range of modulation frequencies tested. This is the same as the hardware measurements for modulation frequencies from 10 MHz to 100 MHz. The dip in electrical input power, observed in the hardware measurement for modulation frequencies above 100 MHz, is not seen in the simulation results. Given that operating above 100 MHz is outside of specification, there are probably many possible reasons for this difference. However, one we consider is the drop off in the inductor's inductance at frequencies above 100 MHz for the real inductor, but an increase in inductance at these frequencies for the inductor model used in the simulation (Figure 3.3.2). When the inductance drops off, the voltage across the laser diodes is not boosted so the current through the laser diodes decrease therefore decreasing the input current and so the input power decreases.

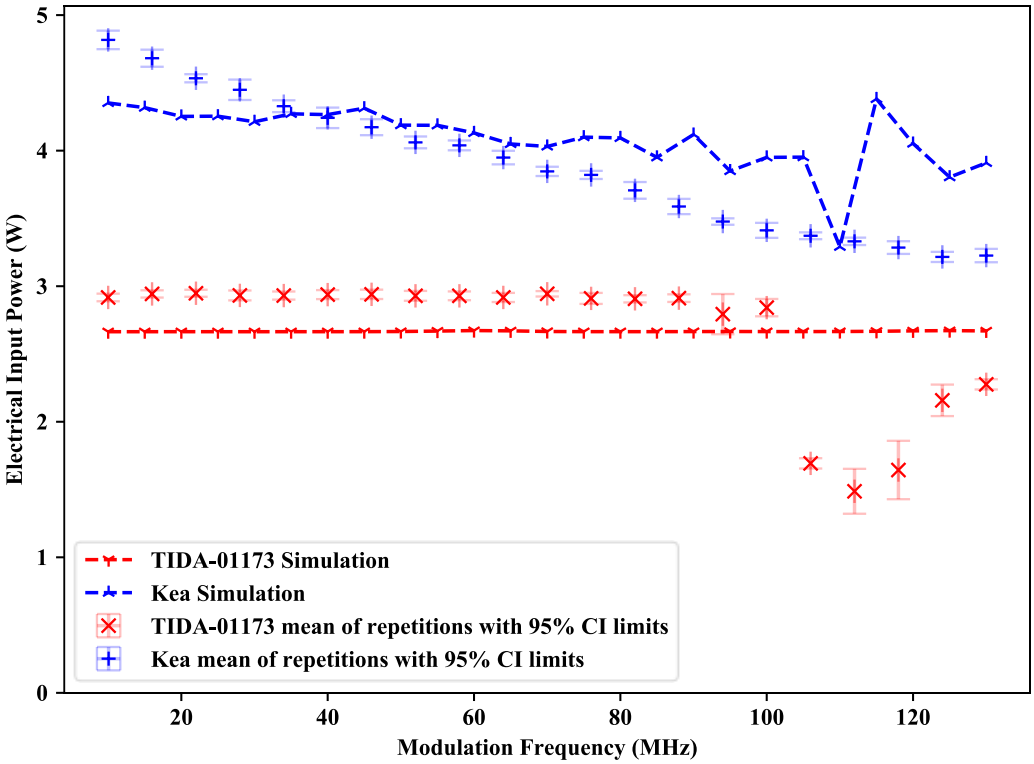

Figure 6.1.1: Plot of electrical input power vs modulation frequency for the TIDA-01173 and Kea light sources showing mean of the repeated measurements with 95% confidence limits as error bars, and the simulation results (dashed lines of the simulated results are for eye guidance only).

6.1.2 Optical output power

The optical output power plot (Figure 6.1.2) shows that the optical output power from modulation frequencies from 10 MHz to 100 MHz of the TIDA-01173 light source is greater than that of the Kea light source. For modulation frequencies greater than 100 MHz, the optical output power of the TIDA-01173 light source dips off just as it does in the electrical input power plot (Figure 6.1.1). The optical output power of the Kea light source steadily decreases as the modulation frequency increases. The optical output power of the TIDA-01173 light source decreases for modulation frequencies from 10 MHz to 70 MHz but increases from 70 MHz to 90 MHz.

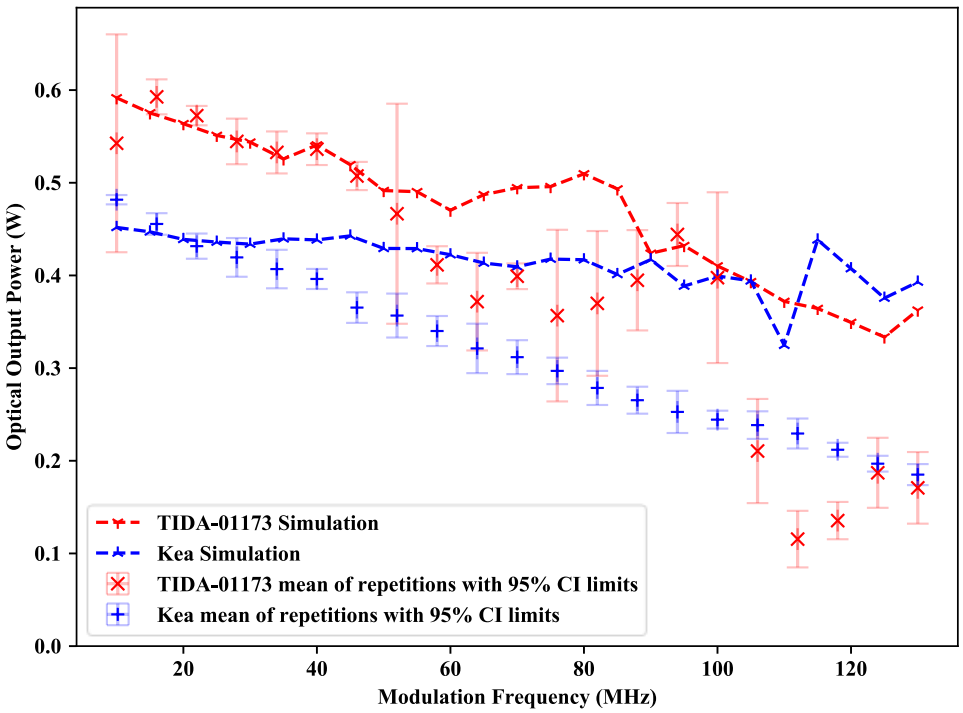

Figure 6.1.2: Plot of optical output power vs modulation frequency for the TIDA-01173 and Kea light sources showing the mean of the repeated measurements with 95% confidence limits as error bars, and the simulation results (dashed lines of the simulated results are for eye guidance only).

The variability in the measurements, as shown by the larger 95% confidence limits, is greater for some of the TIDA-01173 light source optical power measurements than for the Kea light source's measurements. The same measurement method was used to collect the results for both light sources, so the variability must be due to greater instability in the optical output of the TIDA-01173 light source. So, the Kea light source has a more stable optical output than the TIDA-01173 light source. Even though the TIDA-01173 light source produces substantially more optical output power than the Kea light source, it may be preferable to use the Kea light source as it is easier to calibrate for a constant optical output power.

The optical output power simulation of the TIDA-01173 light source is within the 95% uncertainty (shown by the error bars) of the measured TIDA-01173 light source results for modulation frequencies between 10 MHz and 50 MHz. However, between modulation frequencies of 60 MHz and 90 MHz, the simulation diverges from the measured results. The measured optical output power decreases where the simulation increases. The simulated optical output power results return to within the 95% confidence interval of the measured results at the modulation frequency of 100 MHz. At modulation frequencies greater than 100 MHz, the measured and simulated results diverge again. However, the simulation is only expected to be representative of the hardware TIDA-01173 light source up to modulation frequencies of 100 MHz due to the limitations of the component models such as the inductor, as explained in section 3.3.1.

The Kea light source simulation does not show the steady decrease in optical output power with increasing modulation frequency, instead it has a near constant optical output power value of 0.45 W over all the tested frequencies. This does not follow the measured results for the optical output power plot; however, the simulated results are within the same order of magnitude as the measured results, so it is likely that a frequency dependent component in the Kea light source is not present in the simulation. This may be the switch mode buck voltage regulator used to convert the 12 V input voltage to the laser drive voltage of 5 V as it was not included in the simulation. The buck converter may have some resonance with the

high modulation frequency load switching. However, this could not be tested as the TPS62180YZFR buck converter datasheet [90] does not provide information about load frequency response and a TINA-TI model for the TPS62180YZFR buck converter was not available so it could not be included in the Kea light source simulation.

6.1.2.1 Optical output power waveform

The shape of the optical output power waveform of the TIDA-01173 and Kea light sources is observed by placing a DET01CFC high-speed fibre-coupled photodiode (Thorlabs, Newton, New Jersey), connected, matched with 50 Ω impedance, to a DSOS604A digital oscilloscope (Keysight, Santa Rosa, California), in front of the light source laser diodes. The waveforms are captured for modulation frequencies of 10, 68, and 100 MHz, then plotted along with the equivalent waveforms obtained from the SPICE light source simulations (Figure 6.1.3, Figure 6.1.4, and Figure 6.1.5 respectively). The waveforms captured with the photodiode are calibrated by multiplying the waveform by the ratio between the mean results of the average optical output power measurements of the light sources (from Figure 6.1.2 at the appropriate modulation frequencies) and the average of the photodiode waveform.

The measured and simulated TIDA-01173 and Kea light source waveforms at the 10 MHz modulation frequency (Figure 6.1.3) match very closely, apart from the distortion on the TIDA-01173 light source waveform. The additional distortion in the TIDA-01173 light source optical waveform is detrimental to the ToF camera phase measurement as they cause the linearity distortions [31]. The shapes of the simulation waveforms for the 68 and 100 MHz modulation frequencies, for both the TIDA-01173 and Kea light sources do not match the measurements. The two spikes following the falling edge of the simulated TIDA-01173 light source waveform (at about 55 and 60 ns on the 10 MHz plot) are artefacts due to the size of the time base used in the simulation, the time base had to be set large enough so that the simulations were calculated in a reasonable time.

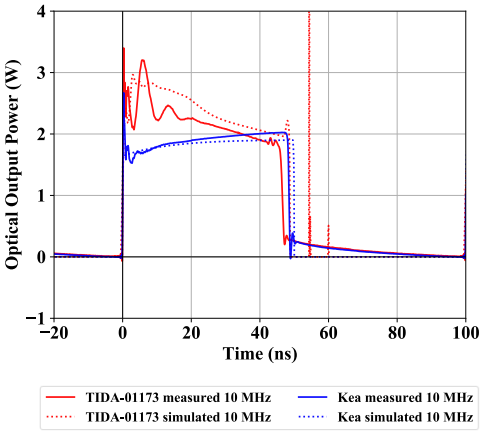

Figure 6.1.3: TIDA-01173 and Kea light source optical output power waveforms at 10 MHz modulation frequency.

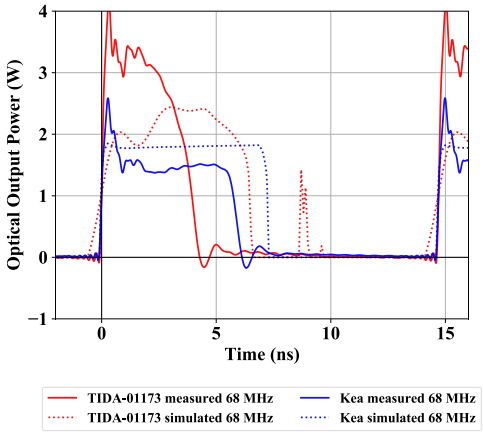

Figure 6.1.4: TIDA-01173 and Kea light source optical output power waveforms at 68 MHz modulation frequency.

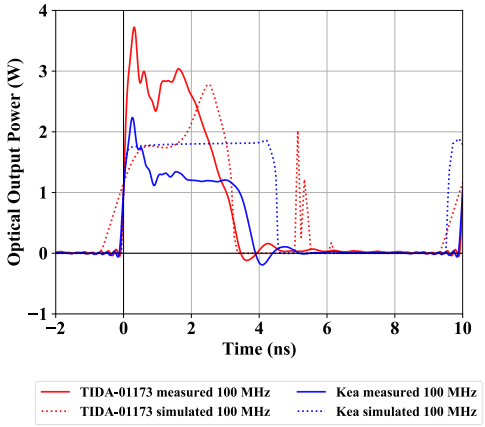

Figure 6.1.5: TIDA-01173 and Kea light source optical output power waveforms at 100 MHz modulation frequency.

At 10 MHz, both the TIDA-01173 and Kea light source's measured optical output power waveforms have roughly square appearance, however, they both exhibit overshoot and oscillations that distort the waveforms following their rising edges. The TIDA-01173 optical output power waveform has much more distortion than the Kea waveform, so at the high modulation frequencies of 68 and 100 MHz. The simulated Kea light source waveform is closer to its measured waveforms for these higher modulation frequencies, however the overshoot after the rising edge does not appear in the simulation. So, the series ToF camera light source topology produces a more consistent optical output waveform than the shunt switching topology, over a wide operating frequency range.

The voltage output of the photodiode detector has a bias level. This bias level is corrected in post. The negative overshoot and ripple on the optical output power plots are artefacts due to voltage ripple in the photodiode, or the coaxial connector between the photodiode and oscilloscope, because optical output power cannot be negative. Indeed, all ripples observable for both light sources and that have a strong correlation are likely to be artefacts of the photodiode measurement system.

There is a difference in the duty cycle ratio between the measured and simulated TIDA-01173 optical output power waveforms at 68 MHz modulation frequency (Figure 6.1.4). The measured duty cycle ratio is 43% at most, and the simulated is 50%. This difference in the duty cycle ratios is likely the reason for the divergence between the measured and simulated optical output power vs modulation frequency plot between 60 and 90 MHz (Figure 6.1.2). The duty cycle ratio of the TIDA-01173 optical output power waveform can be corrected by increasing the duty cycle ratio of the modulation signal for frequencies between 60 and 90 MHz. If the duty cycle ratio is corrected, the measured average optical output power is expected to increase, so the simulated average optical output power vs modulation frequency plot (Figure 6.1.2) will be within the 95% confidence intervals of the measurements.

The TIDA-01773 light source produces more optical output power than the Kea light source but is still eye safe. The shunt topology light source must be continuously modulated to produce substantial optical output power as the inductor and shunt switch acts as a boost converter [54, Ch. 13.4] to increase the laser diode voltage to the laser diode operating voltage, but only when the modulation signal is applied. When no modulation signal is applied, such as when the shunt MOSFET is set to be always on or always off, the voltage across the inductor becomes steady state so it stops boosting the voltage across the laser diode. So, the laser diode voltage falls below its operating voltage and the lasers cease to produce optical output power. As a result, the lasers can never go into continuous wave (CW) mode, so the optical output power does not need to be limited such that at CW operation and given the diffuser optics do not exceed the eye safety requirement (this is shown using a simulation in Appendix B). So, the peak optical output power of the shunt

type light source can be higher than for series as if circuit elements in the series topology fail, such as the modulation MOSFET staying shorted due to component failure or the modulation signal staying on. The advantages of higher optical output power of ToF light sources is higher signal to noise ratio so the ToF camera will perform better in high ambient light conditions such as in day light (ToF cameras don't work well in day light).

6.1.3 Electrical input power to optical output power efficiency

The electrical input to optical output power efficiency of the Kea light source gradually decreases as the modulation frequency increases. The TIDA-01173 electrical input to optical output power efficiency decreases from 10 MHz to 70 MHz then increases from 70 MHz to 90 MHz just as it does for the optical output power.

The simulated efficiency vs modulation frequency curves of either light source is not within the 95% confidence limits of the hardware measurements. However, the overall trend for the simulation and hardware efficiency vs modulation frequency plots are similar for both the TIDA-01173 and Kea light sources. The TIDA-01173 light source simulation follows the decreasing efficiency with increasing modulation frequency as the measured results. The TIDA-01173 light source starts with a 19% mean measured efficiency and 25% simulated at 10 MHz. The efficiency decreases to 14% mean measured and 15% simulated at 100 MHz. However, for modulation frequencies between 60 MHz and 90 MHz the measured and simulated efficiencies diverge then come back together. This is also seen in the optical output power plot (Figure 6.1.2). The largest difference between the measured and simulated efficiencies occurs at 76 MHz, where the measured mean efficiency is 12% and the simulated is 19%. The Kea light source simulation efficiency results are constant at about 10%, however, the measured efficiency of the Kea light source decreases from 10% at 10 MHz to 7% at 100 MHz.

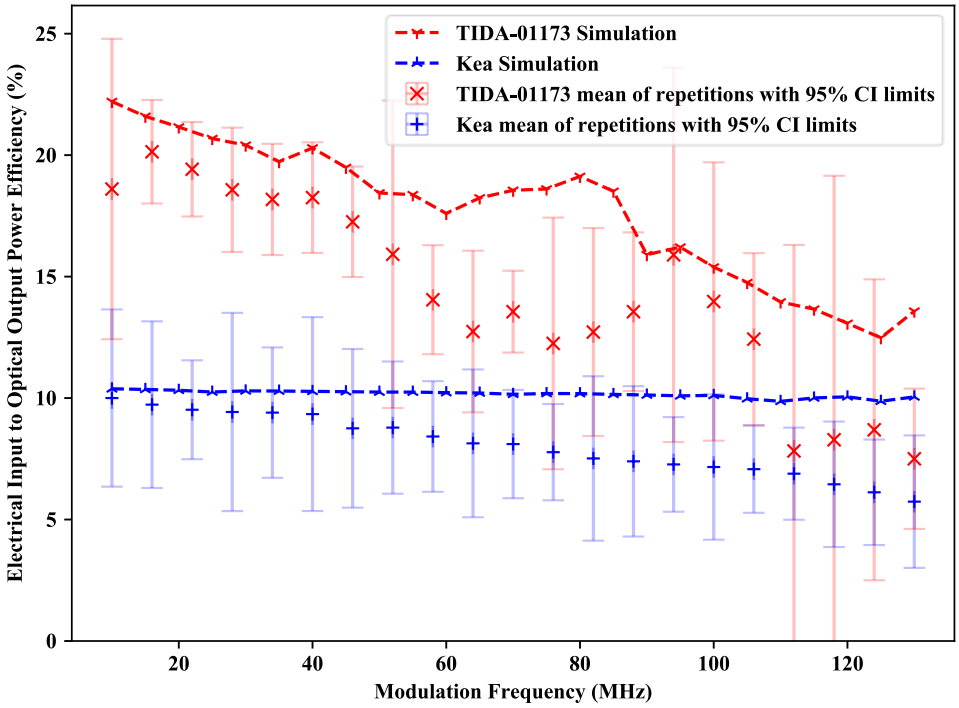

Figure 6.1.6: Plot of electrical input to optical output power efficiency vs modulation frequency for the TIDA-01173 and Kea light sources showing mean of the repeated measurements with 95% confidence limits as error bars, and the simulation results (dashed lines of the simulated results are for eye guidance only).

Even though the light source simulation results do not match the measurements for the real TIDA-01173 and Kea light sources, they are close enough so the simulation can provide an approximate model for how the light sources work in real hardware. In both the hardware measurements and simulations, the electrical input to optical output power efficiency of the TIDA-01173 light source is higher than the Kea light source for all modulation frequencies. This supports the claim made by Texas Instruments and Chronoptics that the shunt switching topology is more power efficient than series topology (section 2.4.5).

6.2 Power efficiency accounting and design improvements

The results from the light source electrical input to optical output power show that the TIDA-01173 has a higher efficiency than the Kea light source. However, the maximum power measured efficiency of the TIDA-01173 light source is only 20% compared to the theoretical maximum efficiency of 34%, as set by the electrical to optical efficiency for the BOB850T1000 laser diode, supplied by the datasheet (Appendix A, Table A.1). To get closer to achieving this maximum power efficiency, the parts of the circuit where power is lost need to be identified. In this section, the light source simulations are used to identify these power losses in the TIDA-01173 and Kea ToF camera light source circuits.

6.2.1 TIDA-01173 power account and design improvement

The power consumption of each of the following components in the TIDA-01173 light source is measured in simulation: Current limiter, inductor, shunt MOSFET, laser diodes, series MOSFET. The voltage regulator and MOSFET driver components were not simulated as their component models could not be sourced so are not included in the power accounting. The TIDA-01173 light source power consumption diagram (Figure 6.2.1) shows that the components that dissipate the most power are the current limiter, laser diodes, and shunt switching MOSFET.

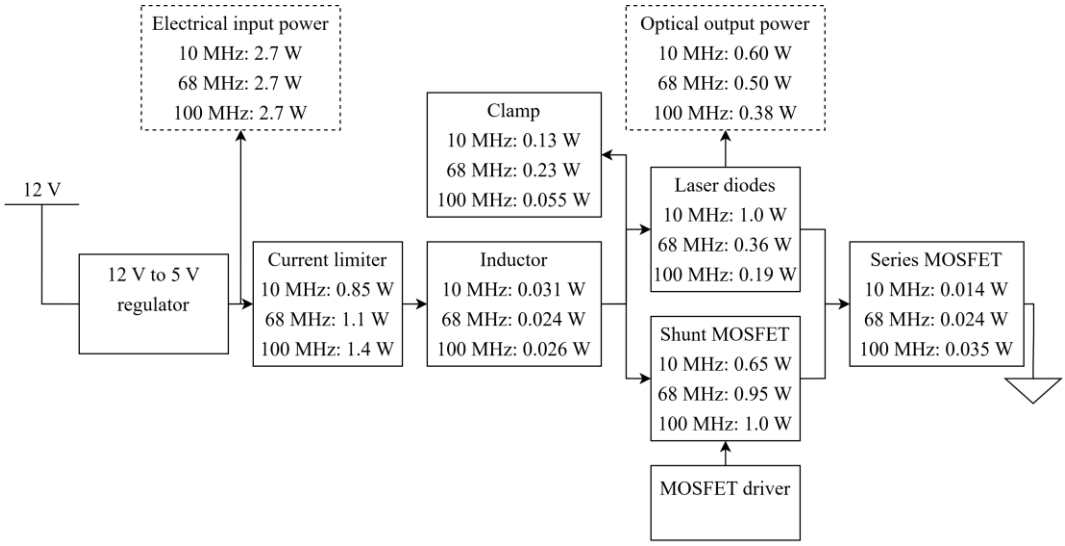

Figure 6.2.1: Diagram showing average power consumption of each component in the TIDA-01173 ToF camera light source simulation for modulation frequencies of 10, 68, and 100 MHz.

It is assumed that all components, except for the laser diode, only dissipate power as heat. For the purposes of calculating laser diode conversion efficiency (electrical to optical output power conversion efficiency), it is important to distinguish between laser total power dissipation and forward power dissipation. The total average power of the laser diodes, as shown in Figure 6.2.1, is less than the average forward power as the total average power includes the power associated with charges leaving the laser diode junctions in the reverse direction, during reverse recovery.

The forward power of the laser diodes is defined as the time averaged product of the forward current through the laser diodes and the voltage across it. The forward power of the laser diode is dissipated as optical power in addition to both heat and optical output power. The reverse power does not contribute to the optical output power so is not included in the conversion efficiency of the laser diode. For example, the reverse power occurs between 50.5 and 56.5 ns in the simulated laser diode power waveform in Figure 6.2.2. The reverse power is, however, dissipated as heat through the shunt MOSFET so is included in the total power consumption of the TIDA-01173 light source to balance the 2.7 W average input power.

The forward power of the laser diode is dissipated as both heat and optical output power. The average forward power consumed by the laser diodes is 1.7, 1.3, and 1.2 W for the modulation frequencies of 10, 68, and 100 MHz respectively. This is calculated by dividing the forward laser diode power by four to account for the 50% duty cycle ratio of the modulation signal, and the 50% duty cycle ratio of the Integration and Off time switching. The forward power of the laser diodes is found from the instantaneous power results (the 10 MHz example is shown in Figure 6.2.2).

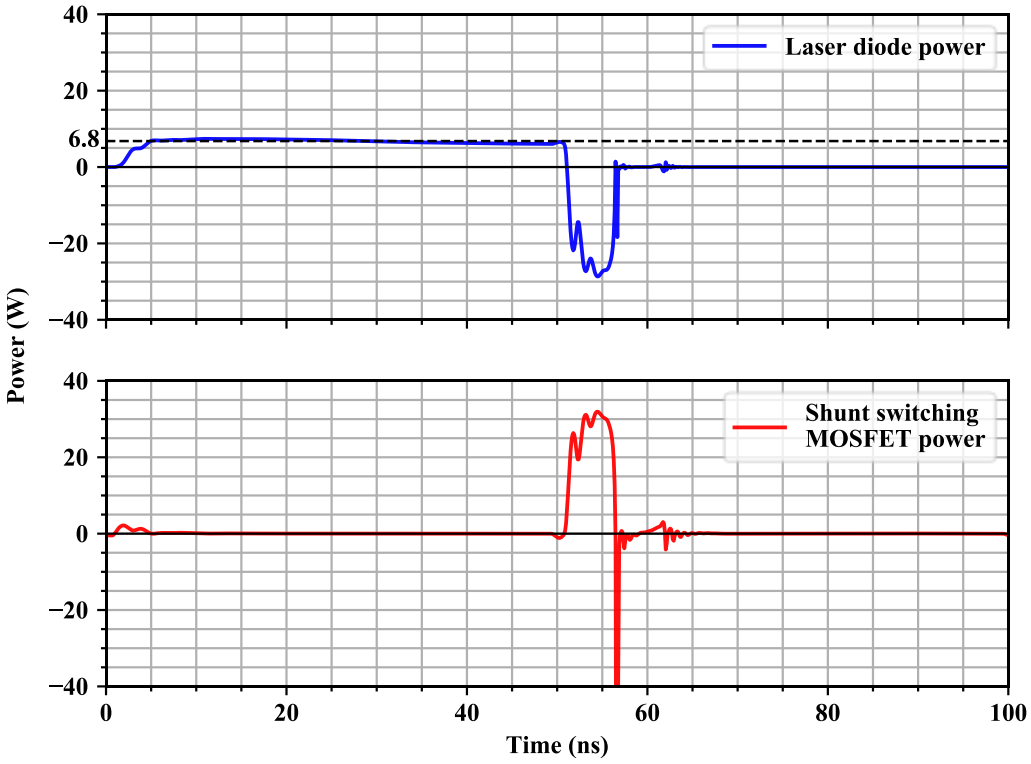

Figure 6.2.2: Laser diode power (top) and shunt switching MOSFET power (bottom) waveforms from the TIDA-01173 light source simulation at 10 MHz modulation frequency.

The ratio between the average forward power consumption of the laser diodes and their optical output power gives their electrical to optical output power conversion efficiency: 35%, 38%, and 32% for the respective modulation frequencies of 10, 68, and 100 MHz. These electrical to optical output power conversion efficiency values are near to the BOB850T1000 laser diode conversion efficiency value of 34%, provided by the BOB850T1000 datasheet (Appendix A, Table A.1). This is another confirmation that the simulation model of the BOB850T1000 laser diode is representative of the real BOB850T1000 laser diode.

The laser diode conversion efficiency sets the maximum limit of the electrical input to optical output power efficiency of the ToF light sources. So, the simplest way to substantially improve the efficiency of the ToF camera light sources is to select a laser diode that has a higher electrical to optical power conversion efficiency. However, as the focus of the investigation is to improve the light source driver efficiency a different laser diode will not be tested.

The inductor and series switching MOSFETs dissipate one to two orders of magnitude less than the current limiter, laser diodes, and shunt switching MOSFET. So substantial improvements in efficiency will not be gained by reducing their power consumption. To improve the electrical input to optical output power efficiency of the ToF light sources, it is best to focus on reducing the power dissipation of the components that consume the most power.

The pie charts (Figure 6.2.3) show that the greatest consumers of power in the TIDA-01173 light source circuit are the current limiter, shunt MOSFET and laser diode. The proportion of power consumed by the current limiter and shunt MOSFET increase as the modulation frequency is increased. This results in a lower portion of power to be consumed by the laser diode, so the power efficiency decreases with increasing modulation frequency, as seen in Figure 6.1.3. To improve the efficiency of the TIDA-01173 light source, the power consumption of the current limiter and shunt MOSFET components must be decreased.

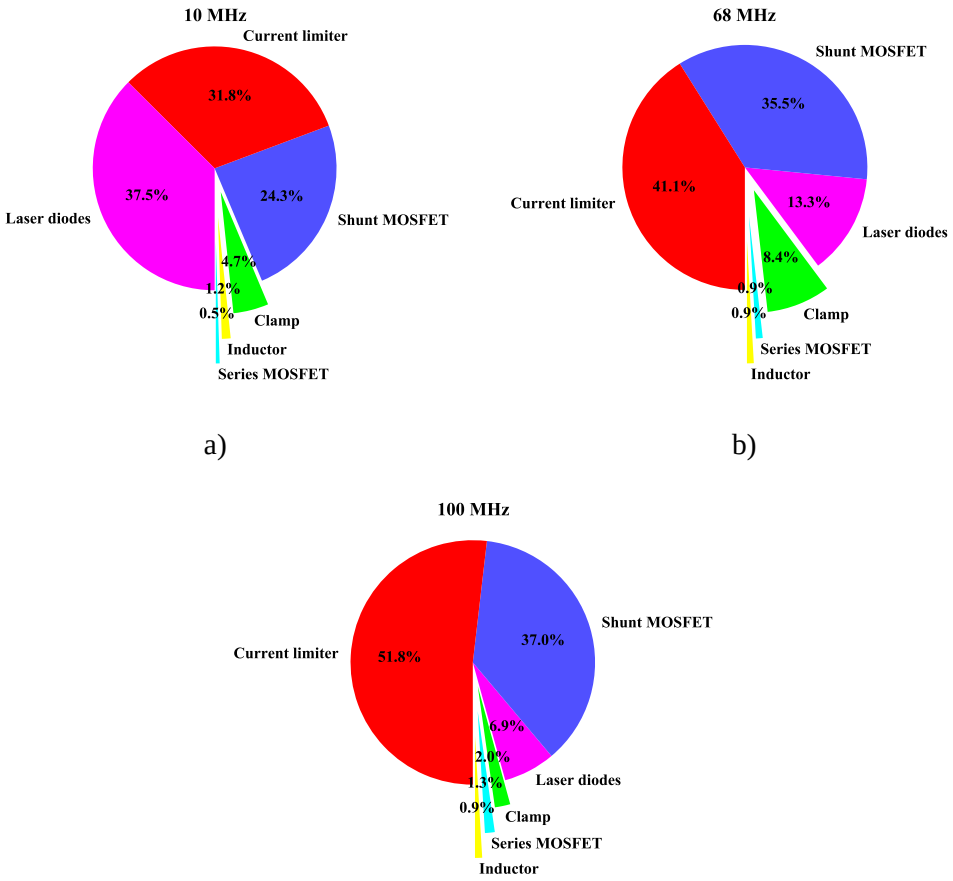

Figure 6.2.3: Pie charts showing the percentage of the total power consumption of the TIDA-01173 light source in simulation for modulation frequencies of: a) 10 MHz, b) 68 MHz, and c) 100 MHz.

The current limiter consumes the most power in the TIDA-01173 light source, so reducing its power consumption is the priority in increasing the efficiency of the TIDA-01173 light source. In constant current mode, the TPS2559 current limiter IC acts as a linear regulator. Linear regulators have low efficiency for high currents, and so, for high current applications, switching regulators are used instead. The range of currents that the current limiter in the TIDA-01173 light source must regulate between is 1.12 to 2.29 A (Table 5.2.1). This is considered high current for a linear regulator. So, we propose that a switching current regulator can be used instead of the linear current limiter. Usually switching regulators are used to regulate voltage not current, however, some switching current regulators exist for LED driver applications, such as the TPS92512 2.5 A Buck LED Driver with Integrated Analog Current Adjust (Texas Instruments, Dallas, Texas). The TPS2559 linear current limiter was replaced by a TINA-TI spice model of the TPS92512 buck current regulator in the TIDA-01173 light source simulation. The buck current regulator is set to source the same current as the linear current limiter, 1.12 A. The simulation is run for modulation frequencies of 10, 68, and 100 MHz.

The simulation results (Figure 6.2.4) show that the buck current regulator substantially improved the electrical to optical power efficiency of the TIDA-01173 light source. For the modulation frequencies of 10, 68, and 100 MHz, the power efficiency is increased from 22%, 19%, and 14% to 28%, 25%, and 23% by using the buck current regulator instead of the linear current limiter. Comparing the power consumption pie charts of the TIDA-01173 light source simulation with the linear current limiter (Figure 6.2.3) and the buck current regulator (Figure 6.2.5), it is apparent that the buck current regulator consumes a lower portion of the total power. When the linear current limiter is replaced with the buck current regulator, the shunt MOSFET becomes the component that consumes the most power. The shunt MOSFET power consumption can be decreased by selecting a MOSFET with a lower on-state drain-source resistance. Aside from the improved efficiency, the supply voltage of the TIDA-01173 light source using the buck current converter is reduced to 5 V, potentially allowing it to be powered via a USB power source if the modulation current is kept within the USB standard maximum current (1.5 to 5.0 A for the USB battery charging specifications [91]).

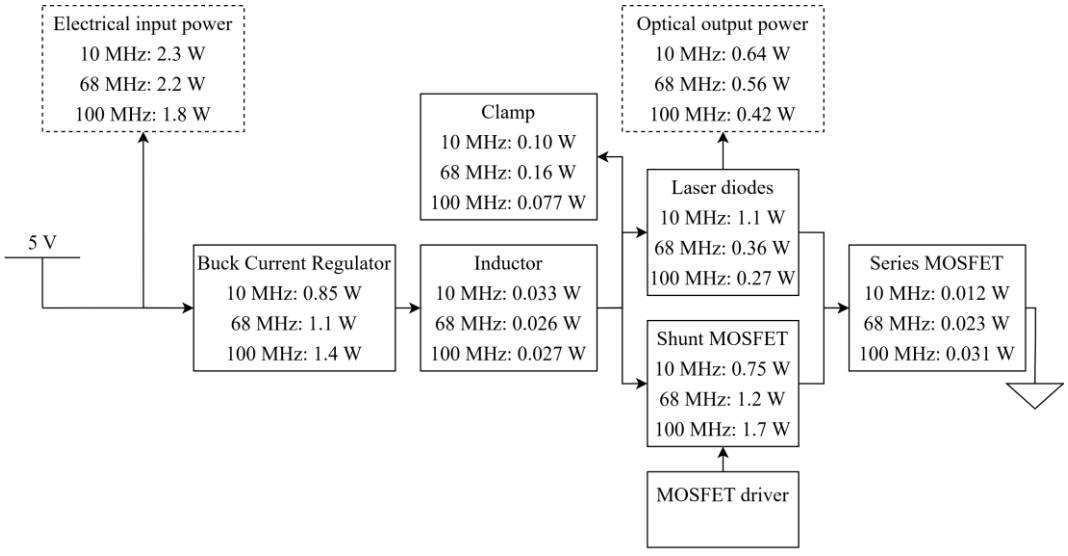

Figure 6.2.4: Average power diagram for the buck current regulator TIDA-01173 light source.

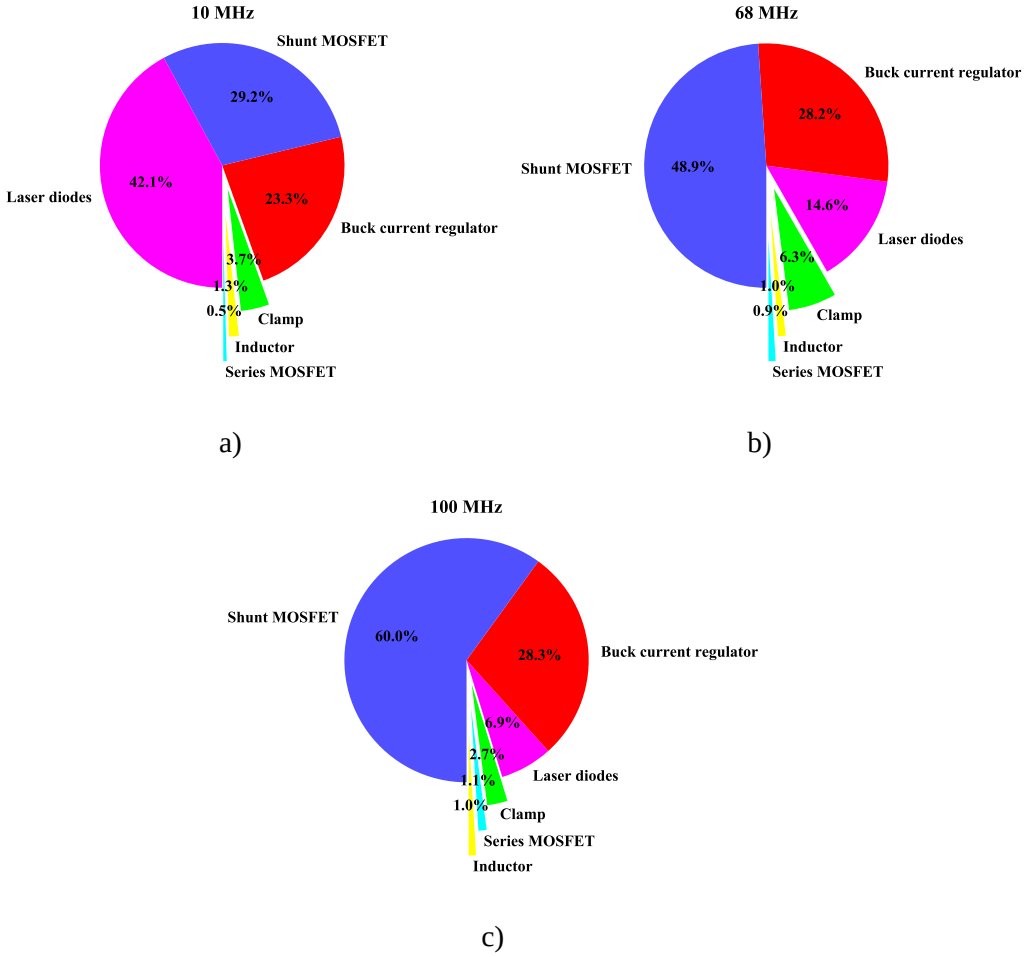

Figure 6.2.5: Pie charts showing the percentage of the total power consumption of the TIDA-01173 light source with the current limiter replaced with the buck current regulator in simulation for modulation frequencies of: a) 10 MHz, b) 68 MHz, and c) 100 MHz.

6.2.2 Kea power account and design improvement

The power consumption of each of the iC-HG and laser diodes in the Kea light source is measured in simulation. The 12 V to 5 V voltage regulator is not included in the simulation as a TINA-TI model is not available. The Kea light source power consumption diagram (Figure 6.2.1) shows the breakdown of the power consumption of each of these components in the Kea light source simulation.

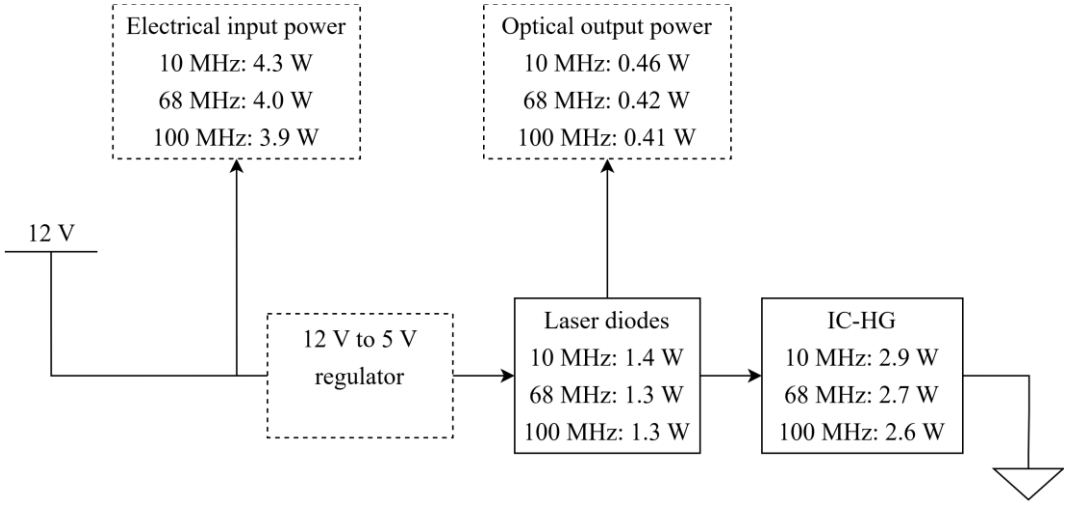

Figure 6.2.6: Average power consumption diagram for the Kea light source.

The pie charts of the percentage of the total power consumption of the Kea light source in (Figure 6.2.7) show that the iC-HG consistently consumes substantially more power than the laser diodes (67.3% compared to 32.7%) for all of the tested modulation frequencies. The iC-HG IC contains two series MOSFETs for each laser driver channel. One of these MOSFETs switches the laser diode current on and off according to the modulation signal, and the other MOSFET acts as a resistor to set the modulation current. This method of resistively regulating current is very inefficient at high currents, so the MOSFET that limits the laser diode current dissipates a lot of power as heat, like the linear current limiter in the TIDA-01173 light source.

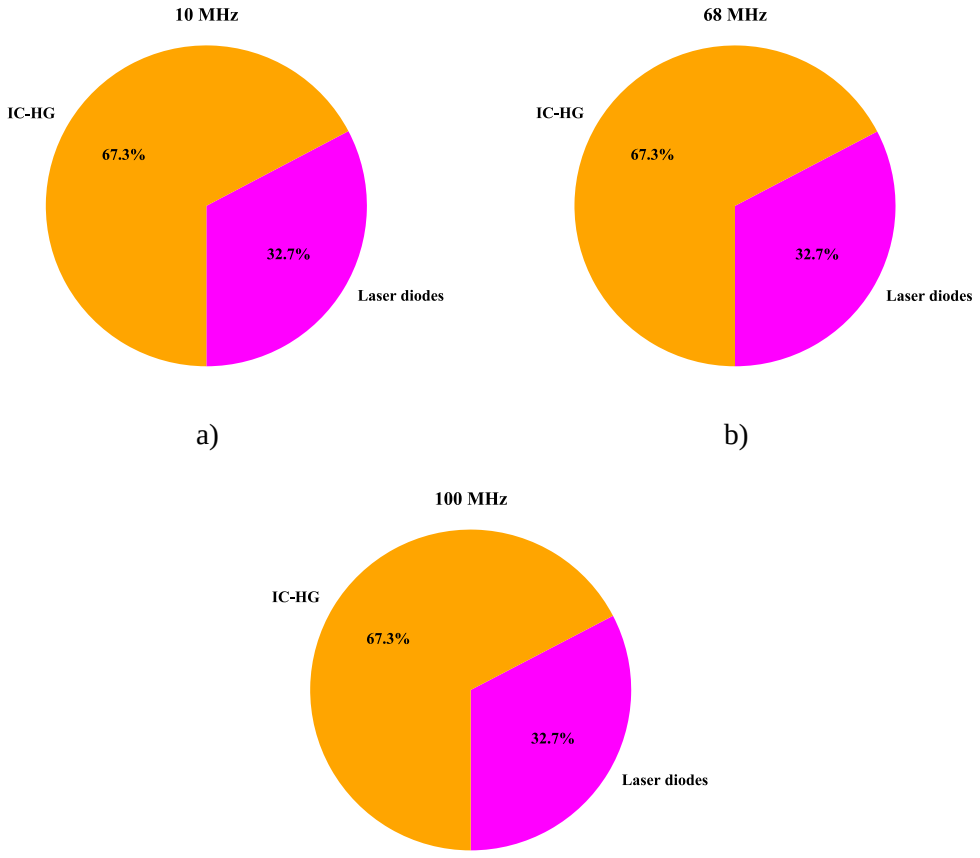

Figure 6.2.7: Pie charts showing the percentage of the total power consumption of the Kea light source in simulation for modulation frequencies of: a) 10 MHz, b) 68 MHz, and c) 100 MHz.

The power efficiency of the Kea light source can be improved by reducing the power dissipated by the current setting MOSFET in the iC-HG. Figure 6.2.8 shows the arrangement of the MOSFETs inside the iC-HG and the arrangement of the laser diodes and iC-HG used in the Kea light source.

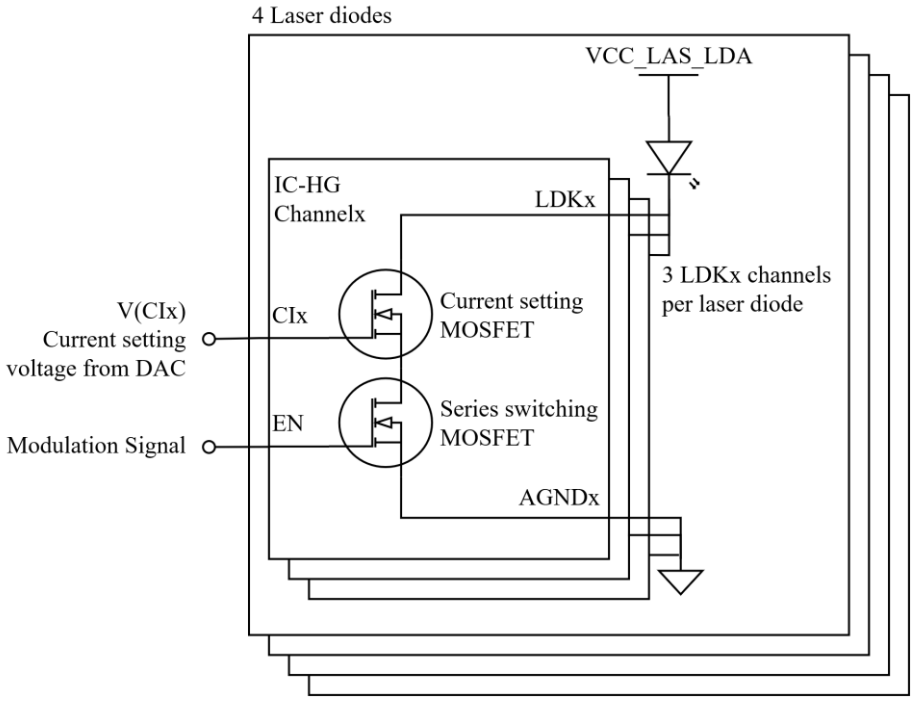

Figure 6.2.8: Diagram showing the MOSFETs inside the iC-HG laser diode driver IC, and the arrangement of the laser diodes and iC-HG as used in the Kea light source.

The typical output characteristics of the laser diode input, LDKx, channels in the iC-HG laser driver, used by the Kea light source, are shown in Figure 6.2.9. The iC-HG datasheet [52] describes the region of the curves where V(LDKx) is greater than 2 V as the current source region, and the region below V(LDKx) is 2 V as the RDSon region. The iC-HG must be operated in the current source region (V(LDKx) > 2 V). In this region, the channel current depends mostly on the current set input voltage (V(CI)) and not on V(LDKx) so the laser current can be controlled by V(CI) in a linear fashion, independent to V(LDKx). V(LDKx) in the present Kea light source design is 3 V, as the VCC_LAS_LDA voltage is set to 5 V and the laser diode forward voltage is assumed to be 2 V at the peak modulation current of 1.48 A (Table 5.2.1). However, V(LDKx) can be reduced to 2 V whilst keeping the iC-HG in the current source region. So, in the present Kea light source design, there is an additional 1 V dropped across each LDKx channel that is not required to operate the iC-HG in the current source region.

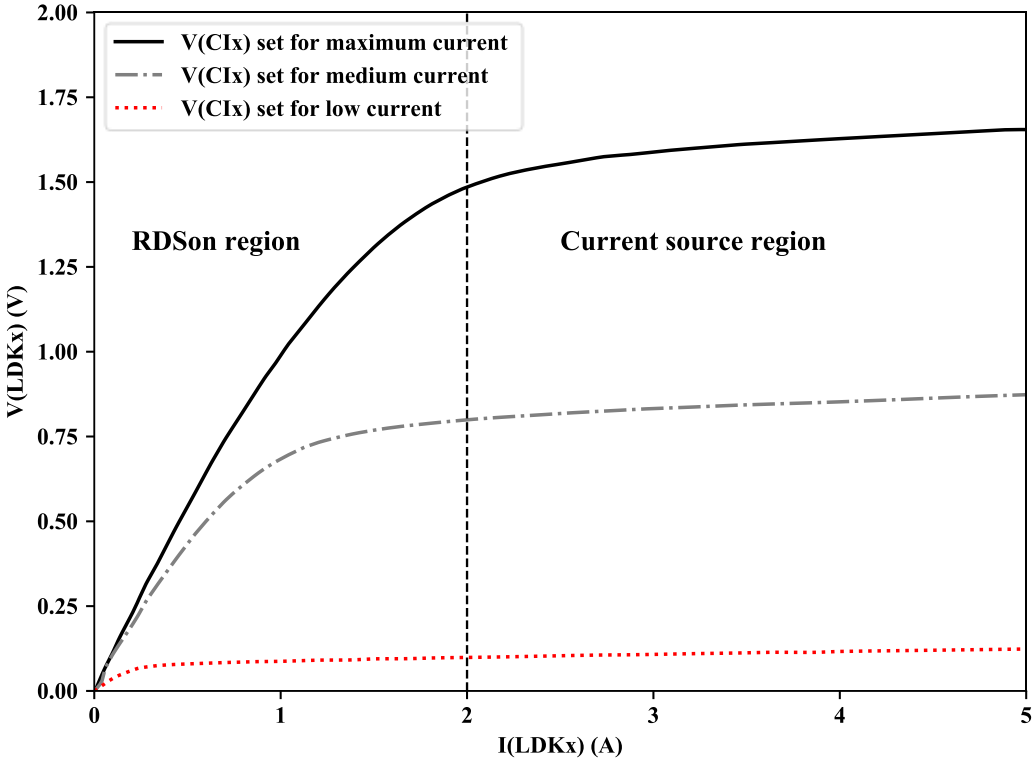

Figure 6.2.9: Output characteristics of the laser diode driver channel, LDKx [52].

It is simple to make this modification to the Kea light source as it only requires the voltage setting resistors on the Kea light source's buck voltage regulator to be changed so that the regulator outputs 4 V instead of 5 V. An adjustment to modulation current setting DAC may also be required to compensate for the slight reduction in LDKx output current at the high current setting values.

This modification is not tested in hardware, but the same simulation used for the efficiency benchmark is run again at a modulation frequency of 10 MHz with VCC_LAS_LDA set to 5 V then 4 V and the modulation DAC value set to the maximum of 470. The average input power and average output power of the input and output power waveforms are recorded, and the power efficiency for each of the measurements are calculated (Table 6.2.1).

Table 6.2.1: Average electrical input and optical output power results for the simulated efficiency measurements of the Kea light source with VCC_LAS_LDA set at 5 V and 4 V, 10 MHz modulation frequency, and 50% duty cycle ratio Integration time switching.

DAC Value	VCC_LAS_LDA	Average Electrical Input Power	Average Optical Output Power	Power Efficiency
470	5 V	4.3 W	0.46 W	11%
470	4 V	3.3 W	0.43 W	13%
478	4 V	3.5 W	0.46 W	13%

These results show that reducing VCC_LAS_LDA from 5 V to 4 V, the average electrical input power has decreased from 4.3 W to 3.3 W, however the average output power also is decreased slightly (from 0.46 to 0.43). This is corrected by increasing the modulation current setting DAC value from 470 to 478 so the optical output power at both 5 V and 4 V VCC_LAS_LDA are the same (0.46 W). After this correction, the average electrical input power with the 4 V VCC_LAS_LDA is 3.5 W compared to the 5 V VCC_LAS_LDA electrical input power of 4.3 W. This is a reduction in the power consumption of the Kea light source circuit of 0.80 W. As a result of this reduction in electrical input power due to reducing VCC_LAS_LDA from 5 V to 4 V, the electric to optical power efficiency of the Kea light source at 10 MHz modulation frequency is increased 2%, from 11% to 13%.

6.3 Conclusion

In this chapter, the electrical input and optical output power of the TIDA-01173 and Kea ToF camera light sources as a function of modulation frequency is measured. The results of these power measurements are used to obtain electrical to optical power efficiency plots of the light sources. These efficiency plots show that the TIDA-01173 light source is more power efficient than the Kea light source. The TIDA-01173 light source power efficiency ranges from about 20% to 15% over modulation frequencies from 10 to 100 MHz and Kea ranges from 10% to 7%. This therefore supports the claim made by Texas Instruments and Chronoptics, that the ToF camera light source shunt switching topology is more power efficient than the series switching topology.

The TIDA-01173 and Kea light source simulations, created in Chapter 3, are compared to the power and efficiency measurements. It is found that the simulations do not perfectly match the measurement results. However, they are close enough to approximate the average power over the light sources operating range of modulation frequencies and the optical output power waveforms. The light source simulations are used to identify the components in the light source circuits that consume the most power. These results are used to propose improvements to the light sources, then the simulation is used to test the proposed improvements. The electrical to optical power efficiency of the TIDA-01173 light source was increased from 22% to 28% at the 10 MHz modulation frequency, by replacing the linear current limiter with a switching buck current regulator. The electrical to optical power efficiency of the Kea light source was increased from 11% to 13% by reducing the laser diode supply voltage from 5 V to 4 V.

This modification has not been tested in hardware. As future work, it is recommended that the Kea light source supply voltage (VCC_LAS_LDA) be reduced from 5 V to 4 V by changing R23 to a 365kΩ resistor and test in hardware to see if there is an improvement in efficiency without compromising the performance of the Kea camera.

The improvements proposed for the TIDA-01173 and Kea light sources allow for less heat dissipation, therefore reducing the heatsinking requirements, and allowing lower power voltage supplies to be used, such as USB.

Chapter 7

Conclusions and Future Work

7.1 Conclusion

The aim of the project is to measure the electrical input to optical output power efficiency of the TIDA-01173 light source and compare it to the Kea light source and to then use these results to develop an improved ToF camera light source. It was found that no apparatuses for measuring ToF camera light source power efficiency were available, so such an apparatus had to be developed. The apparatus measures the electrical input power and optical output power to find the efficiency of the light sources. An input power meter was made to measure the input power. The optical output power was measured by capturing images of the laser beam cross section projected through an optical diffusor. Due to the time required for each measurement and the large number of samples necessary, the capturing of the efficiency measurements was automated.

A simulation of the TIDA-01173 and Kea light sources was produced to aid in the development of the light source improvements. To make the simulation, the characteristics of the BOB850T1000 laser diode were measured and used to make a laser diode simulation model. The light source simulation models provided a good approximation of the real hardware light sources and were used to design and test improvements to the electrical to optical power efficiency of the TIDA-01173 and Kea light sources. The TIDA-01173 light source has a power efficiency of 20% to 15% over modulation frequencies from 10 to 100 MHz, and over the same frequency range, the Kea light source's efficiency ranges from 10% to 7%. Thus, the TIDA-01173 light source was found to have a higher electrical input to optical output power efficiency than the Kea light source. This supports the claim made by

Texas Instruments, that the ToF camera light source shunt switching topology is more power efficient than the series switching topology.

The linear current limiter on the TIDA-01173 light source was found to be the most power consuming component in the light source. In simulation, the linear current limiter was swapped for a buck current regulator. This increased the TIDA-01173 light source's efficiency to 28% at a modulation frequency of 10 MHz. The Kea light source's efficiency was increased to 13% at 10 MHz modulation frequency by reducing the input voltage from 5 V to 4 V. Even though these improvements in efficiency seem small, they are substantial when considering that the maximum electrical input to optical output efficiency of the ToF light source is limited to 34% by the electrical to optical conversion efficiency of the laser diode that was used.

7.2 Future work

Through the course of this project, areas for future work were identified.

The light source test apparatus calibration should be improved by extending the range of measurements to optical output powers above 0.6 W, so the extrapolation of the calibration plot is not required. Also, the calibration should be taken using a standardised light source, or an integrating sphere, to improve the accuracy of the light source test apparatus optical power measurements.

A temperature-controlled enclosure for the light source test apparatus would improve the repeatability and standardisation of the ToF light source measurements. Temperature control of the laser diode in the laser diode characterisation would also benefit the accuracy of the laser diode model and produce more accurate ToF camera light source simulations.

Improvements to the light sources were tested in simulation and found to improve the efficiency. These improvements need to be tested in hardware to confirm that they work.

The TIDA-01173 light source was found to be more power efficient than the Kea light source, however, it was also found that the optical output power waveform of

the TIDA-01173 had more distortion than the Kea light source, and this distortion is detrimental to the ToF camera phase measurement, as it causes linearity distortions.

A shunt topology light source can be designed to be compatible with the Kea ToF camera and tested to see if the greater distortion degrades the performance of the Kea ToF camera. If the performance is degraded, improvements need to be investigated in order to reduce the distortion of the shunt topology light source for use in the Kea ToF camera.

Chronoptics has expressed interest in using the ToF light source power efficiency measuring apparatus. They intend to use it for verification testing of their light source boards to measure each laser's optical output power, checking for out of specification lasers for quality control, and eye safety testing. If this occurs, then the Python script that controls the apparatus needs to be refactored, as it was modified many times throughout the development. It will also be useful for a user interface to be produced for the apparatus. The user interface could take the form of either a Command Line Interface or Graphical User Interface.

The design of the shunt topology TIDA-01173 light source was modified to improve power efficiency by replacing the linear current limiter with a buck current regulator. It was suggested that a shunt switching MOSFET with a lower on-state drain-source resistance be selected to further improve the efficiency of the light source. It is recommended that an appropriate MOSFET be selected and tested in the TIDA-01173 light source simulation before a new shunt switching topology light source board is designed for the Kea ToF camera. It was also suggested that a laser diode with an electrical to optical conversion efficiency greater than the 34% of the BOB850T1000 laser diode, that was used in the Kea light source, be selected. Chronoptics has expressed a preference for the use of Vertical-Cavity Surface-Emitting Laser (VCSEL) diodes over edge emitting diodes, so high efficiency VCSEL laser diodes should be investigated for use in the new shunt switching topology Kea light source.

Appendix A

Laser Diode Datasheet Specification Tables

The datasheet specification tables for the BOB850T1000 laser diode (Bob Laser Co, Guangdong, China) and 22045498 laser diode (Lumentum Operations, San Jose, California) are shown in Table A.1 and Table A.2 respectively.

Table A.1: Parameter table from the BOB850T1000 laser diode datasheet [92].

	Parameter (25°C)	**Symbol**	**Unit**	**Value**
Optical Data	Output power CW	P_o	mW	1000
	Centre wavelength	λ_c	nm	850
	Tolerance of λ_c	-	nm	±5
	Spectral Width (FWHM)	$\Delta\lambda$	nm	<3
	Wavelength stability coefficient	-	nm/°C	~0.3
Electrical Data	Operating current	I_{op}	mA	1300
	Threshold current	I_{th}	mA	200
	Conversion efficiency	η	%	34
	Slope efficiency	η_D	mW/mA	1.1
	Operating voltage	V_{op}	V	2.5
Others	Beam divergence	$\theta_{//}$	°	7.5
		$\theta_{\perp}$	°	35
	Can type	-	TO-18	
	Emitter size	-	µm	50
	Operating temperature	T_{op}	°C	10 to 50
	Storage Temperature	T_{st}	°C	-20 to +80
	Lifetime	MTTF	h	>10000

Table A.2: Parameter table from the 22045498 laser datasheet [93].

Parameter	Minimum	Typical	Maximum
Electrical			
Laser Peak Optical Power at 50% maximum duty cycle, ~10MHz, 1 W for CW			2.4 W
Operating Voltage		1.8 V	2.0 V
Rise Time			1.0 ns
Fall Time			2.0 ns
Operating Current	1.0 A	1.2 A	1.4 A
Threshold Current		0.2 A	0.5 A
Slope Efficiency		1.1 W/A	
Package Inductance		0.9 nH	
Mechanical/Thermal			
Case Thermal Resistance		14°C/W	
Operating Temperature Range	5°C		65°C
Operating Altitude	-300 m		2000 m
Operating relative Humidity (non-condensing)			95% RH
Non-operating Storage Temperature	-40°C		85°C
Optical Performance			
Wavelength Shift Over Temperature		0.3 nm	
Optical Power Temperature Coefficient		-0.4%/C	-1.0 %/C
Beam Divergence - fast axis	14°	18°	21°
Beam Divergence - slow axis	6°	7°	9°
Polarization Ratio	90%		
5% Wavelength at 25°C	845 nm		
95% Wavelength at 25°C			859 nm
Absolute Maximum Ratings (AMR)			
Operating Current			4.5 A
Laser Peak Optical Power			3.7 W

Table A.3: Original Input Power Meter PCB jumper settings for use with the TIDA-01173 light source or the Kea light source.

IPM Jumper Label	IPM Jumper Settings	
	TIDA-01173	Kea
JP_bypass1	Open	Shorted
JP_5V0_IN1	Shorted	Open
JP_5V0_ILIM1	Shorted	Open
JP_CMOS/LVDS1	Shorted	Open

Appendix B

TIDA-01173 Continuous Wave Test

The TIDA-01173 simulation is run with modulation frequency set to 10 MHz and the minimum current setting value that corresponds to 1.21 A peak modulation current. There are three scenarios that may cause the TIDA-01173 to become non eye safe. The first is if the current source fails and becomes a short circuit so that the current is no longer limited. The other two scenarios cause the laser to go into continuous wave mode, if modulation signal remains constantly low so the MOSFET is constantly open circuit, or if the shunt MOSFET fails causing it to also become constantly open circuit. To test these three scenarios, the simulation is run with the following configurations: normal, linear current limiter short circuit, modulation signal set to constantly be low, and shunt switching MOSFET open circuit. The average optical output power results for each of these tests, not considering Integration time switching and Off time, is shown in Table B.4.

Table B.4: TIDA-01173 continuous wave test simulation results.

Configuration	Peak laser diode voltage	Optical output power	Eye safe with diffuser
Normal	6.65 V	1.18 W	Yes
Current limiting switch short circuit	8.30 V	6.96 W	No
Modulation signal set constantly low	5.00 V	0.00 W	Yes
Shunt switching MOSFET open circuit	5.00 V	0.00 W	Yes

The results show that the TIDA-01173 light source is less than normal eye safe optical output power and does not go into continuous wave (CW) mode for two out of the three scenarios: when the modulation signal is set constantly low, and when the shunt switching MOSFET fails open circuit. However, the scenario where the current limiter fails short circuit, does not cause the lasers to go into continuous wave mode, but rather, the optical output power increases substantially above the

normal operating optical output power. This is because there is no current limit, so the current is free to increase to the maximum possible current allowed by the laser diodes, or power supply. It is unknown how likely it is for the linear current limiter to become short circuit if damaged. However, this problem can be mitigated by adding a fuse in series with the current limiter to open the circuit and stop current flow if the current limiter fails short circuit.

TIDA-01173 light source cannot go into continuous wave mode, however the Kea light source can. This may be why the TIDA-01173 light source has a higher optical output power than the Kea light source but is still eye safe.

The reason that the laser diodes optical output power goes to 0 W and does not go into continuous wave mode when the modulation signal is stopped, or if the shunt switching MOSFET fails open circuit is because the inductor stops boosting the laser diode voltage so it falls below the total forward voltage of four series lasers in the TIDA-01173 light source circuit, therefore stopping the current flow.

Figure B.1 shows the measured and simulated voltage waveforms on each side of the inductor, VIN, and VD. VIN is the voltage on the current limiter side of the inductor, and VD is the voltage on the laser diode side, and so is also the voltage across the four series laser diodes. The simulation closely matches the average value of the measurements; however, the measurements have more ripple and distortion on them than the simulation. These waveforms show that the inductor boosts the laser diode voltage (VD) from input voltage (VIN) of just under 4 V, to around 6.5 V. This boosted voltage allows the voltage across of the four laser diodes to be 1.6 V which is enough for them to produce optical output power. If there was no voltage boost, the voltage across each laser diode would be less than 1 V, so the laser diodes would not be able to produce optical output power, as was observed (Table B.4). A modulation signal is required to provide a potentially changing inductor current so that the inductor produces a back Electro-Motive Force (EMF) in response to the changing current therefore boosting the voltage at the VD node.

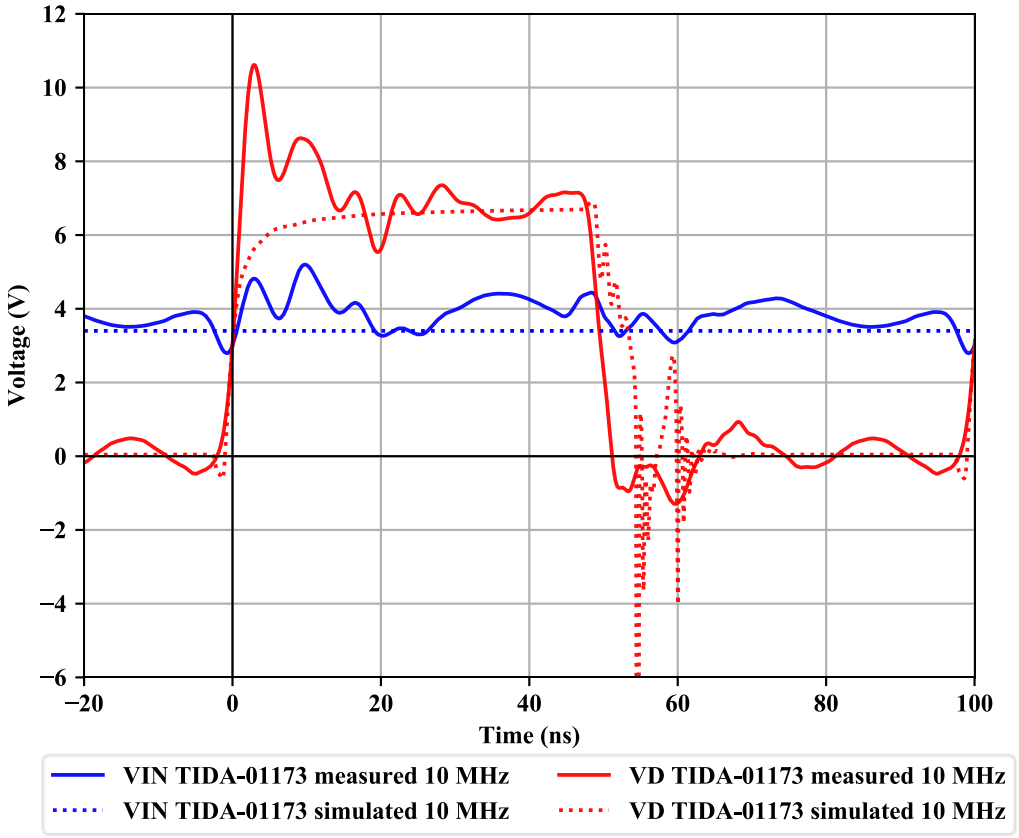

Figure B.1: Oscilloscope traces of the measured and simulated voltage waveforms on each side of the TIDA-01173 light source inductor, VIN, and VD nodes.

References

[1] ‘High Accuracy, 320×240 Voxel 3D Time-of-Flight Robot Vision Reference Design’, p. 34, 2018.

[2] Texas Instruments, ‘Illumination Driving for Time-of-Flight (ToF) Camera System’, Texas Instruments, Application Report, Aug. 2016.

[3] M. Hansard, S. Lee, O. Choi, and R. P. Horaud, *Time-of-Flight Cameras: Principles, Methods and Applications*. Springer Science & Business Media, 2012.

[4] A. Masiero, A. Guarnieri, and A. Vettore, ‘Assessment of A Portable Tof Camera and Comparison with Smartphone Stereo Vision’, *Int. Arch. Photogramm. Remote Sens. Spatial Inf. Sci.*, vol. XLII-2/W17, pp. 187–193, Nov. 2019, doi: 10.5194/isprs-archives-XLII-2-W17-187-2019.

[5] R. Lange, ‘3D Time-of-flight distance measurement with custom solid-state image sensors in CMOS/CCD-technology’, p. 223.

[6] Texas Instruments, ‘Time-of-Flight Camera – An Introduction’. Texas Instruments, Jan-2014.

[7] A. P. P. Jongenelen, D. A. Carnegie, A. D. Payne, and A. A. Dorrington, ‘Maximizing precision over extended unambiguous range for TOF range imaging systems’, in *2010 IEEE Instrumentation & Measurement Technology Conference Proceedings*, Austin, TX, USA, 2010, pp. 1575–1580, doi: 10.1109/IMTC.2010.5488178.

[8] A. P. P. Jongenelen, D. G. Bailey, A. D. Payne, A. A. Dorrington, and D. A. Carnegie, ‘Analysis of Errors in ToF Range Imaging With Dual-Frequency Modulation’, *IEEE Transactions on Instrumentation and Measurement*, vol. 60, no. 5, pp. 1861–1868, May 2011, doi: 10.1109/TIM.2010.2089190.

[9] V. Fang, J. V. Kennedy, J. Futter, J. Manning, and GNS Science (N.Z.), *A review of near infrared reflectance properties of metal oxide nanostructures*. 2013.

[10] T. Ringbeck and B. Hagebeuker, ‘A 3D Time of Flight Camera for Object Detection’, *Optical 3-D Measurement Techniques*.

[11] P. C. D. Hobbs, *Building Electro-Optical Systems: Making It all Work*. John Wiley & Sons, 2011.

[12] R. Henderson and K. Schulmeister, *Laser Safety*. Boca Raton: CRC Press, 2003.

[13] Y. Barkana and M. Belkin, ‘Laser Eye Injuries’, *Survey of Ophthalmology*, vol. 44, no. 6, pp. 459–478, May 2000, doi: 10.1016/S0039-6257(00)00112-0.

[14] K. Petermann, *Laser Diode Modulation and Noise*. Springer Science & Business Media, 2012.

[15] G. Keiser, *Optical Fiber Communications*. McGraw-Hill, 1991.

[16] S. C. Gupta, *Textbook on Optical Fiber Communication and it Applications, Third Edition*. PHI Learning Pvt. Ltd., 2018.

[17] S. R. Salter and D. R. Smith, ‘Injection lasers’, US4355395A, 19-Oct-1982.

[18] J. Lutz, H. Schlangenotto, U. Scheuermann, and R. D. Doncker, *Semiconductor Power Devices: Physics, Characteristics, Reliability*. Springer, 2018.
[19] Thorlabs, 'Laser Diode Tutorial', *Thorlabs.com*. [Online]. Available: https://www.thorlabs.com/NewGroupPage9_PF.cfm?ObjectGroup_ID=1832. [Accessed: 07-Mar-2019].
[20] C. E. Webb and J. D. C. Jones, *Handbook of Laser Technology and Applications: Laser design and laser systems*. CRC Press, 2004.
[21] H. Lin, L. Yang, M. R. T. Tan, and S.-Y. Wang, 'Integration of surface emitting laser and photodiode for monitoring power output of surface emitting laser', US5491712A, 13-Feb-1996.
[22] S. E. Swirhun and W. E. Quinn, 'Integration of laser with photodiode for feedback control', US5577064A, 19-Nov-1996.
[23] T. Yoshida, 'Laser diode optical wavelength control apparatus', US6154474A, 28-Nov-2000.
[24] S. Hava, R. Hunsperger, and H. Sequeira, 'Monolithically Peltier-cooled laser diodes', *Journal of Lightwave Technology*, vol. 2, no. 2, pp. 175–180, Apr. 1984, doi: 10.1109/JLT.1984.1073592.
[25] N. Hori, 'Wavelength/output power stabilizing apparatus of semiconductor laser', US4821273A, 11-Apr-1989.
[26] W. Koechner, *Solid-State Laser Engineering*. Springer, 2013.
[27] J. B. A, R. F. B, and V. J. A, 'Tuning of the laser diode'. [Online]. Available: https://www.rp-photonics.com/laser_diode_drivers.html. [Accessed: 03-Jul-2019].
[28] 'Encyclopedia of Laser Physics and Technology - laser diode drivers, current control, constant power mode, wavelength tuning, protective features, safety, interlocks, temperature control, monitoring, modulation, computer control'. [Online]. Available: https://www.rp-photonics.com/laser_diode_drivers.html. [Accessed: 07-Mar-2019].
[29] IEC, *IEC 60825-1*. 2008.
[30] J. Redd and Q. Tan, 'Interfacing Maxim Laser Drivers with Laser Diodes'. Lightwave magazine, 01-Sep-2000.
[31] A. D. Payne, A. A. Dorrington, and M. J. Cree, 'Illumination waveform optimization for time-of-flight range imaging cameras', presented at the SPIE Optical Metrology, Munich, Germany, 2011, p. 80850D, doi: 10.1117/12.889399.
[32] D. J. Copeland and R. K. Zimmerman, Jr., 'High-current, high-bandwidth laser diode current driver', presented at the Optics, Electro-Optics, and Laser Applications in Science and Engineering, Los Angeles, CA, 1991, p. 412, doi: 10.1117/12.43771.
[33] D. B. Carlin, J. P. Bednarz, C. J. Kaiser, J. C. Connolly, and M. G. Harvey, 'Multichannel optical recording using monolithic arrays of diode lasers: errata', *Appl. Opt., AO*, vol. 23, no. 24, pp. 4613–4619, Dec. 1984, doi: 10.1364/AO.23.004613.
[34] A. Arimoto and S. Saito, 'Laser printing apparatus with device for combining a plurality of optical beams provided with an integral-order wave plate', US4760407A, 26-Jul-1988.

[35] A. Wolozko, M. Lipinski, and P. Korohoda, ‘Circuit For Testing Modulation Properties Of The Semiconductor Lasers’, presented at the Optical Fibers and Their Applications V, Warsaw, Poland, 1990, p. 510, doi: 10.1117/12.953001.
[36] R. B. Thompson, J. K. Frisoli, and J. R. Lakowicz, ‘Phase fluorometry using a continuously modulated laser diode’, *Analytical Chemistry*, vol. 64, no. 18, pp. 2075–2078, Sep. 1992, doi: 10.1021/ac00042a009.
[37] P. -T. Ho, L. A. Glasser, E. P. Ippen, and H. A. Haus, ‘Picosecond pulse generation with a cw GaAlAs laser diode’, *Applied Physics Letters*, vol. 33, no. 3, pp. 241–242, Aug. 1978, doi: 10.1063/1.90312.
[38] G. N. Link, ‘Laser diode driver having automatic power control with smooth enable function’, US5802089A, 01-Sep-1998.
[39] A. D. Payne, D. A. Carnegie, A. A. Dorrington, and M. J. Cree, ‘Full field image ranger hardware’, in *Third IEEE International Workshop on Electronic Design, Test and Applications (DELTA’06)*, Kuala Lumpur, Malaysia, 2006, pp. 6 pp. – 268, doi: 10.1109/DELTA.2006.50.
[40] A. A. Dorrington, M. J. Cree, A. D. Payne, R. M. Conroy, and D. A. Carnegie, ‘Achieving sub-millimetre precision with a solid-state full-field heterodyning range imaging camera’, vol. 18, no. 9, pp. 2809–2816, 2007, doi: 10.1088/0957-0233/18/9/010.
[41] A. D. Payne, A. A. Dorrington, M. J. Cree, and D. A. Carnegie, ‘Improved measurement linearity and precision for AMCW time-of-flight range imaging cameras’, vol. 49, no. 23, pp. 4392–4403, 2010, doi: 10.1364/AO.49.004392.
[42] A. D. Payne, ‘Development of a Full-Field Time-of-Flight Range Imaging System’, Thesis, The University of Waikato, 2008.
[43] R. Z. Whyte, ‘Resolving Measurement Errors Inherent with Time-of-Flight Range Imaging Cameras’, Thesis, University of Waikato, 2015.
[44] I. D. Crawford, J. T. Richter, S. L. Pickles, and J. A. Harwick, ‘Biphase laser diode driver and method’, US8207711B2, 26-Jun-2012.
[45] M. T. Thompson and M. F. Schlecht, ‘High power laser diode driver based on power converter technology’, *IEEE Transactions on Power Electronics*, vol. 12, no. 1, pp. 46–52, Jan. 1997, doi: 10.1109/63.554168.
[46] I. D. Crawford, ‘High-power pulsed laser diode driver’, US6697402B2, 24-Feb-2004.
[47] R. Hui and M. O’Sullivan, *Fiber Optic Measurement Techniques*. Academic Press, 2009.
[48] M. Buchmeier, *Equivalent circuit of a bias tee*. 2018.
[49] Crystek Microwave, ‘RedBox Bias Tee CBTEE-01-50-6000’. Crystek Microwave, 04-Aug-2006.
[50] C. Lee *et al.*, ‘4 Gbps direct modulation of 450 nm GaN laser for high-speed visible light communication’, *Optics Express*, vol. 23, no. 12, p. 6, Jun. 2015, doi: 10.1364/OE.23.016232.
[51] C. Su and V. Lanzisera, ‘Ultra-high-speed modulation of 1.3-μm InGaAsP diode lasers’, *IEEE Journal of Quantum Electronics*, vol. 22, no. 9, pp. 1568–1578, Sep. 1986, doi: 10.1109/JQE.1986.1073192.
[52] iC-Haus, ‘iC-HG 3A Laser Switch Datasheet’. iC-Haus, 08-Jan-2018.
[53] S. Caniggia and F. Maradei, *Signal Integrity and Radiated Emission of High-Speed Digital Systems*. New York, UNITED KINGDOM: John Wiley & Sons, Incorporated, 2008.

[54] M. H. Rashid, *Power Electronics Handbook: Devices, Circuits and Applications*. Elsevier, 2010.
[55] ‘Understanding Optical Power Measurements’, *Electronic Design*, 25-Jun-2012. [Online]. Available: https://www.electronicdesign.com/markets/energy/article/21796124/understanding-optical-power-measurements. [Accessed: 07-Feb-2020].
[56] ILX Lightwave, ‘Accuracy and Repeatability of Power Measurements Using the FPM-8220 Fiber Optic Power Meter’.
[57] Keithley Instruments Inc., ‘Measuring Laser Diode Optical Power With the Keithley Model 2500INT Integrating Sphere’.
[58] ‘Ø2" Integrating Spheres’. [Online]. Available: https://www.thorlabs.com/newgrouppage9.cfm?objectgroup_ID=1658. [Accessed: 08-Feb-2020].
[59] C. Beisbart and N. J. Saam, *Computer Simulation Validation: Fundamental Concepts, Methodological Frameworks, and Philosophical Perspectives*. Springer, 2019.
[60] ‘BRL3225TR51M | INDUCTORS | TAIYO YUDEN CO., LTD. for NA’. [Online]. Available: https://ds.yuden.co.jp/TYCOMPAS/ut/detail?pn=BRL3225TR51M++&u=M. [Accessed: 22-Jan-2020].
[61] Taiyo Yuden, ‘Spec Sheet Wire-wound Chip Power Inductors (BR series)[BRL] BRL3225TR51M’. Taiyo Yuden, 27-Jul-2016.
[62] ‘Engauge Digitizer’. [Online]. Available: http://markummitchell.github.io/engauge-digitizer/. [Accessed: 23-Jan-2020].
[63] Texas Instruments, ‘TPS2559 Precision Adjustable Current-Limited Power-Distribution Switch’. Texas Instruments, Jun-2014.
[64] Texas Instruments, ‘TPS255x Precision Adjustable Current-Limited Power-Distribution Switches’. Texas Instruments, Nov-2009.
[65] V. V. Bodake, A. Jeyakumar, and D. Patel, ‘VERIFICATION OF SPICE MODEL OF MOSFET’, vol. 04, no. 05, p. 5.
[66] Texas Instruments, ‘CSD16301Q2 25-V N-Channel NexFET™ Power MOSFET Datasheet’. Texas Instruments, Oct-2009.
[67] Texas Instruments, ‘TPL0102 Two 256-Taps Digital Potentiometers With Non-Volatile Memory’. Texas Instruments, Mar-2011.
[68] ‘iC-Haus Homepage - product: iC-HG’. [Online]. Available: https://www.ichaus.de/HG. [Accessed: 11-Feb-2020].
[69] Semtech Corporation, ‘uCLAMP1201H 1-Line ESD protection datasheet’. Semtech Corporation, 2005.
[70] K. Petermann, *Laser Diode Modulation and Noise*. Springer Science & Business Media, 1991.
[71] Berkeley, University of California, ‘Circuit Elements’, *CIRCUIT ELEMENTS AND MODELS*. [Online]. Available: http://bwrcs.eecs.berkeley.edu/Classes/IcBook/SPICE/UserGuide/elements.html#618. [Accessed: 03-Dec-2019].
[72] Thorlabs, ‘TCLDM9 Temperature Controlled, Laser Diode Mount for 5.6 and 9 mm LD Operating Manual’. Thorlabs, 26-Jun-2015.
[73] Fluke, ‘Fluke 170 Series True-rms Digital Multimeters’, p. 5.

[74] R. C. Jaeger and T. N. Blalock, *Microelectronic circuit design*, Fifth edition. New York, NY: McGraw-Hill, a business unit of The McGraw-Hill Companies, Inc, 2015.
[75] R. Borràs, J. del Río, C. Oriach, and J. Juliachs, 'Study of a single emitter laser diode: Pspice model and characterization system', in *Semiconductor Lasers and Laser Dynamics VIII*, 2018, vol. 10682, p. 106821K, doi: 10.1117/12.2304747.
[76] S. A. Maas, *Nonlinear Microwave and RF Circuits*. Artech House, 2003.
[77] Solartron Analytical, '1260 Impedance/Gain-Phase Analyzer OPERATING MANUAL'. Solartron Analytical, Dec-1995.
[78] D. I. Zaikin, 'Basic diode SPICE model extension and a software characterization tool for reverse recovery simulation', in *2015 IEEE International Conference on Industrial Technology (ICIT)*, 2015, pp. 941–945, doi: 10.1109/ICIT.2015.7125218.
[79] M. H. Rashid, *SPICE for Power Electronics and Electric Power*. CRC Press, 2017.
[80] 'numpy.trapz — NumPy v1.18 Manual'. [Online]. Available: https://numpy.org/doc/1.18/reference/generated/numpy.trapz.html. [Accessed: 16-Feb-2020].
[81] K. Walters, 'How to Quickly Obtain Spice Parameters for Diodes', p. 4.
[82] R. Borràs, J. del Rio, C. Oriach, and J. Juliachs, 'Laser diodes optical output power model', *Measurement*, vol. 133, pp. 56–67, Feb. 2019, doi: 10.1016/j.measurement.2018.10.007.
[83] jimblom, 'Arduino Shields - learn.sparkfun.com', *Sparkfun*. [Online]. Available: https://learn.sparkfun.com/tutorials/arduino-shields/all. [Accessed: 17-Jan-2020].
[84] Arduino, 'Arduino - ArduinoShields'. [Online]. Available: https://www.arduino.cc/en/Main/arduinoShields. [Accessed: 17-Jan-2020].
[85] Texas Instruments, 'INA226 High-Side or Low-Side Measurement, Bi-Directional Current and Power Monitor with I2C Compatible Interface Datasheet'. .
[86] Thorlabs, 'S302C Thermal Power Head Spec Sheet'. [Online]. Available: https://www.thorlabs.com/drawings/f845aaae3b6efc05-D0EF259E-F4C1-2759-D9F8B90D82411FE7/S302C-SpecSheet.pdf. [Accessed: 26-Feb-2020].
[87] 'numpy.polyfit — NumPy v1.17 Manual'. [Online]. Available: https://docs.scipy.org/doc/numpy/reference/generated/numpy.polyfit.html. [Accessed: 26-Feb-2020].
[88] D. T. Larose, *Data Mining Methods and Models*. John Wiley & Sons, 2006.
[89] N. Gupta, '[Resolved] [FAQ] TINA/Spice: Calculating Efficiency for a Power Supply with TINA-TI - Simulation, hardware & system design tools forum - Simulation, hardware & system design tools - TI E2E support forums', *E2E support forums*, 23-May-2018. [Online]. Available: https://e2e.ti.com/support/tools/sim-hw-system-design/f/234/t/692610. [Accessed: 07-Mar-2020].
[90] Texas Instruments, 'TPS6218x 4-V to 15-V, 6-A, 2-Phase Step-Down Converters with AEE^{TM} Datasheet', May-2017. [Online]. Available: http://www.ti.com/lit/ds/symlink/tps62180.pdf. [Accessed: 07-Mar-2020].

[91] USB Implementers Forum, Inc., ‘Battery Charging Specification’, p. 72, Mar. 2012.
[92] Bob Laser Co, ‘850nm 1000mw laser diode TO-18 infrared illumination, View 850nm laser diode, BOB Product Details from Bob Laser Co., Ltd. on Alibaba.com’, *www.alibaba.com*. [Online]. Available: //www.alibaba.com/product-detail/850nm-1000mw-laser-diode-TO-18_60539297671.html. [Accessed: 11-Feb-2020].
[93] Lumentum, ‘22045498 2 W Peak Power TO-56 Packaged Diode Laser Rev003 Datasheet’. Lumentum.